RAIDING THE TOOLBOX – TECHNIQUES FOR ASSESSING HISTORICAL, HIGH-RESOLUTION RECORDS OF COASTAL AND ESTUARINE SEDIMENT EROSION, TRANSPORT AND SEDIMENTATION

Emily Anne Elliott

A dissertation submitted to the faculty of the University of North Carolina at Chapel Hill in partial fulfillment of the requirements for the degree of Doctor of Philosophy in the Department of Marine Sciences.

Chapel Hill
2017

Approved by:

Brent A. McKee

Antonio B. Rodriguez

Harvey Seim

Jaye Cable

W. Joe Lambert

ABSTRACT

Emily A. Elliott: Raiding the toolbox – Techniques for Assessing Historical High-Resolution Records of Coastal and Estuarine Sediment Erosion, Transport and Sedimentation
(Under the direction of Brent A. McKee and Antonio B. Rodriguez)

Estuaries act as a buffers to material transport from terrestrial to oceanic environments. Characterizing mechanisms of erosion, transport and deposition within estuaries is crucial for understanding material flux to the marine environment and compositional transformations. However, obtaining multi-decadal high-resolution records of sediment flux, source, and composition within estuaries is a major challenge in coastal research due to dynamic processes that actively erode, resuspend and/or rework the sedimentary record. For this reason, estuarine sedimentology has dominantly focused on either long-term (decadal to millennial) records that show constant sedimentation rates often matching the rate of sea-level rise, or short-term (multi-year to decadal) studies that show variable sedimentation rates associated with events.

This dissertation presents a monthly record of estuarine sedimentation that spans ~40 years within a highly accreting mini-basin, Cape Lookout Bight (CLB), NC, utilizing existing and newly-developed methods. This long-term high-resolution record is used to identify the dominant physical drivers of sediment flux within the estuary.

Chapter 1 of this dissertation uses the lithologic and the long-term geochronology of this basin to determine its formation and sediment sources through time. Chapter 2 presents and tests the efficacy of a modified uni-directional time-integrated mass suspended-sediment sampler for use within the bi-directional flow of a tidal (estuarine) environment. Modified collectors are then used to verify the dominant estuarine sediment source to the CLB basin. Chapter 3 applies and

tests different geochronological models for excess ^{210}Pb within the estuarine system, showing the strengths and weaknesses of each model application within our system, and presents a method for applying tempestite horizons for increased resolution and accuracy of estuarine geochronologies. Finally, Chapter 4 uses this established high-resolution multi-decadal geochronology, along with historical physical data obtained for the system, to identify sediment source and drivers of sediment transport within the estuary to the coastal ocean through time. This study identifies multiple sedimentation events that are triggered by conditions that have a recurrence interval of ~1 year (+/- 0.5) and advances our understanding of how storms, and therefore climate change may impact sediment erosion, transport and deposition within the coastal zone.

To the loves of my life, Mark Elliott and our beautiful children, Grace and Jacob;
You are my joy, my love and my inspiration.

Jalowska, who not only trained me in geochronological methodology, but mentored and supported me as a researcher, mother and friend throughout the dissertation process. Thanks also to Elaine Monbureau for her incredible support in both laboratory and field analysis, and whose friendship I deeply value. To Dr. Christopher Martens, Dr. Glenn Walters, Dr. Ethan Theuerkauf, Dr. Justin Ridge, Dr. Theresa O'Meara, Dr. Robin Mattheus, Dr. Maggie Esch, Dr. John Gunnell, Dr. Lisa Nigro, William Flowers, Sherif Ghobrial, Molly Bost, Anna Atencio, Patricia Rodriguez, Beth VanDussen, Glenn Safrit, and Jill Arriola for invaluable expertise and assistance in the lab and field. I also owe a great deal of gratitude to all of the faculty, staff and students of the UNC Department and Institute of Marine Sciences, whose guidance, support and friendship made my time at UNC so special.

I want to thank my family and friends, especially my parents Nancy and Tony Timmons and my in-laws Marcia and Herschel Elliott, whose unconditional love and unwavering support have been a guiding force and source of strength. To my amazing husband, Dr. Mark Elliott, who has been my constant cheerleader and refuge throughout this process, and to our beautiful children, Grace and Jacob, who are the joy and inspiration in our lives.

Finally, I would like to thank God for the incredible opportunity pursue work that I love with brilliant colleagues who are truly working to make this world better now and into the future.

TABLE OF CONTENTS

LIST OF TABLES

LIST OF FIGURES

LIST OF ABBREVIATIONS AND SYMBOLS

CLB	Cape Lookout Bight, North Carolina
RSLR	Relative Sea-Level Rise
DEM	Digital Elevation Model
OGF	Open Grounds Farm
CIC	Constant Initial Concentration Model
CRS	Constant Rate of Supply Model
SSL	Suspended Sediment Load
TIMS	Time Integrated Mass Sediment Sampler
OD	Outer Diameter
ID	Internal Diameter
PIV	Particle Image Velocimetry
PVC	Polyvinylchloride
PS	Point Sample
SS	Sediment Sampler
SAR	Sediment Accumulation Rate
SAE	Sediment Accumulation Event
SSAE	Significant Sediment Accumulation Event
Pb^{210}	Lead 210
Cs^{137}	Cesium 137
Be^{7}	Beryllium 7
$\delta^{15}N$	Stable Nitrogen
g	grams
i.e.	that is

e.g.	for example
km	kilometer
m	meter
mm	millimeter
μm	micrometers
NAVD88	North American Vertical Datum of 1988
MSL	mean sea level
NOAA	National Oceanic and Atmospheric Administration
NC	North Carolina
s	seconds
SD	standard deviation
Hz	Hertz
yr	year
~	around
Φ	Porosity
λ	^{210}Pb radioactive decay constant (0.03118)

CHAPTER 1: THE UTILITY OF ESTUARINE BASINS FOR CONSTRUCTING MULTI-DECADAL, HIGH-RESOLUTION RECORDS OF SEDIMENTATION[1]

1.1 Introduction

Long-term records of sediment flux and source within estuaries are difficult to obtain,

due to the dynamic physical and biological processes that remove and mix the sediment bed.

Estuaries have numerous sediment sources, including riverine, direct shoreline erosion, and off-

shore marine, each with unique sediment-transport processes (Dalrymple et al., 1992). The river

flux generally involves uni-directional flow of freshwater and sediment to the estuary (Dyer,

1995). Estuarine shoreline erosion can increase overall sediment load and change the shape of

the estuary, causing increased fetch and a feedback loop that will exacerbate shoreline retreat

(Schwimmer, 2001; Cowart et al., 2011). Erosion along the shoreline also creates

accommodation space for additional sediment accumulation (Zaitlin et al., 1994; Cooper, 2002;

Slagle et al., 2006). Marine inputs to the estuary result from episodic storm events that

overwash barrier islands and form washover fans and more continuous marine-sediment

delivery through the mouth of the estuary.

Sediment flux to estuaries from each of those sources outlined above is not constant

through time. Episodic events like storms result in greater sediment flux from rivers due to

---

[1] This chapter was previously appeared as an article in the journal of *Estuarine, Coastal and Shelf Science.* The original citation is as follow: Elliott, E. A., McKee, B. A., & Rodriguez, A. B. (2015). The utility of estuarine settling basins for constructing multi-decadal, high-resolution records of sedimentation. Estuarine, Coastal and Shelf Science, 164, 105-114., doi: 10.1016/j.ecss.2015.06.002

runoff, increased estuarine shoreline erosion from waves, remobilization of previously

deposited sediment on the estuary floor, and increased sediment influx from marine

contributions (French and Spencer, 1993; Day et al., 1995; French, 2002; Yang et al., 2003;

Ralston and Stacey, 2007; Ralston and Geyer, 2009). Daily to monthly tidal fluctuations can

remobilize sediment within the estuary, and seasonal variations (e.g., spring freshet,

winter/summer storms, dry and wet seasons) can increase estuarine flow regimes, turbidity and

overall sediment flux to and from the estuary, causing continual erosion, transport and

deposition within the estuarine basin (Allen et al., 1980; Geyer et al., 2001; Fain et al., 2001;

Grabemann and Krause, 2001). Over decadal to millennial timeframes, variations in

anthropogenic influences (e.g., dams, land-use and cover modifications, shoreline armoring),

sea level, and climate can also affect changes in sediment flux to the estuary (Patton and Horne

1992; Small and Cohen, 2004; Poff et al., 2006; Mattheus et al., 2008); Walling 2012).

Constructing high-resolution records of estuarine sedimentation and linking measured

changes in accumulation rate to an associated change in the process of sediment transport,

deposition, and/or preservation is important for coastal management, predicting estuarine

response to climate change, and improving models of strata formation. Variation in sediment

flux to the central basin of an estuary with low accommodation can be preserved in the

sedimentary record over short time scales (storm deposition examined shortly after the event)

(Olsen et al., 1978; Corbett et al., 2007); however, over scales greater than 1 year, those

variations in sedimentation are much more difficult to resolve (Olsen et al., 1993). This is

primarily due to the dynamic processes that control sedimentation within the estuary.

Conceptual models of estuarine sedimentation emphasize a balance between the rate of

accumulation and provision of accommodation space by the rate of relative sea-level rise

(RSLR) (Stevenson et al., 1986; Nichols, 1989; Nichols and Boon, 1994). These conceptual models show that energy dissipation through waves and currents resuspending and redistributing estuarine-bottom sediment and exporting some portion of that sediment through tidal inlets is a significant factor in determining the base level of sediment accumulation. Nichols (1989) and Simms and Rodriguez (2015) presented a significant direct relationship between the fetch and depth of estuaries arguing that estuarine accumulation rates in the central basin over decadal-millennial time scales should be in equilibrium with the rate of RSLR. Additionally, biological activity within the estuary will cause bioturbation and disturb the long-term profile. These processes make resolving long-term records of changes in sediment flux within the estuarine central basin difficult, which in turn will make identifying the forcing mechanisms that cause changes in sediment flux in and out of estuaries problematic.

Nevertheless, determining changes in sediment flux to the estuary, which could be due to changes in discharge, shoreline erosion rates, or changes in estuarine hydrodynamics from changing the configuration of the estuary (e.g., changes in the width or number of tidal inlets) may be possible in estuarine mini-basins or low areas that capture sediment below the regional sedimentation base level. Deep mini-basins are not affected by sediment resuspension and redistribution in the same way as adjacent more shallow areas, due to the greater sediment accommodation within. A mini-basin with these characteristics should contain a continuous sedimentary record of changes in the source of sediment and/or process of sedimentation and can be scaled and used as a proxy of sediment flux. This study examines the potential of using the sedimentary record preserved in the Cape Lookout Bight (CLB), NC estuarine mini-basin, placed in context with changes in the coastal geomorphology of the basin, as a proxy to identify changes in the rate of sedimentation and relative contribution of various sediment sources and

sedimentation processes through time.

1.2   Study Area

Cape Lookout Bight (CLB), North Carolina, USA is a well-studied, constrained

estuarine mini-basin, shown to have high rates of sediment accumulation (Martens, 1976;

Bartlett, 1981; Chanton et al., 1983; Martins and Klump, 1984; Wells, 1988; Canuel et al.,

1990). The basin is 7.5-m deep, located near the southern Outer Banks chain of barrier islands

and is centered at the apex of two previously connected barrier islands, Shackleford Banks that

trends east-west, and Core Banks that trends north-south (Figure 1.1). A hurricane in 1933

formed an inlet between these two barriers, which has been maintained by dredging as Barden's

Inlet. Upon formation of Barden's Inlet in 1933, a rubble-stone groin, previously placed along
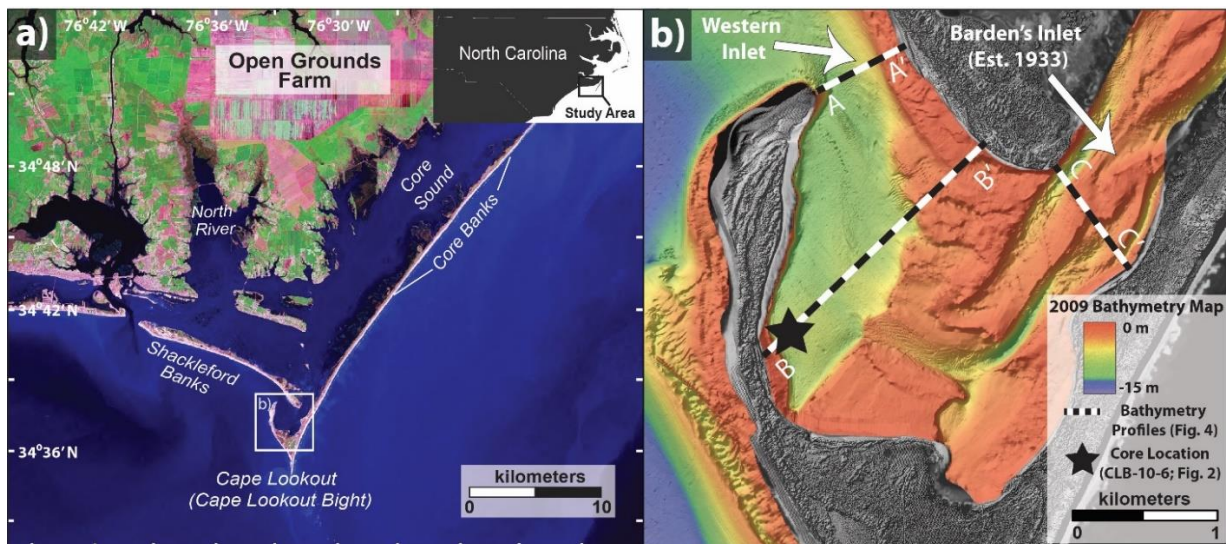
Figure 1.1 - Study area map showing (a) location of Cape Lookout Bight, NC (CLB) and surrounding estuary (USGS Landsat image) and (b) closer view of CLB with location of core CLB-10-6 (34°37.1840N, 76°32.9650W; Fig. 1.2) and bathymetry transects (Fig. 1.4) overlain on 2009 high resolution multi-beam bathymetry survey (Geodynamics Group).

Core Banks in 1915 to enlarge the barrier, helped to facilitate rapid north-northwest spit

migration. Recurved-spit growth created the mini-basin and formed a second inlet, the Western

Inlet, between Core Banks and Shackleford Banks. The Western Inlet is the entrance where

marine water enters the semi-enclosed CLB basin northwest of Cape Lookout over what used to be the shoreface and inner continental shelf (Figure 1.1). The formation of this basin created an effective sediment trap for fine-grained material moving through Barden's Inlet from Core Sound and North River Estuaries (Chanton et al. 1983; Wells, 1988; Canuel et al., 1990).

The efficiency of CLB as a sediment trap is, in part, due to the steep margins and high shoals near the Western Inlet and relatively deep (~7 m), flat basin floor (Wells, 1988; Figure 1.1; Figure 1.5). It has been shown that resuspension and mixing of sediments in the basin by currents and bioturbation is minimal due to the cohesive nature of the sediment and the suboxic condition of bottom waters (Martens, 1976; Bartlett, 1981; Martins and Klump, 1984; Wells, 1988). Previous work in the area established a geochronology for CLB by extracting sediment cores from the central region of the basin (Chanton et al., 1983; Wells, 1988). At the base of all cores, clearly visible well-sorted sand beds and sandy mud dominated the profile. Sand decreased in occurrence to the upper most 4-cm thick sand layer. It was noted that these sand beds represent material that was washed over the barrier spit into the basin during large storm events, namely hurricanes. These washover deposits or tempestites were used by Chanton et al. (1983) as time horizons, most notably the upper most 4-cm thick sand layer, which represents deposition from Hurricane Ginger (1971). Above that sand layer, sediment within the core was predominantly composed of black, carbon-rich mud (3-4% carbon; Martens and Klump, 1984; Chanton et al. 1983; Wells, 1988; Canuel et al., 1990). The fine-grained, organic material was shown to be largely derived from salt-marsh detritus and peat material, likely from erosion of the fringing marsh along the shoreline of Core Sound (Chanton et al., 1983; Canuel et al., 1990). Excess ^{210}Pb profiles established down core showed high rates of sediment accumulation, with an accumulation of excess ^{210}Pb thirty times its estimated atmospheric supply, indicating

sediment focusing into CLB from a much larger area outside of the basin.

That previous work demonstrated that CLB is an effective trap for sediment transported from a large region within the estuary and adjacent watershed over a range of time-scales, indicating the potential for a high-resolution record of sedimentation from multiple sources. Sediment from both marine (lower unit) and estuarine (upper unit) inputs are exhibited within the basin. Estuarine sedimentation within the basin should be relatively unmodified, as indicated by the lack of bioturbation and resuspension of sediment by currents within the upper portion of those cores collected over four decades ago by Chanton et al. (1983) and Wells et al., (1988)

1.3 Methods

1.3.1 Sampling and Grain-size Analysis

On July 27, 2010, we collected core CLB-10-6, from the central region of the CLB basin near the location of previously extracted cores (34° 37.184'N, 76° 32.965'W); after Chanton et al., 1983 and Wells, 1988). Core extraction was accomplished by lowering a 10.16 cm diameter, 6-m long aluminum core barrel through a well in the center of the boat. The core barrel was lowered to the sediment surface with a one-way valve attached to the upper portion of the barrel to create suction during extraction, and pounded into the basin floor using a jack-hammer and extension rods. After retrieval, the core was cut into 152-cm sections while still in the upright position to prevent mixing. At the laboratory, each section was then turned on its side, split in half longitudinally, and the working portion of each section was photographed and described. The working half of each section was sampled at 1-cm intervals, sampling the entire length of the 465-cm core for detailed grain-size and radio-isotopic analysis. Samples were freeze dried, establishing water content for each sample by pre-and post- weighing. Subsamples were run for

grain-size analysis using a Cilas 1180 Particle Size Analyzer, which measures particle sizes from 0.04 µm to 2500 µm in 100 size classes by laser diffraction.

1.3.2 Radioisotope Analysis

Excess ^{210}Pb was determined utilizing alpha particle spectrometry analysis. Freeze-dried samples were spiked for [209]Po tracer, underwent nitric and hydrochloric acid microwave digestion leach, electroplated onto stainless steel planchets, and analyzed using silicon barrier detectors and alpha spectrometer (standard alpha particle spectrometry methods after Nittrouer et al. 1979, Mckee et al. 1983, DeMaster et al. 1985). Samples were decay corrected to date of sampling, corrected for grain-size (sand) and background ^{210}Pb, using a values of 0.73 dpm g^{-1}, which Chanton et. al. (1983) measured using the radon emanation method. Interpretations of overall changes in sedimentation within the core were determined based on 5-cm binned averages. Binning samples in this way and correcting for sand allows for better comparability in scope to previous work (Chanton et al., 1983) as verification of results.

Ages for associated ^{210}Pb were determined using the constant initial concentration sedimentation rate model (CIC; Robbins and Edgington, 1975; Sanchez-Cabeza and Ruiz-Fernández, 2012). Changes in slope of the excess ^{210}Pb profile down core document changes in sedimentation rates that result from changes in sediment supply (McKee et al., 2005; Ruiz-Fernández et al., 2009). Break points in slope were distinguished based on linear regression and best fit, with associated error bars and linear regressions reported (Figure 1.2d).

1.3.3 Aerial photography and Bathymetry Analysis

Time series of northward migration of the western spit was conducted by utilizing spatially-referenced aerial photography from 1947-2010 (Table 1.1). Using ArcGIS, width was measured through time for both the Western Inlet and Barden's Inlet. The Western Inlet was

Table 1.1 - Reference, including acquisition date, resolution/scale, technique and agency for high-resolution aerial photography and satellite imagery utilized for time-series analysis inlet width through Western and Barden's Inlet.

Date	Resolution (m)/ Scale	Technique	Agency
06/25/2008	0.30 (m)	Satellite	USGS, Digital Globe, Microsoft
09/23/1999	41,667	Vertical Reconnaissance	FEMA
04/02/1989	65,000	Vertical Reconnaissance	NASA - Ames Research Center
12/22/1983	24,713	Vertical Cartographic	National Park Service
12/22/1982	23,979	Vertical Cartographic	National Park Service
12/09/1977	21,000	Vertical Reconnaissance	NASA - Wallops Island
01/30/1973	126,000	Vertical Reconnaissance	NASA - Ames Research Center
04/01/1964	50,000	Vertical Cartographic	U.S. Air Force
01/01/1958	40,000	Vertical Cartographic	U.S. Navy

measured at the narrowest cross-section between the tip of the northward migrating spit and the shoreline of Shackleford Banks, NC; likewise Barden's inlet was measured at the narrowest cross-section between the tip of Shackelford Banks, NC and Cape Lookout, NC. For the analysis of bathymetric change, a high-resolution bathymetry dataset and historical nautical charts were used. A Simrad EM 3002 dual head multi-beam system was used to collect a high resolution 16.3-sq km bathymetric survey of Barden's Inlet into Cape Lookout Bight by Geodynamics Incorporated in 2009, and was provided for further analysis in this work. We converted from NAVD88 to MLLW based on Beaufort tide gauge (Hess et al., 2005). This high-resolution digital elevation model was then compared directly to the NOAA-NOS 1978 nautical chart (scale 1:40000) to determine relative change in basin morphology through time.

1.4 Results and Interpretation.

1.4.1 Lithologic Units

Core CLB-10-6 is composed primarily of fine silts and clays, with higher concentrations of sand below ~300-cm depth (Figure 1.2). CLB-10-6 sampled three distinct
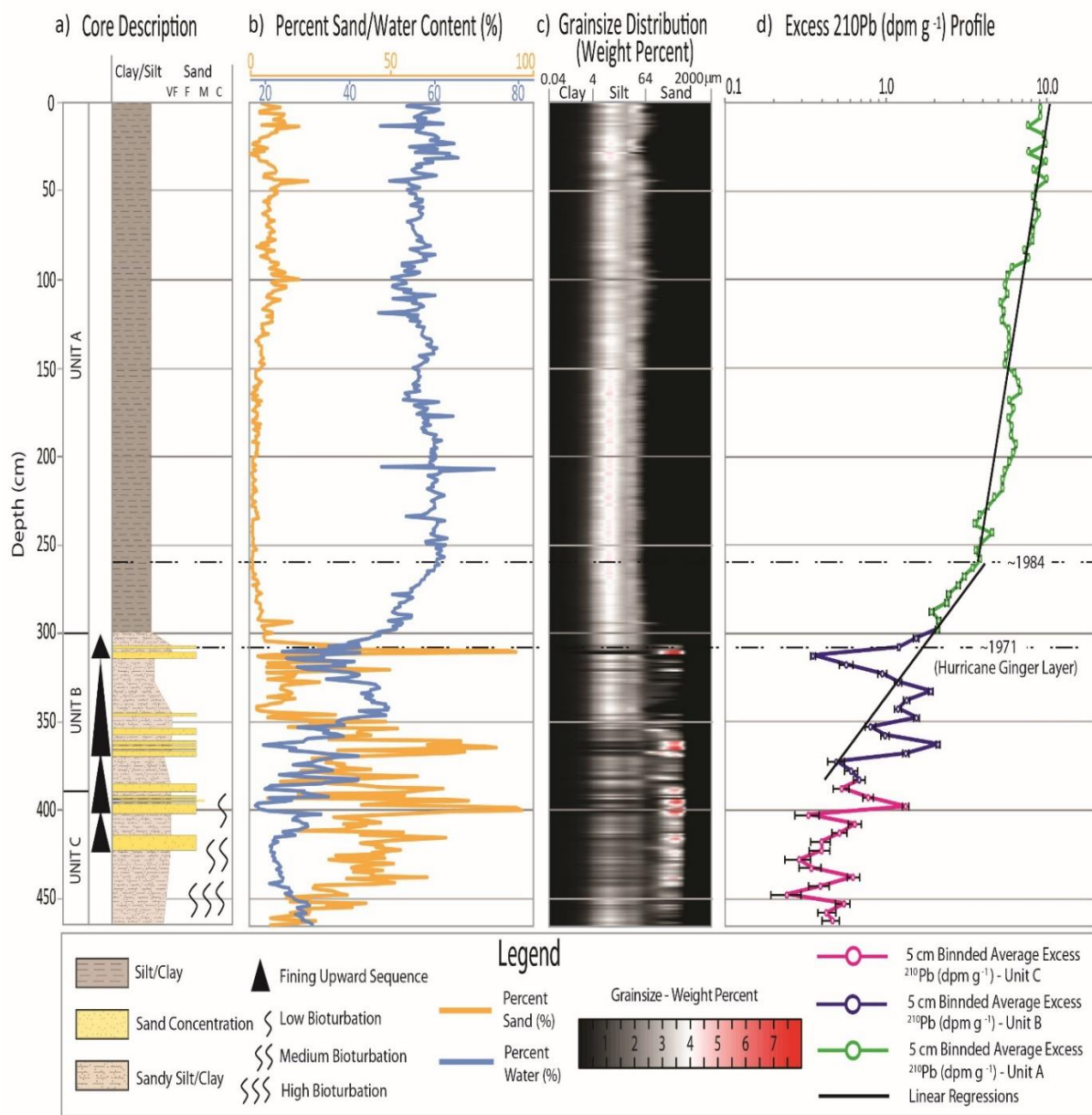
Figure 1.2 - Core CLB-10-6 (a) Descriptive analysis of lithologic units; (b) percent sand and water content; (c) Grain-size distribution by weight percent from 0 (dark) to 8 (red), relative to overall sediment classes (clay, silt, and sand); (d) 5-cm binned average excess ^{210}Pb profile for three units down core with ^{210}Pb analytical error bars, linear regressions above and below transition at 262 cm depth, and time of deposition based on age model calculations. Analytical error bars for intervals in the upper ~300 cm of the cores are smaller than, or equal to, the size of the symbol. The R^2 value for the lower regression (385-262 cm) is 0.498, and the value for the upper regression (262-0 cm) is 0.801 (as shown in Table 1.2).

units (Figure 1.2a). The basal unit (unit C; 460 to 385 cm) is a bioturbated, muddy fine-grained sand (average grain-size of sand 167 µm; Figure 1.2a,c). Burrows decrease in abundance from the base of the core to a depth of ~385 cm, where there is a gradational contact with Unit B. Unit B (385-300 cm) is a sandy mud unit with well-defined sand beds, ranging from ~1-5 cm thick (Figure 1.2a,c). Fining upward sequences occur between sand layers, and sand layers decrease in occurrence up the core. Between 340 and 315-cm depth, sand content reaches a relative minimum for Unit B of 15% (overall average of Unit B is 33%). A 4-cm thick fining upward sand bed exists, centered at 309-cm depth. Water content is at a minimum at the base of the core, and highly variable through units C and B, mirroring percent sand content through unit B to 300-cm depth. Unit A (300-0 cm) is the thickest unit sampled, extends to the top of the core, is homogeneous with a low sand content (average of 4.61%) and is composed predominantly of organic-rich mud (silt and clay; Fig. 1.2a,c). Although lithology is consistent through Unit A, water content consistently increases to a depth of 262 cm, where there is an abrupt change in slope, and water content remains relatively constant (average of 57.5%) to the top of the core. In comparing water content to sediment texture, the water content transition at 262-cm depth appears to be completely independent of any change in grain-size (Fig. 1.2b).

1.4.2 Geochronometric Units (Pb-210)

Excess ^{210}Pb distribution in the lower portion of the core (between 465 cm and 300 cm; units C and B; Fig. 1.2d) exhibits a high degree of variability, likely related to fluctuating grain-size composition, multiple sources of particulate materials during this period of sedimentation, and post-depositional redistribution (i.e., bioturbation, resuspension, etc.). Linear regression fit to the excess ^{210}Pb profile from 465 cm through the gradational transition at ~385 cm depth (Unit C) is nearly vertical, indicating high mixing and disturbance, and

10

further identifies the transition from bioturbated Unit C (465-385-cm depth) to Unit B (385-300-cm depth). The high disturbance present in this portion of the core violates the assumptions of the CIC model, and thus Unit C has been excluded from the linear regressions associated with the age model reported in this work. The predominant sand layers in Unit B results in a poor linear regression fit for the excess ^{210}Pb profile in this unit. The upper geochronologic unit (300 cm to the top of the core; Unit A) is delineated by a notable change in the ^{210}Pb profile at a depth of ~262 cm (between 255 and 270 cm), where there is an increase in the slope of the profile, indicating an increase in the rate of sedimentation, and a much lower degree of ^{210}Pb variability.

To determine if the change in excess ^{210}Pb slope and water content at 262-cm depth represents a shift in sedimentation rates within the core, a sensitivity analysis was performed. Multiple depths between 202.5 cm and 302.5 cm were selected as possible break points signifying where the slope of the excess ^{210}Pb profile changes. Linear regressions values for the slope of the excess ^{210}Pb profile above and below the break point were calculated along with the associated R^2 values (shown in Table 1.2). For each selected break point value and associated linear regression, the age of the shallowest sand layer (at 307 cm) was calculated. From previous work (Chanton et al., 1983; Wells, 1988), it has been established that the shallowest sand layer was deposited during Hurricane Ginger (1971).We use 1971 as the age of the sand layer at 307 cm because the general bedding between our core and those previous cores are similar. Within the constraints of the CIC model, the best fit for both linear regression R^2 value and a calculated age of 1971 for the sand bed at 307 cm, was for a break point at 262.5 cm (the mid-point of that interval), with an associated date of 1984 and associated rates of sedimentation of 3.05 cm yr^{-1} and 9.92 cm yr^{-1} for below and above the transition,

Table 1.2 - Linear regressions based on 5-cm binned average (centered at midpoint of bin) excess ^{210}Pb profile with calculated sedimentation rates, associated R^2 values and the final column which shows calculated age of the the sand layer at 307-cm, referenced as the 1971 Hurricane Ginger layer in previous work.

Depth of Rate Change	Sedimentation Rate Below (cm yr^{-1})	Sedimentation Rate Above (cm yr^{-1})	R^2 Below Break	R^2 Above Break	Sand Layer Year (Reference 1971)
No Break – All Data (Excluding Unit C)	5.001		0.8156		1949
202.5 cm	2.716	11.624	0.7973	0.6250	1956
222.5 cm	2.682	11.581	0.7403	0.6881	1961
242.5 cm	2.673	10.562	0.6610	0.7496	1965
252.5 cm	2.894	10.236	0.5929	0.7773	1968
257.5 cm	2.900	10.101	0.5488	0.7899	1969
262.5 cm	3.053	9.919	0.4984	0.8014	1971
267.5 cm	3.074	9.405	0.4632	0.7955	1971
272.5 cm	3.208	9.085	0.4120	0.8016	1971
282.5 cm	3.563	8.430	0.3037	0.8081	1971
292.5 cm	3.533	7.626	0.2494	0.7878	1969
302.5 cm	3.260	7.137	0.5700	0.7959	1968

respectively. Although this best fit is reasonable, especially in light of the corresponding transition in water content which abruptly shifts at 262-cm depth, it could also be argued that there are a range of depths between ~255 and 270 cm for break points that yield reasonably good R^2 values and dates for the sand layer at 307 cm that are close to the established date of 1971. Any break point selected within this depth range (255-270 cm) yields sedimentation rates of ~3 cm yr^{-1} below the break and ~10 cm yr^{-1} above the break. Given the range of possible transition depths, and the depth of the water content shift, we have designated 1984 as the date of the sedimentation rate change, with a real uncertainty on the order of a few years.

1.4.3 Geomorphologic changes to CLB

Time series of the width of the Western Inlet shows a constant rate of closure at ~22 m yr^{-1} as the northward migration of the western spit encapsulated the basin. In comparison,

Barden's Inlet has consistently widened over the same period of time at an average rate of between 6 to 8 m yr^{-1} (Figure 1.3).

Aerial photographs and the DEM of Core Banks topography derived from the North Carolina Floodplain Mapping Program (ncfloodmaps.com; Figure 1.3) exhibit recurved dune
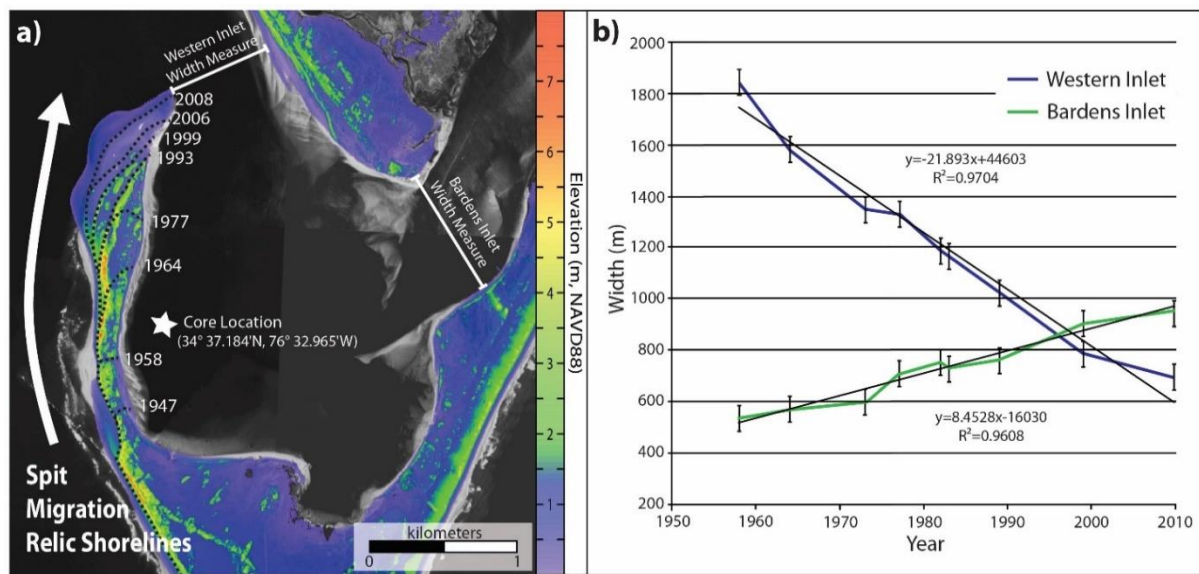
Figure 1.3 – (a) Positions of spit shoreline through time marking inlet narrowing overlain on DEM (derived from North Carolina Floodplain Mapping Program) for Core and Shackleford barrier islands; (b) Graphic showing width of Western Inlet and Barden's Inlet through time.

ridges that flank the previous shorelines of the northward migrating spit. It is likely that as the spit accreted northward, it widened and grew in elevation as a result of dune-growth along the shoreline. This increase in elevation likely prevented overwash and restricted the marine source from reaching the basin. Three separate bathymetry transects are presented through the basin (Figure 1.1; Figure 1.4), one near the Western Inlet (A-A'), one in the central basin (B-B') and one through Barden's Inlet (C-C'). In transects A-A' near the Western Inlet, narrowing and deepening is apparent. In contrast, transect C-C' through Barden's Inlet shows widening along the entire inlet and shallowing along the main channel (in addition to the relocation of the ship channel near the edge of Shackleford Banks; Figure 1.1; Figure 1.4). Transect B-B'
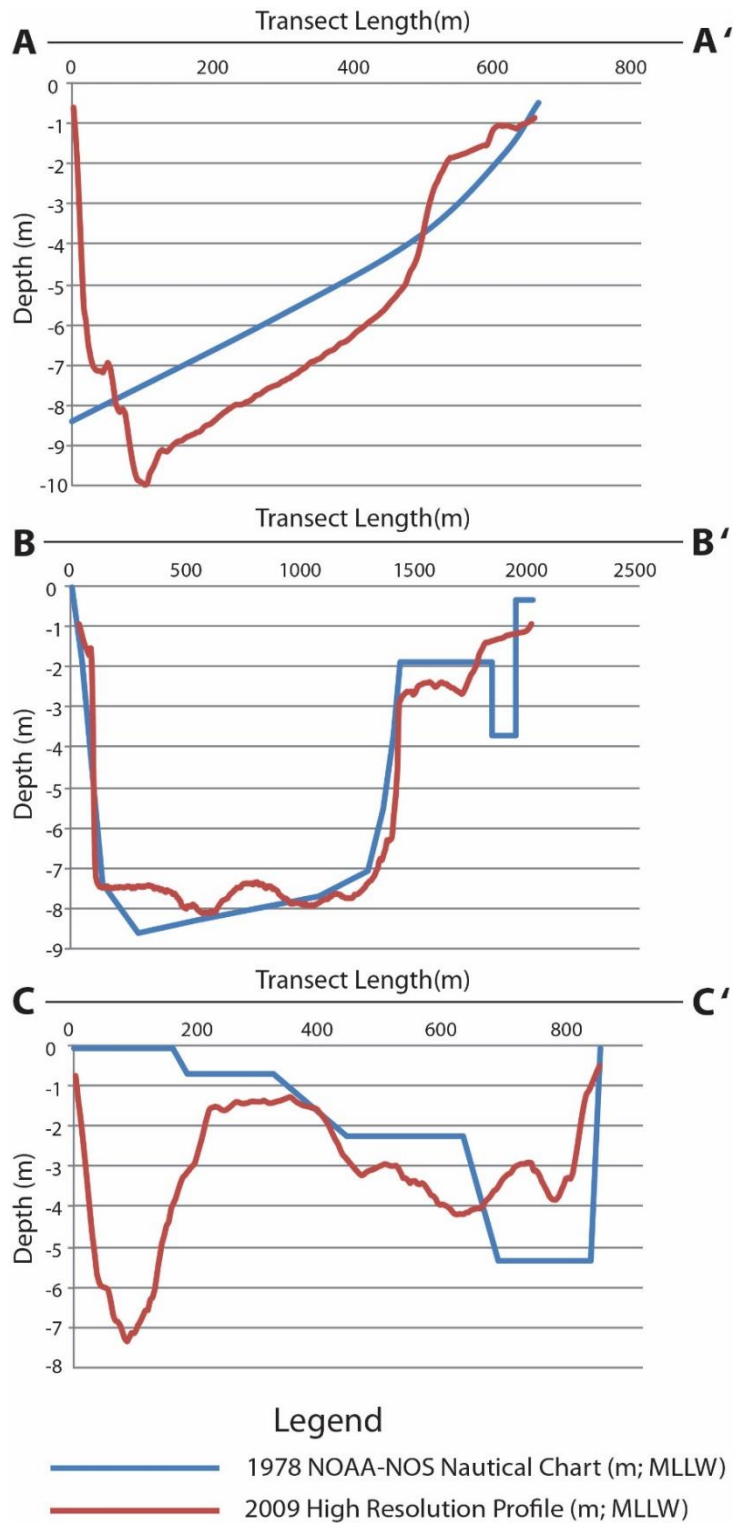
Figure 1.4 - Bathymetry profiles taken in CLB through Western Inlet (A-A'), the central basin and core location (B-B') and Barden's Inlet (C-C'), showing changing basin bathymetry through time utilizing a low resolution 1978 NOAA-NOS nautical chart (m) relative to a more recent, high resolution 2009 multi-beam bathymetry survey (Figure 1.1b).

through the central portion of the basin shows little change in basin-floor morphology. Although the earlier profiles are based on nautical charts that have a lower spatial resolution (Grid Spacing: ~182 m) than the 2009 multi-beam data set (Grid Spacing: ~ 3.05 m), there is an indication of central basin shallowing by ~1 to 1.5 m, consistent with rapid sedimentation.

1.5 Discussion

Three distinct depositional units were established in core CLB-10-6. Each unit represents changes in the sediment profile, which can be explained by forcing mechanisms like changing basin morphology influencing sedimentation processes and changes in sediment source and/or flux. A three-phase model is used to illustrate the dominant forcing mechanism for each change in the sediment profile through time (Figure 1.5).

1.5.1 Phase 1 - Formation of Mini-basin

Depositional unit C, extending from the base of the core to a gradational transition ~385-390 cm depth, is interpreted as being deposited on the inner continental shelf prior to formation of the mini-basin, as evidenced by extensive bioturbation indicating oxygenated bottom water (Figure 1.5). Bioturbation is exhibited in unit C not only in the sediment profile (i.e. burrows and mixed layers), but also in the excess ^{210}Pb, which exhibits nearly uniform activity through this unit, indicating extensive mixing. Based on the depth of the top of unit C (385-390-cm), the age model places the formation of the mini-basin at 1946 (+/- 1.6 yrs), which coincides with spit growth being in-line with the core location, as presented in historical nautical maps/aerial photography. The formation of Barden's inlet occurred in 1933, followed by formation of the mini-basin due to extensive growth of the spit after ~1946. During the decade preceding mini-basin formation, the shoreface of Shackleford Banks was likely contributing sand to the core site

15
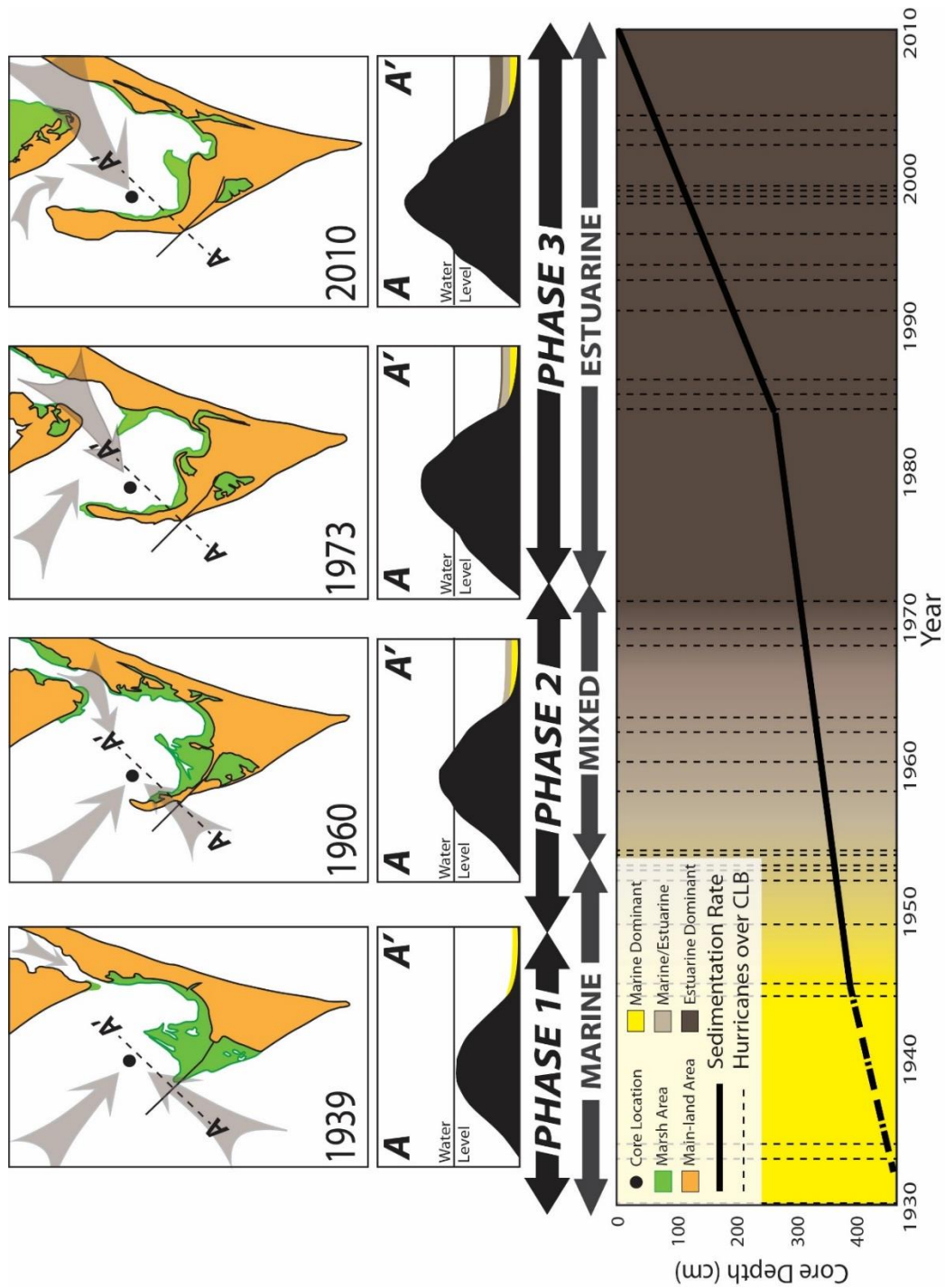
Figure 1.5 - (Left to Right, Top to Bottom) Bird's eye view of CLB (modified nautical maps after Chanton et al., 1983) marking phase changes within the basin, noting core location of CLB-10-6 and transect A-A'; Profile view of transect A-A' at various time points indicating sediment source (marine, estuarine or mixed) layers and shifts, as well as relative elevation change along dune ridge of migrating spit; Graphical representation of changing basin sedimentation through time, including sedimentation rate and dominant source, relative to hurricane activity (category 1 to 4 hurricanes within 100 miles of CLB) over the same period.

16

during storms, and that sand was mixed with fine estuarine sediment supplied through Barden's

Inlet; the dominant sediment source to the basin during this time was marine.

1.5.2 Phase 2 - Storm Influence and Changing Sediment Source

Unit B (385-300-cm depth) has a similar lithology to unit C, but can be differentiated

based on the absence of burrows and extensive mixing, and higher frequency of distinct, well

sorted sand beds relative to unit C. The unit was deposited as the spit was migrating to the

northwest from 1946 through the early 1970s. As storms (namely hurricanes) overwashed the

migrating spit of CLB, sand would wash over the spit and into the mini-basin forming distinct

sand beds. The percent sand in unit B from ~340-cm depth to 315 cm shows a marked decrease

in concentration. Within the constraints of the age model used, 340-cm to 315-cm depth

corresponds to a period between 1960 and 1968 (+/- 1.6 yrs), respectively. Aerial photographs

show that by 1960, the spit had migrated past the core location. Therefore, it is likely that the

observed decrease in overall sand concentration starting at 340-cm represents disconnection

between the basin and the barrier island that began as the spit migrated past the core location in

the early 1960's. As noted from both aerial photography and the DEM (Figure 1.3), dune ridges

developed along the migrating spit, increasing both elevation and width of the barrier. The

decrease in overall sand content and discrete beds above 340-cm reflects the change in spit

geomorphology and a decrease in contribution of marine sediment through overwash. As the spit

increased in elevation and width, the intensity of storms required to overwash the barrier and

deposit sediment within the central mini-basin would have increased.

The transition between units B and A is gradual, starting at 340-cm where marine inputs

to the basin were limited due to increased dune ridge elevation along the migrating spit.

Although marine influx was limited, the regression of the excess ^{210}Pb profile indicates no

apparent change in the rate of sedimentation during this time. Therefore, as marine (sand) overwash decreases, estuarine (fine grained material) deposition must increase to compensate and sustain the same rate of sedimentation within the basin. The increased capture of fine grained material from 340 to 315-cm depth indicates a period of increasing trapping efficiency within the basin as the Western Inlet crossed a threshold width, which reaches a maximum at 300-cm depth (the start of unit A). Wells (1988) comes to a similar conclusion, asserting that the transition from sand to mud (silt and clay) within the basin represents the beginning of the period of maximum trapping efficiency, and that the deposition of homogenous fine-grained material (unit A) indicates the trapping efficiency has reached a constant maximum. Like the lower sand beds within the core, the upper sand bed centered at 309-cm depth shows a general fining upward sequence. That sand bed was deposited during Hurricane Ginger, which was a category H1 hurricane that made landfall over Bogue Banks (~15 km west of CLB) on September 30, 1971. After 1971 (+/- 1.6 yrs), the dominant sediment source to the basin is from Core Sound through Barden's Inlet. No sand resulting from overwash was preserved in basin sediments after this time (Figure 1.2a-c; Figure 1.5).

1.5.3 Phase 3 - Isolated Mini-Basin

The upper Unit A (300-0 cm depth), is composed of homogeneous fine-grained mud (silt and clay) and is interpreted as being deposited when the mini basin was isolated from overwash deposition. Unlike the lithologic profile of unit A that shows very little variation in grain-size from 300-cm depth through the top of the core, both water content and the sedimentation rate determined by the excess ^{210}Pb profile exhibit an abrupt transition at ~262-cm. At this transition point, the rate of sedimentation more than doubles; the age model places this transition between 1983 and 1985 (+/- 0.5 yr). One possibility is that the increase in the rate of sedimentation could

18

be the result of an increase in trapping efficiency of the mini-basin due to changing morphology

of the barrier spit, Western Inlet and/or Bardens Inlet. As the width of Western Inlet shrunk, it is

possible that the transfer time of sediment-laden water moving through the basin to the open

ocean increased and/or physical processes (e.g., bottom current speed) within the basin changed,

allowing for further sediment fallout and an increased rate of sedimentation within the basin.

1.5.3.1 Increase in Trapping Efficiency and Threshold Response within the Mini-Basin

Changes to inlet morphology could impact residence times in the mini-basin. The

investigation of Western Inlet width through time (Figure 1.3) indicates that the rate of spit

growth has been consistent. Spit growth encapsulated the area around core CLB-10-6 between

1960 and 1972, with predominant growth west – northwest along the spit after this time. Basin

bathymetry (Figure 1.4) shows that over time Western Inlet narrowed and deepened as the main

channel of Barden's Inlet shallowed and the overall inlet widened. The consistency of the

Western-Inlet narrowing through time argues against a dramatic shift in sedimentation rate

between 1983 and 1985 as a result of rapid spit growth. Rather, any increased residence time

within the basin related to changing inlet width must have been the result of a second threshold

response to closure of the Western Inlet. The threshold inlet width that was crossed between

1960 and 1972 as the spit migrated past the core location changed the process of sedimentation,

increased the sediment trapping efficiency of the core location, shifted the basin lithology

towards finer grains, and was marked by a gradual increase in water content. In contrast,

between 1983 and 1985 the only change observed in the core was an increase in sedimentation

rate and a sharp transition to constantly-high water content. Although it is possible that a second

threshold inlet width was crossed between 1983 and 1985 that shifted the basin circulation

towards increased sedimentation, we interpret that to be unlikely based on reconstructions of

19

inlet width and bathymetry and comparing this sudden increase in sedimentation rate to the striking differences in mini-basin sediment that occurred between 1960 and 1972 when we interpret a threshold inlet width was crossed (the gradational contact between units B and A).

1.5.3.2 Additional Sedimentation from Estuary

In the absence of any coupled morphologic-hydrodynamic explanation, we propose that the increased sedimentation within the basin between 1983 and 1985 resulted from an increase in the sediment flux coming through Barden's Inlet from Core Sound and/or the Western Inlet from the marine environment. Considering that the Western Inlet is far removed from any large river system delivering fine-grained material into the ocean, we disregard the possibility that an increase in sediment flux from the marine environment increased sedimentation rates in the mini-basin. Therefore, since increased rates of sedimentation are unlikely to be the result of internal basin dynamics, the observed increase in the rate of sedimentation is more likely to have resulted from increased estuarine sediment flux through Barden's inlet from Core Sound and the upper estuary. We interpret estuarine sediment flux increased abruptly starting around 1983-1985, causing the increased rate of sedimentation observed within the basin. Sedimentation within the basin is currently dominated by the estuarine sediment source, and we interpret the increase in the rate of sedimentation marks a change in the amount of estuarine sediment delivered to the basin through time as opposed to an increase in marine sediment or trapping efficiency of the mini-basin (Figure 1.5).

1.5.3.3 Potential Estuarine Sediment Sources

The primary source of sediment to the basin from the estuary has historically been salt marsh detritus derived from back-barrier fringing marsh erosion (Chanton et al., 1983; Canuel et al., 1990) and $\delta^{13}C$ data support that interpretation (Canuel et al., 1997). Marsh shorelines in

core sound have experienced high rates of retreat (up to 1-m/ yr) over the past 25 years, largely as a result of sea-level rise (Riggs, 2001). It is also likely that fringing marsh erosion will increase as a result of increasing storm frequency and sea-level rise brought about through global climate change, which could result in increased sedimentation rates within the basin.

Anthropogenic influence within the basin has also increased over the last 32 years through commercial, residential and agricultural development. Unlike the estuarine salt marsh shoreline, which acts as a natural buffer to over-land sediment flow, developed land has a higher potential to increase suspended sediment load to the system through direct runoff from the land. Mattheus et al. (2009) showed rapid accretion along the Newport River Bayhead delta front as the result of runoff from a large silviculture operation directly adjacent to the watershed. That increase in sedimentation rate occurred between 1964 and 1967, just as suddenly as what we measured at CLB (Mattheus et al., 2009). Another land-use change in the area has been farming. For example Open Grounds Farm (OGF), a 160 km^2 farm that lies directly adjacent to the fringing marshes that supply sediment to CLB (Figure 1.1). The farm transitioned to a large row-crop enterprise from the late 1970's to the early 1980's. Since runoff from the farm would run directly into adjacent tidal creeks, it is not completely buffered, adding a potential new estuarine sediment source to CLB.

It is therefore possible that the increased sediment flux to the basin through Barden's Inlet starting between 1983-1985 (+/- 0.5 yr) could have resulted from 1) an increase in the same source (fringing marsh erosion) as a result of external forcing mechanisms (i.e., sea-level rise, increased storm frequency/intensity) and/or 2) a source addition through land-use modification. A high R^2 value (0.8) for the excess ^{210}Pb slope regression since 1983-1985 suggests that the increased sediment flux has been relatively constant since that time. Whatever the cause, it is

likely that the sedimentary record of CLB indicates an increase in the sediment load from Core Sound since 1983-1985, and requires further investigation to isolate the cause and implications of this increased sediment loading to the system.

1.5.4 Implications for Paleotempestology

The abrupt cessation of marine and barrier sand being transported into the mini-basin during overwash events shown in this work has important implications for paleotempestology. Many studies reconstruct prehistoric storm records from washover sand beds preserved in coastal lakes and lagoons located directly behind a barrier (Lui and Fearn, 2000; Donnelly and Woodroof, 2007; Scileppi and Donnelly, 2007; Mann et al., 2009). This research highlights the importance of changing barrier geomorphology (i.e., spit accretion, barrier regression, etc.) in altering the fidelity of storm records that are based on washover sand beds. Since Hurricane Ginger there have been 14 category 1, 2, 3 or 4 hurricanes within 100 miles of CLB, with average wind speeds >76 miles per hour (Figure 1.5). Many of these large storms exceeded the power of Hurricane Ginger and previous storms in CLB that resulted in deposition of sand in the basin; however, there is no indication of their existence within the sediment record of CLB. This work indicates that the resolution of the storm record is not constant through time. Similarly, Hippensteel (2008) reported that paleo-storm records from saltmarsh strata show decreasing storm frequency through time, interpreted as an artifact of reworking rather than decreasing storminess. In the mini-basin behind Cape Lookout, preservation potential of washover sand beds is extremely high given that the basin is deep and sub-oxic; however, the increase in width and elevation of the barrier shifted the resolution of the sedimentary record towards higher-magnitude storms. Given a large-enough hurricane, a new sand layer could be deposited in the

basin and that event would likely lower the elevation of the barrier spit and make the basin more sensitive to recording overwash from smaller storms once again.

With uncertainty surrounding increased storm frequency and intensity as a result of Global Climate Change, the field of paleotempestology has never been more important. However, as stated by both Hippensteel et al. (2014) and Donnelly et al. (2014), when interpreting paleo-storm records, careful consideration must be made to overwash susceptibility, preservation potential, local geomorphology, and archive fidelity. As shown in this work, even within rapidly accreting mini-basins, where reworking is minimal and a pristine long-term sediment record should exist, it is critical to consider the changing forcing mechanisms and dynamics of the system before interpreting the paleo-record, as changes in the geomorphology and/or physical dynamics of the system can hide or eliminate portions of the lithologic profile, leading to misinterpretation of the paleo-storm record.

1.6 Conclusions

Obtaining long-term records of changing estuarine sediment flux is difficult, due to the dynamic processes present within the low-accommodation estuary that actively remove the high-resolution long-term sediment record. An alternative method for investigating the sources and fluxes of sediment to an estuary is through examining sedimentation in an associated mini-basin, where a long-term record of sedimentation can be exploited. Cape Lookout Bight, NC presents a unique coastal environment to capture a long-term record of sedimentation.

Lithologic analysis of core CLB-10-6, extracted from the central region of the basin in 2010 reveals three distinct units within the core; basal unit C, which is defined as marine shelf sediment, followed up the core by unit B, basin deposits of mud and sand overwash as the spit encapsulates the basin, and unit A, a massive fine-grained mud estuarine unit with very little

variation up the core. A high-resolution excess ^{210}Pb profile was established for core CLB-10-6, measuring sedimentation rates within the basin over much finer time scales and over a much longer period of time than was previously available. The high resolution excess ^{210}Pb profile allowed for the development of an age model so that timing of deposition could be assigned to each unit. Unit C reflects the encapsulation of marine shelf by the northward migrating western spit, separating CLB from the marine shelf, developing the CLB depositional basin by 1946 (+/- 1.6 yrs). Unit B reflects the transition from dominant marine deposition into the basin through storm induced over-wash events to estuarine-dominant deposition to the basin through Barden's Inlet. This transition reflects the increased trapping efficiency of fine estuarine mud from 1960 to 1972, due to the changing geomorphology of the mini-basin.

Unlike the earlier units within the core, Unit A primarily reflects estuarine sediment from Core Sound coming through Barden's Inlet. The homogeneity of sediment within this unit is further indication that trapping efficiency reached equilibrium by the start of deposition at 300-cm depth or 1973 (+/- 1.6 yrs). An abrupt increase in the rate of sedimentation within the basin occurs at ~262-cm (255-270-cm) depth, more than doubling the rate of sedimentation between 1983-1985 (+/- 0.5 yr). This increased rate of sedimentation is attributed to increased estuarine sediment flux through Barden's Inlet from Core Sound and the upper estuary. The most likely explanation for the increase in sedimentation rates is increased erosion of fringing salt-marshes due to increased rates of sea-level rise and storms, and/or the potential addition of a new sediment source as a result of land-use modification. This is worthy of further investigation to identify specific sources through time.

The elimination of overwash storm layers as a result of changing barrier geomorphology within the sediment record of this study indicate the importance of understanding the dynamics

of a system when using estuarine sediment records as proxies for long-term paleo-storm records. This work underscores the importance of placing any long-term record of sedimentation within an estuary in the context of the geomorphology and physical processes (e.g., overwash susceptibility, preservation potential, local geomorphology, archive fidelity) active within a specific system.

This work indicates that preservation of long-term high-resolution proxy records of sediment fluxes for the estuary is possible in systems that drain into deep, confined mini-basins like CLB, that are not limited by available accommodation space as rates of RSLR increase. Unlike records collected within the low-accommodation central estuary, which are prone to modification and can be incomplete, rapidly accreting mini-basins like CLB have the potential to collect long-term records of estuarine sedimentation through time. However, even within rapidly accreting mini-basins, it is important to consider the dynamics of the system before interpreting the paleo-record, as changes within the system can hide or eliminate long-term lithologic signatures from the sediment record. By carefully considering the changing forcing mechanisms present within the basin through time (e.g., geomorphology, sediment source, flux), we have established a long-term, high-resolution geochronology for this system, which can be used in association with sediment finger-printing techniques to identify the source and changing processes associated with the increased estuarine sediment flux for this system.

CHAPTER 2: A NOVEL METHOD FOR SAMPLING SUSPENDED SEDIMENT LOAD IN THE ESTUARINE ENVIRONMENT USING BIDIRECTIONAL TIME-INTEGRATED MASS-FLUX SEDIMENT (TIMS) SAMPLERS[2]

2.1 Introduction

Coastal watersheds and estuaries directly connect terrestrial and oceanic environments with fine-grained (<62.5 µm) sediment dominating the material transported within these systems (Frank, 1981; Meybeck, 1984; Allan, 1986; Walling, 1989; Ludwig and Probst, 1998; Bianchi and Allison, 2009). The fine-grained suspended sediment load (SSL) directly influences coastline evolution (Syvitski et al., 2005), habitat maintenance and development (Fagherazzi et al., 2012), and ecological health within the estuary and coastal habitats (Syvitski et al., 2005). Nutrient and contaminant transport have been shown to be intimately tied to the sediment flux (Smith et al., 2001; Syvitski et al., 2005), as trace elements bind to the SSL while in transport within the aquatic environment (Correll et al., 1992; Turner and Millward, 2002; Kronvang et al., 2003; Jha et al., 2007; Horowitz et al., 2008). Anthropogenic influence through land-use modification, urbanization and industrialization have significantly modified sediment, nutrient and contaminant load to rivers and coastal environments (Syvitski et al., 2005). Sediment-associated heavy metals within river and estuarine environments, often from anthropogenic sources, account for a significant portion (at times >90%) of the overall metal load (Chueng et al. Chemosphere (2003), Martin and Meybeck (1979), Audrey et al., 2004). Additionally, global

---

[2] This chapter was submitted as an article to the journal of *Estuarine, Coastal and Shelf Science*. The original citation is as follow: Emily A. Elliott, Elaine Monbureau, Glenn W. Walters, Mark A. Elliott, Brent A. McKee, Antonio B. Rodriguez (2017), A novel method for sampling the suspended sediment load in the estuarine environment using bi-directional Time-Integrated Mass-Flux Sediment (TIMS) samplers, **IN REVIEW.**

climate change and sea-level rise are thought to further impact the overall SSL within the watershed and estuary (Walling and Webb, 1996; Walling and Fang, 2003; Kirwan et al., 2010). These findings highlight the importance of quantifying the source and abundance of the SSL within the coastal watershed.

Representative samples of SSL are critical in the quantification of geochemical fluxes and water quality within the watershed, specifically with sufficient mass of sediment for analysis of particle size composition, organic matter and carbon content, isotopic and geochemical concentrations, and nutrient and contaminant abundance (Smith and Owens, 2014). Unfortunately, traditional methods of SSL collection, including manual and automatic sampling protocols, are often labor intensive, expensive and/or inadequate for analysis of the physical and geochemical properties of the SSL (Phillips et al., 2000). SSL transport has been shown to be highly episodic, with up to 90% of the annual load transported in only 10% of the time (Walling and Webb, 1987). Therefore, fine-sediment delivery to the watershed may be highly temporally variable, causing even the most intensive sampling protocols to misrepresent the SSL (Perks et al., 2014; Keestra et al., 2009; Grieve, 1984; Ongley, 1992; Cuffney and Walace, 1988). Manual sampling techniques, while the traditional standard for accuracy relative to automated and indirect approaches (Wren et al., 2000), can be time and labor intensive, especially when attempting to capture SSL during an event. Given the episodic nature of SSL transport, it is difficult to obtain high temporal resolution sampling and capture infrequent high-magnitude events when using manual sampling alone (Perks et al., 2014). Automated samplers, including rising and falling limb bottle samplers (Frank, 1981) and pump/vacuum operated equipment (e.g., Russell et al., 2000), while less time and labor intensive, are expensive and cannot be deployed in areas where inundation is likely, which prevents large-scale deployment within the

watershed and system-wide characterization of SSL. With both of these sampling techniques mass of sediment is generally insufficient to conduct geochemical analyses except from integrated samples or samples of high-magnitude runoff events.

An innovative solution for the collection of suspended sediment transported in small, lowland river catchments was first proposed by Phillips et al., 2000. The Phillips time integrated mass sediment (TIMS) sampler was designed to trap sediment through the principles of sedimentation, with the ability to collect representative suspended sediment samples over the sampling period with enough sample mass for assessment of the physical, geochemical and magnetic properties of the sediment (Phillips et al., 2000; Russell, 2000; Smith and Owens, 2014; Perks et al., 2014). Given the sampler's ability to constantly sample suspended sediment over a range of flow conditions, a continuous multi-event record of the suspended sediment flux can be obtained from a single deployment (Phillips et al., 2000; Russell, 2000; Walling, 2005; Perks et al., 2014). Due to its cost-effective simple design and construction, with relatively little maintenance and no power requirement upon deployment, the TIMS sampler has been implemented around the world in a variety of fluvial environments (e.g., Ankers et al., 2003; Laubel et al., 2003; Evans et al., 2006; Fox and Papanicolaou, 2007, 2008; McDowell and Wilcock, 2007; Walling et al., 2008; Poulenard et al., 2009; Fukuyama et al., 2010; Collins et al., 2010; Wilson et al., 2012; Owens et al., 2012; Voli et al., 2013; Smith and Owens, 2014), with modifications for optimal operation within higher energy systems (Perks et al., 2014; McDonald et al., 2010).

In this paper, we describe modifications to the original Phillips design which allows for the collection of SSL in a bi-directional flow regime, typical of a tidal environment. Where possible, laboratory and field assessment were replicated from the work of Phillips et al., 2000

for comparison to the original sampler function and efficiency. To characterize the new flow regime within the modified sampler design, laboratory testing, including flume tests with dye and particle image velocimetry (PIV), and chemically-dispersed sediments were analyzed to identify stagnation points and quantify particle-settling velocity within the sampler. Field testing was conducted under natural conditions within tidal creeks in two distinct locations. To assess if the TIMS sampler collects an unbiased sample, particle-size composition and overall mass were compared with single time point samples collected over the same period.

2.2 Methods

2.2.1 Sampler Design and Modifications

The Phillips sampler was designed to continuously trap suspended sediment load in fluvial channels with uni-directional flow. Phillips et al. (2000) presents a full description of flow characteristics within the sediment sampler and relationships between ambient, inlet and sampler velocities. Flow enters the sampler at ambient velocity through a narrow (4 mm diameter) inflow tube. As flow moves into the sampler's main body (98 mm diameter x 1 meter length), velocity decreases in proportion to the change of cross sectional area, promoting sedimentation of particles in the sampler, with water exiting the sampler through a similar 4 mm outflow tube to allow for unimpeded flow (Figure 2.1). The bi-directional TIMS sampler design proposed in this study was built following the original design description from Phillips et al. (2000), with modifications for use in systems with bi-directional flow (i.e. tidally influenced environments). Like the original design, the body of the sampler is made of commercially-available polyvinylchloride (PVC) pipe, 98 mm internal diameter by 1 meter length, sealed using end caps with internal 'O-ring' seals (Phillips et al., 2000). The opaque PVC prevents fouling from photosynthetic processes during deployment within the estuarine environment.

The inflow and outflow tubes and connectors were modified from the original design, which were made of semi-rigid nylon pneumatic tubing (6 mm (OD) x 4 mm (ID) x 150 mm) with an internal cross-sectional area of 12.6 mm^2 with a polyethylene funnel placed over the inlet tube to streamline the sampler body and minimize turbulence or disruption of ambient flow (Phillips et al. 2000). In the bi-directional sampler design the inflow and outflow tubes are made of rigid 9.5 mm (OD) x 4 mm (ID) x 150 mm long nylon tubing to keep inflow tube aligned with ambient flow within the tidal environment. Exposed ends were chamfered at 45 degrees at the entry and exit points (Figure 2.1) to reduce turbulence in a similar fashion to the funnel proposed in Phillips. Inflow tubes were attached to sampler end-caps using a ¼ NPT pipe to Swagelok tube fitting screwed flush to the internal surface of the endcap (Figure 2.1). To prevent air bubbles within the sampler, which could impede normal flow conditions, two sealable vents were added along the top of the samplers main body. Given the changes in water-level that occur in the tidal environment, these vents allow for any air that may have entered the sampler during low water-level conditions to escape prior to peak flow.

The most important modification made to the original Phillips TIMS design is the 'L' shaped outflow tube which prevents sediment entry into the sampler during flow reversal (Figure 2.1). Outflow tubes are identical to inflow tubes in tapering and internal diameter, cut to a length of 150 mm. Outflow tubes are attached to sampler end caps using a ¼ NPT pipe to Swagelok elbow fitting screwed flush to the internal surface of the end cap. The perpendicular
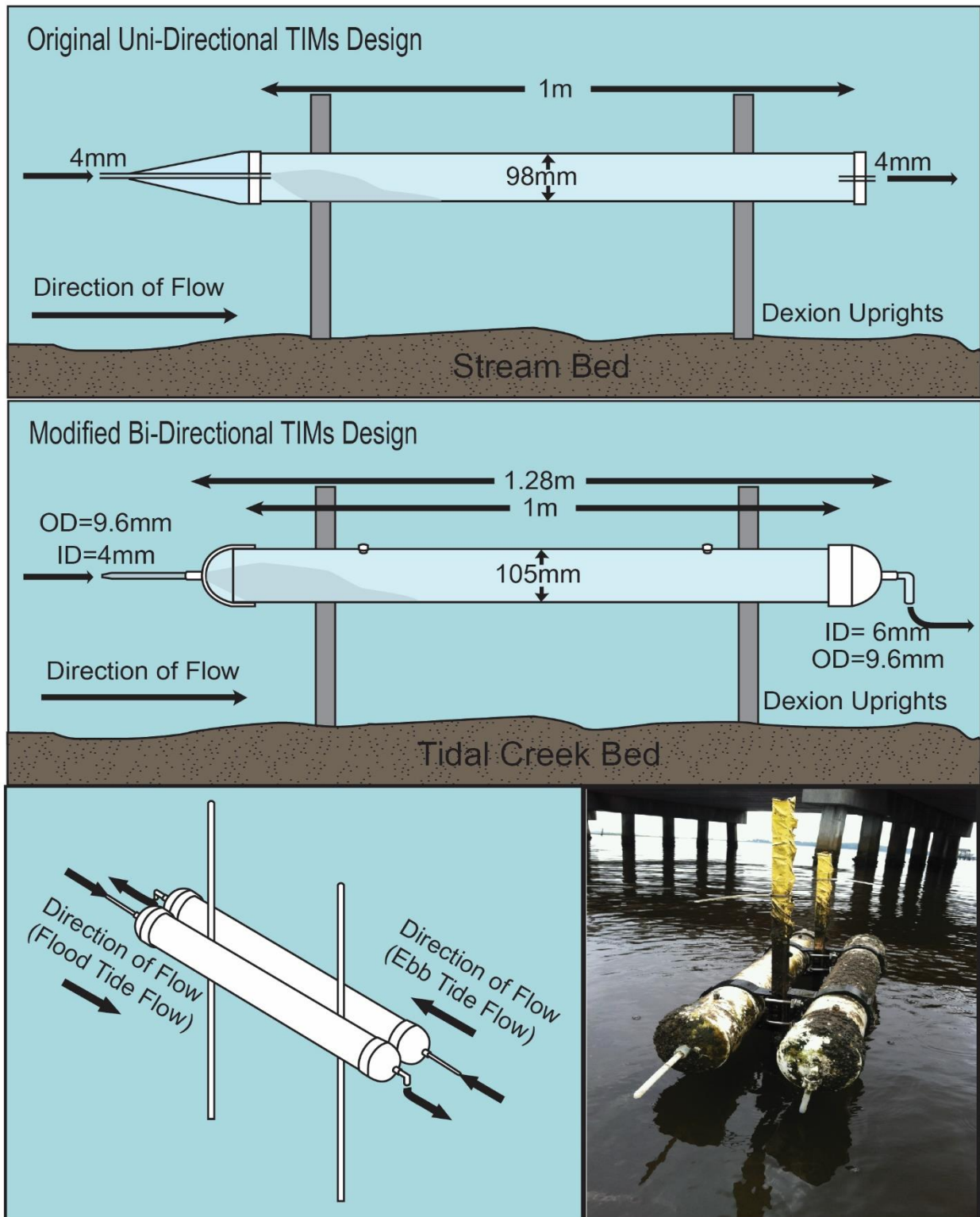
Figure 2.1 – (From top to bottom, left to right) Cross-sectional view of the original Phillips et al. (2000) TIMS design; Cross-sectional view of modified bi-directional TIMS design for collection of suspended sediment tidal flow; Three dimensional view of modified bi-directional design, showing how sediment is collected uniquely in each direction of tidal flow, with picture of the mounted modified design in a tidal creek.

orientation of the outflow tube relative to ambient flow prevents sediment laden water from re-entering the sampler when flow reverses. Epoxy-coated dexion uprights were used to hold the samplers in place to prevent corrosion within the marine environment, as corrosion could impact the geochemical signature of the collected sample. Samplers (2) were mounted parallel to each other and flow vectors, with inflow tubes oriented in opposing directions, held onto uprights using 'C' PVC-pipe clamps attached with fabricated stainless steel holders. Mounting the samplers parallel to each other in opposing sampling directions allows for collection of material uniquely in each direction of flow.

2.2.2 Fluid Dynamics

2.2.2.1 Flume and Modified Design for Bi-Directional Flow

To assess flow dynamics during reversal of flow within the modified sampler, a bi-directional TIMS sampler with a transparent acrylic body and the new 'L' shaped outflow tube was placed in a race-track flume. Velocity within the flume reached a maximum of 0.6 m s^{-1} in each direction of flow, with a minimum speed near zero reached when flow was reversed. Fluorescent dye was injected into the stream near the inflow and outflow tubes to monitor flow dynamics within the sampler during reversal of flow. The sampler was mounted within the dimensions of the flume-viewing window, with a video camera mounted at the height of the sampler. Video was captured continuously throughout the experiment to monitor flow structures and dynamics.

2.2.2.2 Dye Experiment

For further investigation of the fluid dynamics within the sampler, with particular attention paid to dead zones, dye experiments were undertaken similar to those described in Phillips et al. (2000). A bi-directional sampler with a transparent acrylic body was used to

visualize dye and internal flow dynamics throughout the experiment (Figure 2.2a). A ¼ inch

polyethylene tubing was attached to the inlet and inserted into a 5 L glass beaker. The beaker

was filled with 5 L of water and 1 g of Bengal rose dye ($C_{20}H_2Cl_4I_4Na_2O_5$), mounted on a stir

plate and kept continually mixed by a magnetic stir bar. The outlet
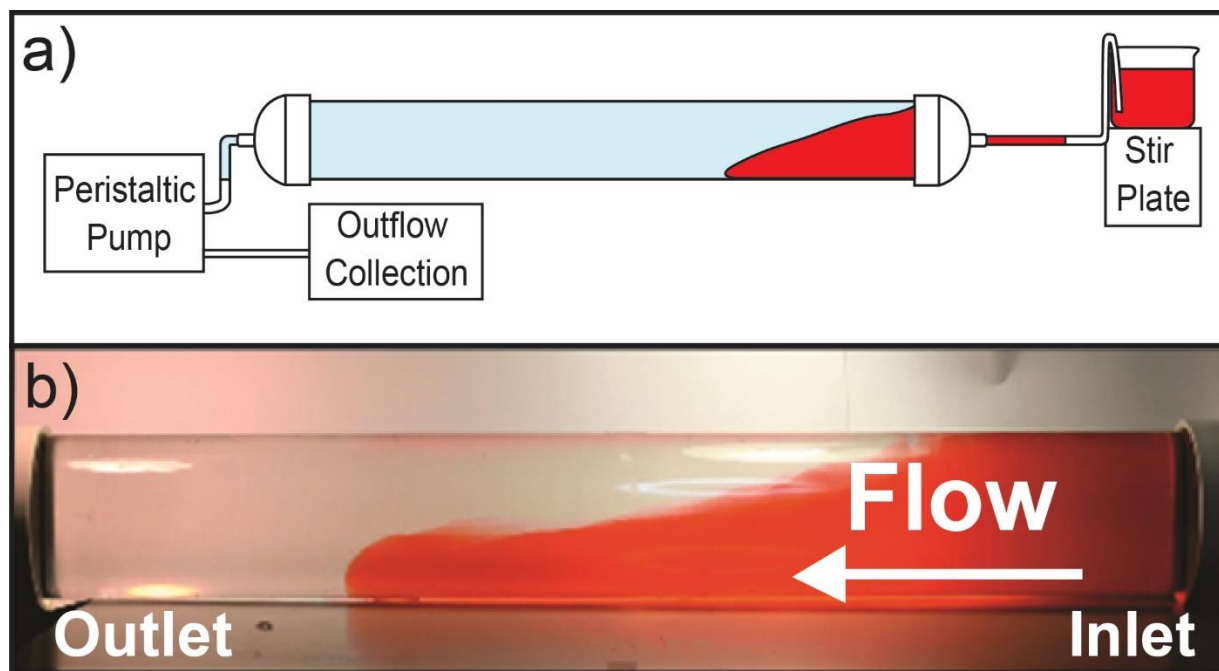
Figure 2.2 - (a) Diagram of dye/suspended sediment lab experiment setup; dye/sediment is constantly mixed on stir plate, and drawn through collector at constant speed through use of peristaltic pump, outflow collected (b) Image of rose dye drawn through collector during experiment, flow direction, inlet and outlet indicated.

pipe was connected through similar tubing to a peristaltic pump which allowed for pump speed,

and therefore flow speed, of dye and water to be drawn through the sampler at a relatively

constant rate throughout the experiment. For comparison to the work conducted by Phillips et al.

(2000), the same flow velocity of 60 cm s^{-1} was chosen, resulting in a maintained discharge rate

of 242.1 ml min^{-1}. Flow structures were noted and photographs were taken throughout the

experiment. The experiment was terminated when dye filled the main body of the sampler and

outflow tube.

2.2.2.3 Particle Image Velocimetry

Particle Image Velocimetry (PIV) is an optical method for tracking flow and obtaining instantaneous velocity measurements. In PIV, neutrally buoyant particles are seeded into the fluid, and a laser is used to illuminate the particles during flow. Cameras are used to record images of the particles with a timing unit for triggering the laser and the cameras synchronously (Figure 2.3). Images of the particles are analyzed to determine the velocity of each particle as it moves through the sampler.
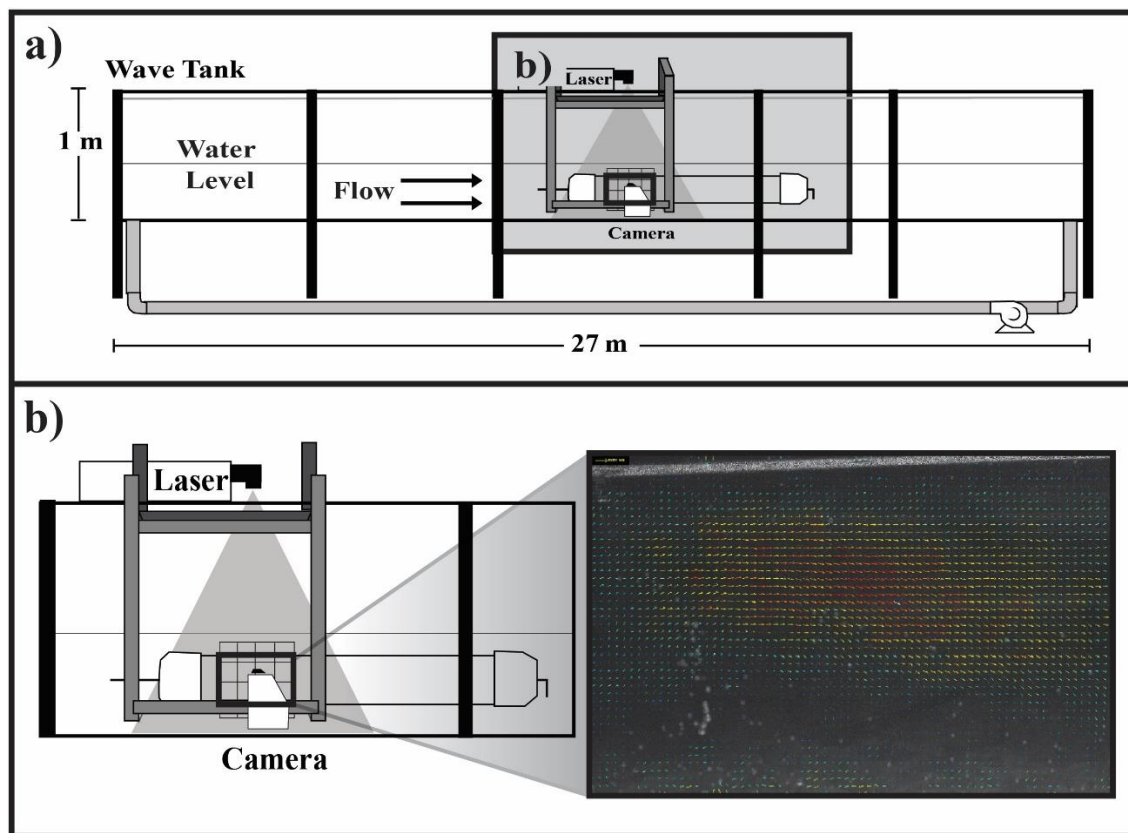
Figure 2.3 – (a) Schematic of the experimental wave tank setup with water depth of 30 cm to generate uniform channel flow via centrifugal pump; (b) Closer view of camera and laser mounts relative to sediment collector throughout experiment, imagining glass particles inside collector by laser generated sheet perpendicular to the camera; an example of the raw camera image with flow vectors superimposed.

In laboratory testing of the bi-directional TIMS design, PIV allowed for qualitative and quantitative assessment of fluid motion within the main body of the sampler (Westerweel, 1997).

Assessment using 2D Planar PIV was conducted in a 27-m long wave tank, with a 130-mJ, Dual Cavity Nd:YAG laser pulsed at approximately 14 Hz and a LaVision Imager Pro camera with 1800x1200 resolution (14-bit digital output, 14 frames sec^{-1}, with a pixel size of 7.4 x 7.4 μm). To visualize the particles, the laser was mounted to a cart above the collector and a laser sheet, which was generated by adding a 10-mm focal length cylindrical lens to the laser optics, illuminated an x-z section (x is along the length of the collector and the wave tank and z is along gravity) of the collector while the camera took images of the region of interest from the side (Figure 2.3 a, b). The same transparent body bi-directional TIMS design from the dye investigation was used, so assessment of particle movement could be made. Using a water depth of 30 cm and centrifugal pump, a quasi-uniform channel flow of 0.06 to 0.1 m s^{-1} was established and sustained throughout testing. During assessment, 10-μm diameter hollow glass spheres, with a specific gravity of 1.05 were seeded into freshwater within the sampler. The laser on top of the tank generated a laser sheet perpendicular to the two mounted cameras, bisecting the long-axis of the sampler and illuminated the glass particles inside of the sampler. The camera mounted to the side of the tank obtained images of the entire internal diameter of the sampler throughout the analysis. Initial images were acquired at 2 Hz, but required subsampling to 0.2 Hz for the analysis due to the reduction of speed within the sampler. The images of the particles are then analyzed using a software program that scans an image pair to see where the particles have moved via cross-correlation. The time between images is known, and the distance between particles can be measured; therefore, the velocity of each particle can be determined. The maximum ambient flow velocity achieved during the experiment was 0.1 m s^{-1} with a viewing window 11.0 cm x 147.0 cm. Final images were taken at a distance that achieved easiest visualization (Figure 2.3b). To further inspect the velocity field within the sampler, 3 vertical

profiles of the 2D vectors were obtained at 3 different distances along the length of the sampler, and are presented as velocity vectors along sampler depth (Figure 2.5).

2.2.3 Sampler Efficiency

2.2.3.1 Laboratory Sediment Efficiency Assessment

Following the laboratory investigation from Phillips et al. (2000), sediment-sampler efficiency was assessed prior to field deployment through a series of experiments that compared the total mass and particle composition of sediment retained in the sampler and outflow material to the known input sample at different ambient flow velocities. A sample representative of sediment from Core Sound, North Carolina, was obtained by combining and homogenizing 8 grab samples taken from bed sediment throughout the estuary. The homogenized sample was placed in a muffle oven at 550°C for four hours to remove organic material, 5-g sub-samples were disaggregated ultrasonically in a solution of 5% sodium metaphosphate. The same design used in the dye-fluid dynamics study described in section 3.2.2 was implemented during the sediment efficiency experiment (Figure 2.2 a), but we replaced the dye solution with the 5-g sample dispersed in 5 L of water (concentration of 1000 mg L^{-1}). The same flow velocities used in Phillips et al. (2000) of 0.3 m s^{-1} and 0.6 m s^{-1} were applied by maintaining discharges from the peristaltic pump of 24.9 and 242.1 mL min^{-1}, respectively. After the entire sediment sample had passed through the sampler, 5 L of DI water was passed through to flush the system. Discharged material from the outflow tube was collected throughout the experiment in a 25 L container. At the end of the experiment material in the outflow container and the sample retained in the sediment sampler were individually centrifuged, freeze dried and weighed to obtain retained sediment mass. The grain-size distributions were subsequently determined for input, retained and discharged samples using a Cilas 1180 Particle Size Analyzer, which allows

for particle size measurement between 0.04 to 2500 µm in 100 size fractions by laser diffraction.

2.2.3.2 Field Assessment

      To understand the sediment sampler efficiency during field deployment, samplers were deployed in two tidal creeks that flow into Core Sound, North Carolina. The first sampler was placed in a tidal creek directly adjacent to a fringing marsh (Figure 2.4) and the second sampler was deployed in a tidal creek that drains overland flow from a large (160 km^2) agricultural site (Figure 2.4). Both sampling locations are within the semi-diurnal tidal environment, allowing for
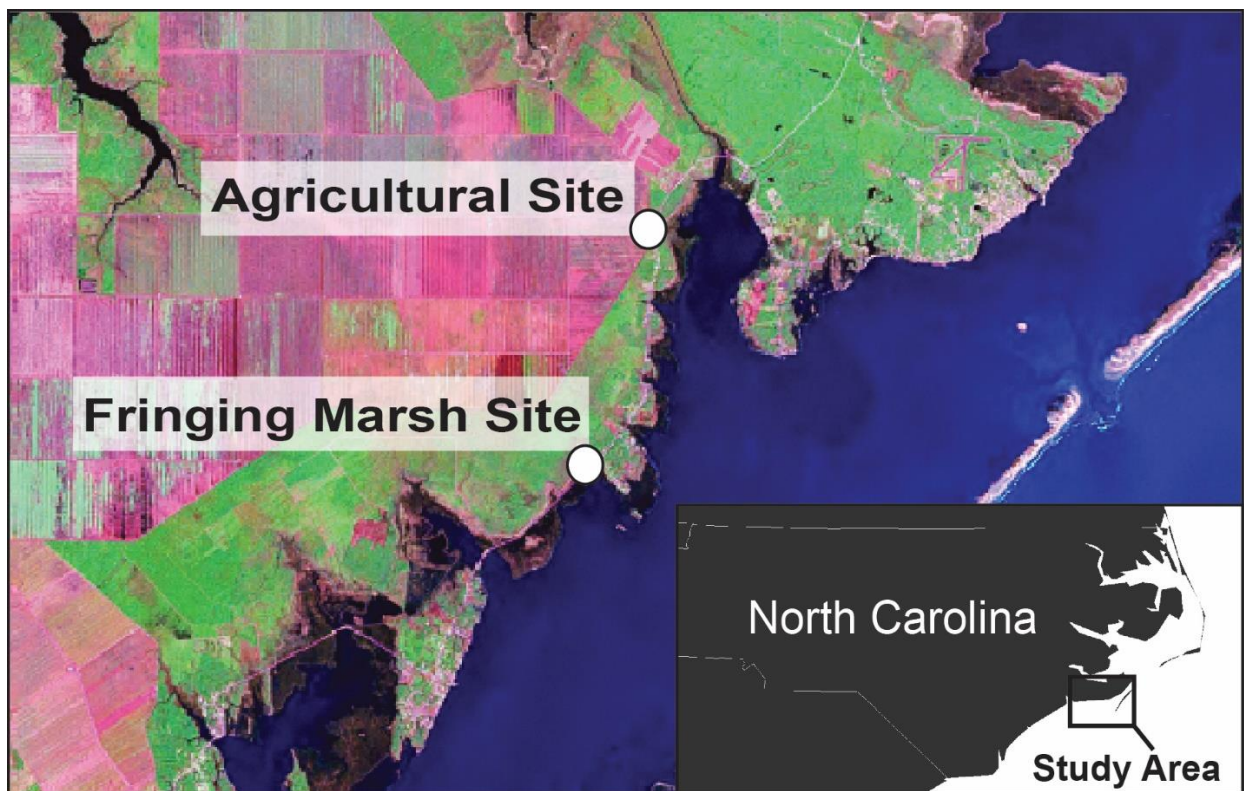
Figure 2.4 – Field map showing sediment collector sampling locations at agricultural and fringing marsh locations along the shoreline of Core Sound, North Carolina.

the unique collection of suspended sediment in reversing flow and variable velocities multiple times a day. HOBO U20 water-level loggers (0-4 m range) were mounted to the center of the sampler at each site to determine water level relative to the sediment sampler during the sampling period. Samplers were deployed at both sites over a 3 ½ day period from May 25th,

2014 through May 28th, 2014, with no precipitation occurring at either site over sampling period. Manual single time point samples were collected daily around high and low tide throughout the semi-diurnal tidal cycle, allowing for a total of 16 manual point samples throughout the multi-day sampling period. Manual point samples were collected through bucket retrieval, filling a 20 L carboy at each sampling. At the end of the sampling period, sediment from the bi-directional TIMS sampler was extracted by manual swirling and draining of the main body into a 20L carboy through the inlet spout, followed by flushing of the sampler with site water into a carboy until all sediment was retrieved. Sediment from both the manual point samples and the samplers was recovered through centrifugation. All samples were freeze dried, weighed and underwent particle-size analysis using the Cilas 1180 Particle Size Analyzer. Distributions of particle size are presented as weight percent distributions, d_{50} range and mean d_{50} values for both the single time point samples and retained sediment from the samplers.

2.3 Results

The bi-directional TIMS sampler was modified to sample suspended sediment uniquely in each direction of tidal flow, and therefore peak performance requires that when tidal direction reverses, suspended sediment is not allowed to re-enter the sampler. To assess whether the modified design prevents sampling of sediment during reversal of flow, flume experiments with a scaled sampler were conducted under bi-directional flow conditions (2.4.1). Modifications of the outflow tube to prevent sediment sampling during flow reversal could also impact the operation and performance of bi-directional TIMS, making it necessary to assess and quantify the internal fluid dynamics under uni-directional flow conditions (2.4.2, 2.4.3). Once a theoretical understanding of how particle fallout should be impacted by internal fluid dynamics within uni-directional flow, testing of the trapping efficiency of the sampler was

assessed in the laboratory (2.4.4) and the field (2.4.5) to verify expected performance.

2.3.1 Fluid Dynamics - Bi-Directional Flow Flume Experiment

Flow within the flume was parallel to the inflow tube of the scaled sampler and started at 0 m s^{-1} and increased to a maximum velocity of approximately 0.6 m s^{-1}. The fluorescent dye that was introduced by syringe near the entrance of the inflow tube showed an immediate reduction in speed, with dye tending to both eddy and move toward the bottom of the tube. Although difficult to quantify in the scaled experiment, the speed of the dye within the sampler was substantially reduced relative to the speed of dye in the ambient flume flow, and appeared to settle and move very slowly along the bottom of the main body of the sampler.

As direction of ambient flow was reversed within the flume, dye within the sampler remained along the bottom, with no apparent movement within the sampler during flow velocities less than 0.6 m s^{-1}. To further clarify this, dye was input with a syringe near the opening to the outflow and inflow tubes during reverse flow conditions. Dye traveled in the ambient flow of the flume, but did not enter the sampler through the L-shaped outflow tube at any point during reverse flow conditions. As reverse flow conditions peaked at 0.6 m s^{-1}, flow over the opening of the outlet tube appeared to displace water within the sampler, creating a slight pressure gradient within the main body of the sampler.

2.3.2 Fluid Dynamics – Uni-Directional Flow Dye Experiment

Unlike the TIMS sampler initially proposed in Phillips et al. (2000), the inlet tube for the bi-directional sampler design is sealed flush with the end cap interior with a ¼ NPT pipe to Swagelok tube fitting, and therefore does not extend into the main body of the sampler. As a result, the 'dead zones' discussed in the Phillips work were very small in the bi-directional TIMS design. Instead, the bi-directional sampler appeared to show an initial dispersion and

reversal of flow upon entering the main body of the sampler as a result of the abrupt change in velocity from the inlet tube to the much wider main body of the sampler. Although not the same size or extent of the dead zone discussed in the Phillips work, which was noted would promote substantial deposition of very-fine particles, the dispersion, reverse flow and circulation upon entry into the main body of the sampler did create a very small 'dead-zone' near the entry to the collector, which would allow for longer residence time at the entry of the sampler prior to movement through the sampler. Once circulation occurs, like the original design, dye settles along the bottom of the collector (Figure 2.2 b). Likewise, sediment laden water entering the sampler will experience a sudden decrease in velocity, and after initial dispersion and circulation, will settle along the bottom of the collector.

2.3.3 Fluid Dynamics – Uni-Directional Flow Particle Image Velocimetry

PIV gives both a qualitative and quantitative analysis of the velocity field within the sediment sampler. The velocity is assumed to reach steady-state through the length of the sampler, after which it is likely that there is little change in the characteristic velocity field over time. Clear flow dynamics emerged within the upstream 1/3 of the sampler, and assuming steady-state dynamics, allowed for general qualitative and quantitative analysis of flow within the sampler.

Theoretically, for efficient collection of the suspended-sediment load, the velocity field within the sampler should be slow enough to allow particulates to fall out of suspension. Additionally, as eddies are mainly what keeps particles in suspension (Oroskar and Turia, 1980), it is important to measure fluctuations in vertical velocity, w'. Along the upstream 1/3 of the sampler, there was free-stream flow in the upper part of the sampler, with some weaker return flow at the bottom. Neutrally buoyant particle paths projected by the PIV data show a

downward trend for most starting heights. These particle paths of water showed overall downward trend in flow, which will be more pronounced with the addition of sediment. Qualitatively, this was expected and shows that aliquots of water (and sediment) will be directed downward toward the bottom of the sampler. Much of the time, flow in the upstream 1/3 of the sampler was exceedingly slow relative to ambient flow, with an average flow in the sampler of 10^{-4} m s^{-1} relative to ambient flow between 0.06 and 0.1 m s^{-1}.

Using Reynold's number, a dimensionless quantity that determines the ratio of inertial to viscous forces, it is possible to characterize expected flow regimes in ambient flow versus expected flow within the sampler design itself. The corresponding Reynold's number within the sediment sampler is ~0.5, consistent with what would be expected for laminar flow, with an external flow Re that exceeds 20,000, consistent with turbulent flow, indicating the high potential for sediment fallout within the main body of the sampler during through flow conditions.

To further inspect the velocity field, 3 vertical profiles of the 2D vectors at 3 different down collector distances were obtained along the length of the upstream 1/3 of the sampler, showing the velocity vectors along the depth of the sediment sampler (Figure 2.5). Note that the laser sheet bisected the 10.5 cm diameter sediment sampler along its long axis, so these vectors are in the center of the cylinder. In the vertical, starting at y = 0 cm, velocity increases from the top of the sampler down. Maximum velocity is from 2 cm to about 6 cm from the top (y = 0). Flow velocity decreases from 6 cm – 10 cm at the bottom, where there is a slight return of flow. This is expected due to boundary layer dynamics and mass-balance.
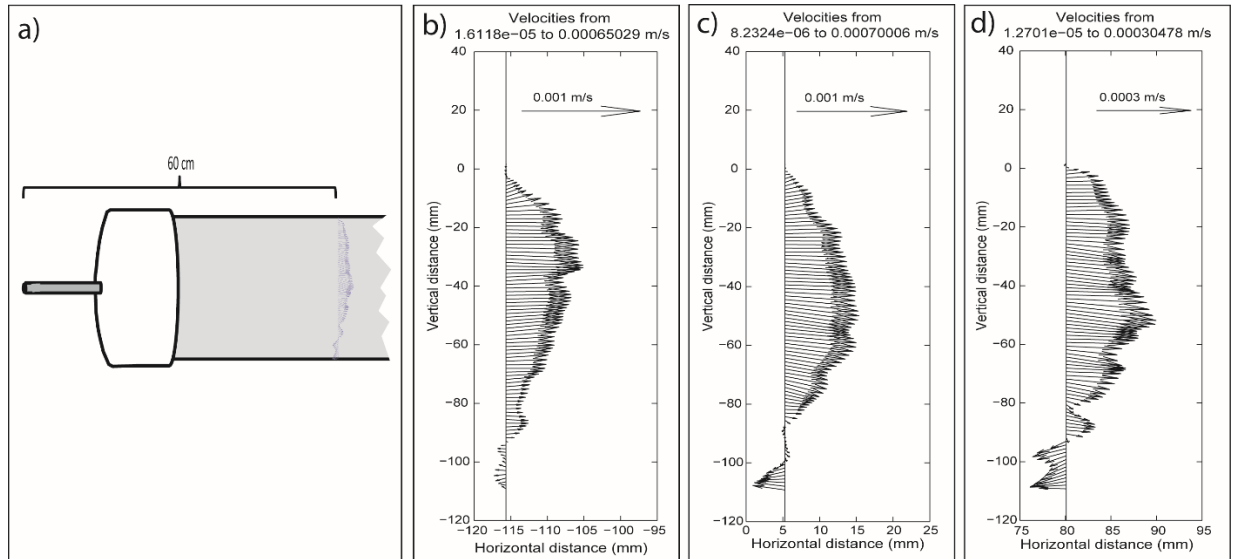
Figure 2.5 – (a) Cartoon of velocity profile within the sediment collector and 60 cm from the nozzle inlet tip. Velocity vectors along collector at (b) 48 cm, (c) 53 cm and (d) 60 cm.

The Durand method for critical velocity has been widely used to characterize critical flow (Onishi et al., 2002). Although different methods for estimating the critical velocity can produce varied results, the Durand method is one of the more well-known and established (Wasp et al., 1977; Oroskar and Turian, 1980). Using this method, critical velocity is determined by the equation:

$$v_t = F * \sqrt{2(1 - s)D} * (d_p/D)^{1/6}$$

where F is an empirical factor, s is the ratio of the particle density to the water density, d_p is the particle size, D is the pipe size, and g is gravity (Oroskar and Turian, 1980). This equation predicts that for a 0.1-mm particle, the critical velocity needed to keep the particles from forming bedforms is 0.9 m s^{-1} to 1.4 m s^{-1}. With this in mind, even for clay particles, the critical velocity based on the Wasp-modified Durand equation above is 0.5 m s^{-1}, with a range from 0.12 to 0.48 m s^{-1}, dependent on the eddy fraction within the Sampler, as calculated from the method found in Oroskar and Turian (1980), which are two to three orders of magnitude higher than the velocities measured in the sediment sampler.

42

2.3.4 Sampler Trapping Efficiency – Laboratory Assessment

Like results from Phillips et al. (2000), the sampler was effective in retaining the silt

and clay fraction through a range of flow velocities. However, some of the coarse fraction

started to settle in the tubing prior to entry into the sampler, particularly at the lower 0.3 m s^{-1}

velocity. This complication is not noted in the Phillips work, and is likely due to 1) the

presence of a coarser fraction in the sample used during our experiment or 2) the tubing that

was used to draw the sample into the sampler from the glass beaker, rather than directly

inserting the inflow tube into the bottom of the beaker as was done in the Phillips experiment.

Despite this complication sediment retention within the sampler, which was calculated based

on the overall dry weight of retained and outflow material, accounted for 93-96 (+/- 1.5)

percent of the overall retained and outflowing material during laboratory experiments (Table

2.1). Like Phillips et al. (2000), the sampler retained sediment across the range of particle sizes

present within the inflowing sample, but did show an over sampling of coarser sediment

Table 2.1 – Sediment percent (%) mass retention and d_{50} values for laboratory studies of full-scale sampler

Ambient Flow Velocity (m/s)	Sediment Retained by Sampler (%)	Inflowing Sediment d_{50} (μm)	Retained Sediment d_{50} (μm)	Outflow Sediment d_{50} (μm)
0.3	95.6 (+/- 1.5)%	26.8	22.7	2.6
0.6	93.3 (+/- 1.5)%	29.1	30.1	6.7

relative to the inflowing suspended sediment (Figure 2.6). Likewise, the outflowing sediment

not retained within the sampler is substantially finer than the inflowing sediment (Figure 2.6).

As expected and reported in Phillips et al. (2000), sediment retention efficiency decreases with
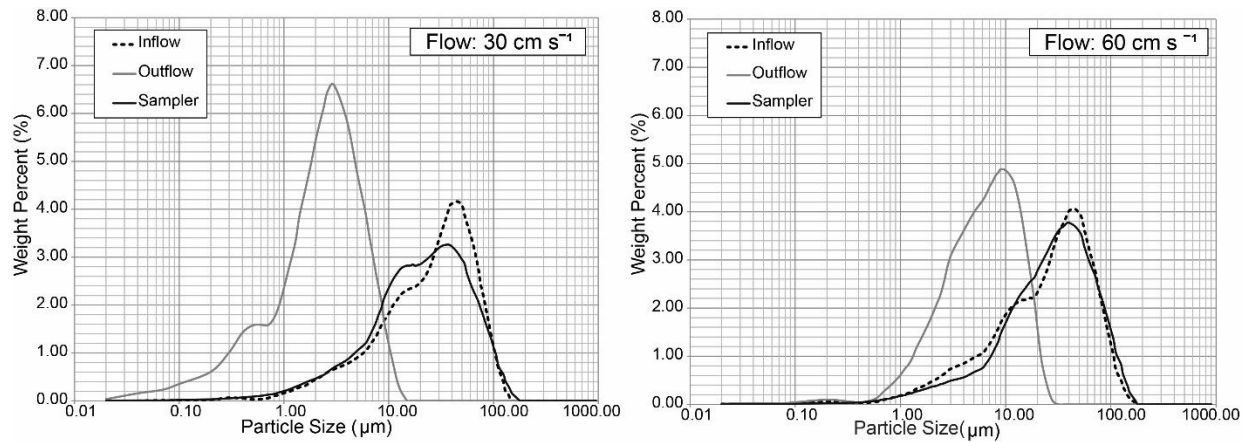
Figure 2.6 – (Left to right) Comparison of particle size distribution by weight percent for inflow, outflow and retained sediment within the collector for velocities of 30 cm s^{-1} and 60 cm s^{-1} (respectively).

increasing velocity, although the difference in efficiency between the velocities is much less in

the modified sampler design relative to the original sampler presented in Phillips et al. (2000).

This warrants further investigation of flow regimes within the sampler to determine if the

modifications to the bi-directional TIMS sampler design increase sampling efficiencies overall

relative to the original TIMS sampler design, making this modified design more efficient than

the original design for deployment in both uni-directional and bi-directional flow regimes. It is

also worth noting that the outflowing material is significantly finer than that of the inflowing

sample, with a d_{50} value for outflowing material under 7 µm at the highest tested velocity

(Table 2.1). The Kolmogorov-Smirnov two-sample statistical test was applied, after Phillips et

al. (2000), to statistically test comparability of the particle size distributions of the inflowing

material relative to retained sediment in the sampler and outflow material and are presented in

Table 2.2. The p-values from this test indicate that the outflow material was significantly

Table 2.2 – Kolmogorov Smirnov (K-S) test results for similarity of particle size distributions in laboratory experiments with full-scale sampler

Ambient Flow Velocity (m s^{-1})	Inflowing vs. Retained Sediment p-value	Inflowing vs. Outflowing Sediment p-value
0.3	0.794	0.0004
0.6	0.961	0.003

different than the inflowing sample at both velocities, but there was not a significant difference

in the distribution of the inflowing material relative to the retained sample at either velocity.

2.3.5 Sampler Trapping Efficiency - Field Assessment

Grain-size distributions are comparable between the sediment collector and the single-

time point samples for each site and tidal current flow direction (Figure 2.7 & Figure 2.8, Table

2.3). An average of the single-time point distributions at each site are presented for each tidal

current flow direction (Figure 2.7 & Figure 2.8) relative to the sediment sampler distribution.

There are differences in the distributions of sediment grain-size between locations, with larger

d_{50} values representing coarser sediment in the agricultural site. Within site variations in

Table 2.3 – Characteristics of sediment (i.e. dry mass of sediment (g), d_{50}, Kolmogorov Smirnov (K-S) test for similarity between samples) collected from single point samples (P.S.) and full-scale sediment samplers (S.S.) in both ebb and flood directions of tidal flow in field placements at two locations

Site Location and Tidal Current	No. of Point Samples (P.S.)	d_{50} P.S. Range (μm)	Dry Mass (g)	Average d_{50} P.S. (μm)	d_{50} Sediment Sampler (S.S.) (μm)	Dry Mass (g)	K-S Test p-value
Marsh – Ebb	4	10.5-14.1	0.2-0.6	12.2	14.3	1.13	1
Marsh - Flood	5	10.9-15.0	0.1-0.4	13.0	14.0	1.61	0.961
Agricultural - Ebb	3	12.0-16.9	0.2-0.5	14.2	15.0	1.17	1
Agricultural - Flood	4	13.1-17.2	0.2-0.4	15.2	14.9	1.62	1

distributions based on tidal flow directions show only minimal differences in the averaged single

time point samples, and single time point samples and sediment collector samples corresponded
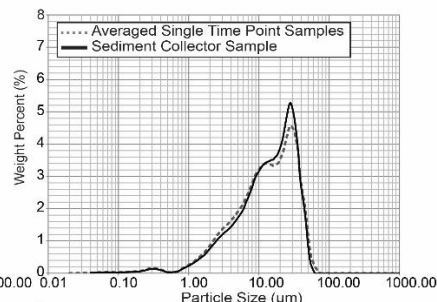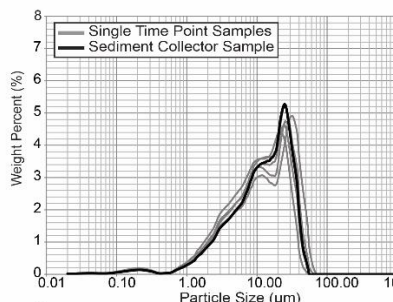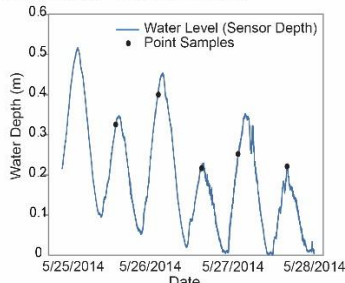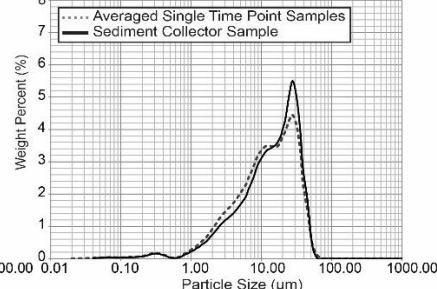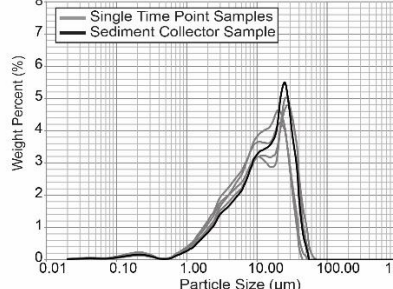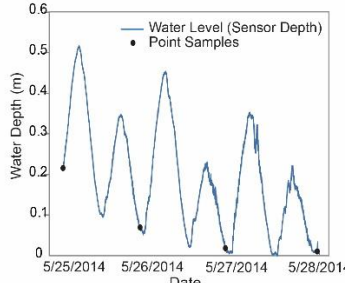
Figure 2.7 – Marsh site water level in tidal creek based on sensor depth (mounted in center of collector), with sample collection date and comparison of particle size distribution by weight percent at each point sample and average point sample with sediment retained in collector over sampling period relative to collector samples for (a) Flood and (b) Ebb current conditions.
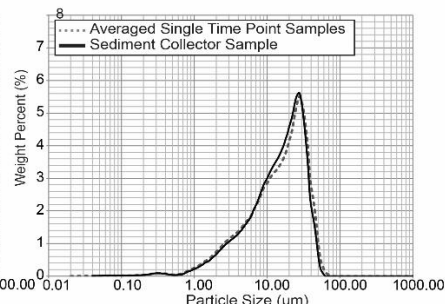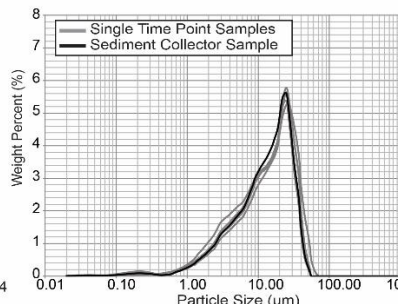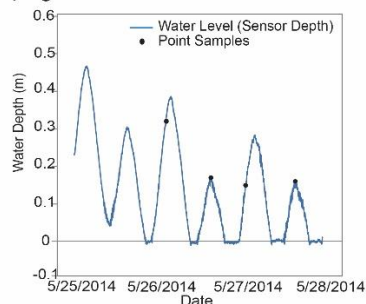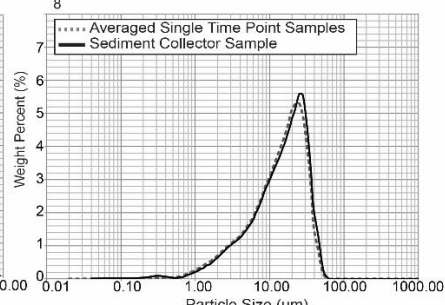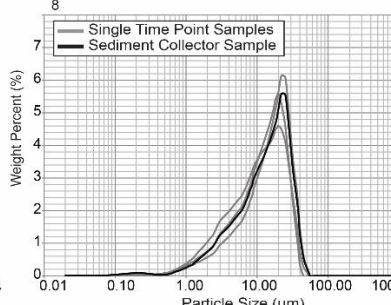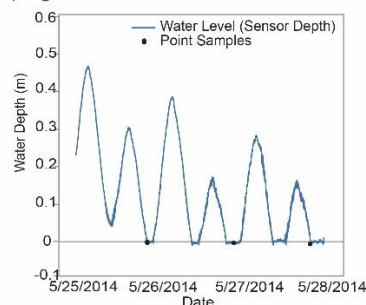
Figure 2.8 – Agricultural site water level in tidal creek based on sensor depth (mounted in center of collector), with sample collection date and comparison of particle size distribution by weight percent at each point sample and averaged point sample with sediment retained in collector over sampling period relative to collector samples for (a) Flood and (b) Ebb current conditions.

well between ebb and flood current samples in both the marsh and agricultural sites (Figure 2.7 and Figure 2.8, respectively). Statistical analysis through the Kolmogorov-Smirnov test verified that there is no significant difference in the averaged distribution of single-time point samples and sediment sampler samples for each site and current direction (Table 2.3). Similar to the correspondence in distribution, d_{50} values for single-time and sediment sampler samples were comparable within the two environments.

Although biofouling did not occur while deployed during the field testing over the week long study, it is important to note that biofouling of the outside of the collector occurred when deployed within the estuarine environment for a period of 2 months. This biofouling was present on the outside of the main-body PVC, however, biofouling was never observed internally within the collector, or along the inside or outside of the inlet or outlet tubes. The opaque body of the PVC main-body of the collector prevents photosynthesis and biofouling internally. Though not completely opaque, the lack of biofouling along the internal or external portion of the inflow and outflow tubes indicates that the semi-rigid nylon pneumatic tubing is resistant to the biofouling observed along the outside of the PVC collector.

2.4 Discussion

2.4.1 Modified TIMS Design

2.4.1.1 Outflow Tube and Pressure Gradient

During flume studies the modified 'L' shaped design of the outflow tube was tested to assess its ability to collect an unbiased sample during reversal of flow. As observed, the modified design did not allow for entry of dye through the outflow tube when flow was reversed, with stagnation of dye primarily occurring within the sampler upon initial reversal of flow. Although no back flow into the sampler occurred when flow within the flume was

reversed, a small negative pressure gradient was created within the sampler when flow was reversed to the peak tested speed of 0.6 m s^{-1}, as water was displaced from within the outlet tube due to flow along the outlet surface. This effect could cause a small amount of sediment laden water to be pulled into the inflow tube when flow is reversed. However, any sediment reuptake would be very small relative to the overall retained sample even in the most extreme of conditions. To fully characterize whether uptake and retention of fine grained material is possible during normal, much lower estuarine flow conditions, which are more on the order of ~0.03 to 0.10 m s^{-1} (Leonard and Luther, 1995), further testing with PIV analysis may be useful.

Some proposed further modifications to the sampler design to address the potential of a negative pressure gradient developing in reverse flow include asymmetrical tapering around the outlet or a check-valve along the entry point of the outflow tube. However, these modifications pose a risk of increased turbulence around the mouth of the outflow tube, or, in the case of the check-valve, increased probability of failure under field conditions. Therefore, the potential disadvantages of these further modifications are likely to outweigh their advantages in the field and the simple modified 'L' shape outflow tube design tested in this study is likely a better fit for field deployment.

2.4.1.2 Inlet Tube and Dead Zones

In the original Phillips design, the inflow tubes extended 20 mm into the main body of the sampler, resulting in the 'dead-zones'. The Phillips work references the importance of these features for further reduced flow and increased ability for sediment fallout to occur (Phillips et al. 2000). Within the proposed modifications to the design, the inflow tube is installed directly into the ¼ NPT pipe to Swagelok fitting, allowing for a flush entry point into

the main body of the sampler. This begs the question of whether or not it would be possible to further reduce flow speeds within the sampler by extending the inflow tube into the main-body of the sampler like the original design, thus creating the noted dead-zones.

Although useful to consider, quantification of the fluid dynamics within the collector indicates that the modified design should be capable of velocities that would be conducive to fine-grained sediment fallout equal to or even better than what is reported in Phillips et al. (2000). This is further verified in the results from the laboratory sediment efficiency experiments, which indicate the modified design is able to capture the fine-fraction, with no significant difference in distribution between the inflowing and captured sediment, with greater retention rates overall reported in the modified design relative to what was reported in the original TIMS design.

From a practical standpoint, the modified design, which does not have the inflow tube inserted into the main body of the sampler, allows for easier and more complete sample collection in the field. In the modified design, sediment is drained through the sampler inflow tube into a 20 L sample collection carboy and flushed with clean water prior to removing the end cap. Having an inflow tube that is flush with the surface of the interior of the sampler prevents build-up or even loss of material, especially the fine fraction, which would be more likely to adhere to the inserted inflow tube. Since sediment loss, especially of the fine fraction, has the potential to bias the physical and chemical signal of the sample, it is critical to avoid this during field collection.

Draining and flushing the sediment through the flush Swagelok fitting into the inflow tube prior to taking off the end cap in the field prevents any accumulated sediment from accidental release. Given the complexity of sampling in the field, allowing for direct drainage

and flushing of the sediment sampler into a collection unit/carboy will result in lower potential for sample loss. With the lack of quantitative evidence for increased efficiency with the dead zones within the modified design, and the ease of collection with the flush inflow tube while in the field in the modified design, the trade-off for slightly increased sediment trapping efficiency with the inserted inflow tubes does not appear worth the potential for sediment loss. Overall, the modified design with inflow tube flush with the sampler entry has a number of practical advantages for sample collection during field deployment, which needs to be weighed against claimed improvement in sediment trapping efficiency in the Phillips design.

2.4.2 Laboratory Performance and Efficiency

Both dye and PIV experiments indicated the downward trend in particle movement, with substantial reduction of velocity within the sampler relative to ambient flow velocities. Critical velocity, as calculated by the Durand method, further indicates that clays should fall out of suspension within the sampler.

Sampler efficiency experiments of overall mass of sediment retained within the sampler relative to outflow material indicated up to 96% retention, with only a small reduction of retention to 93% with a doubling in velocity. Likewise, the grain-size distributions and d_{50} values of the inflowing and retained sampler samples correlated well. Of the fraction of material that was able to make it through the sampler, the grain-size was fine silt to clay (Table 2.1).

As noted, laboratory experiments utilized chemically dispersed or disaggregated sediments for grain-size analysis. This allowed for a high-resolution grain-size distribution to be analyzed for both retained and outflow material from the sampler. However, as discussed in Phillips et al. (2000), in the natural riverine environment fine sediment is often transported in

50

aggregate form. Due to the larger particle size and density of aggregates, a higher velocity is required to keep particles in motion, allowing for greater fallout and therefore higher trapping efficiency within the sampler when sediment is transported as an aggregate rather than individual particles. The transport of particles as aggregates within the estuarine environment is well documented and potentially more prominent than in rivers due to conditions within the estuarine environment like ionic strength, bi-directional collision potential, higher biogenic content, that facilitate particle aggregation during transport (Avnimelech et al., 1982; Van Leussen, 1988; Winterwerp, 1998; Milligan and Hill, 1998). Therefore, relative to laboratory testing, this would indicate that aggregation of fine-grained material within the estuarine environment would further facilitate increased trapping efficiency of the modified bi-directional TIMS design.

2.4.3 Sediment Trapping Efficiency in the Estuarine Environment

Field experiments indicate good retention of sediment in the modified sampler design relative to single time point samples extracted at the marsh and agricultural sites. Sediment distributions between sites did appear different, with material collected from the agricultural site being overall coarser than the marsh sampling location. Sediment sampler grain-size distributions fit the range of grain-size distributions measured for the corresponding single time point samples. Distributions from the averaged single time point samples and the sediment samplers were nearly identical at each site. This indicates the potential of the modified design to collect an unbiased integrated sediment sample through time in diverse estuarine sub-environments.

Ebb and flood current grain-size distributions were similar at each site for both the sediment sampler and single time point samples. Since the samplers are mounted in the same

location, oriented in opposing directions of flow, it is unlikely that the material would be significantly different between the ebb and flood current directions, as the samplers are likely sampling the same material in each direction of flow. Within the constraints of the sampling done for this work, it is apparent that the grain-size distributions and d_{50} values for the single time point samples for each site and current direction matched the equivalent retained sediment sampler sample well. Although distributions between the sampling methods were comparable, single time point samples yielded between 0.1 to 0.6 grams of sediment, while the sediment sampler retained between 1.2 to 1.6 grams of sediment over the one-week sampling period. This additional sediment mass is essential for comprehensive geochemical analysis of the sample. Additionally, this time integrated sediment sample incorporates sediment transported during peak flow conditions, allowing for the capture of event scale, daily and monthly variation in sediment flux within the estuarine environment, a resolution that is difficult and expensive to achieve using traditional sampling methods. Although this work clarifies the fluid dynamics of the modified design within the laboratory setting, performance and retention is likely to vary based on the environment in which the sampler is deployed. When implementing this modified design within a new environment, it is recommended that a field assessment of sediment distribution through grain-size analysis of single time-point samples relative to sediment sampled in the sampler be implemented to verify trapping efficiency prior to large scale deployment.

2.5 Conclusions

The modified bi-directional TIMS design represents a new and novel approach to collection of suspended sediment in environments where flow direction reverses, making it ideal for use within the estuarine environment. Through extensive assessment of the fluid dynamics

within the sampler, including flume, dye and PIV analysis, this work validates that flow within the sampler is substantially reduced relative to ambient flow velocity. Additionally, influent dye aliquots tended to flow downward in the sampler, indicating that influent sediment-laden aliquots will also flow downward upon entry into the sampler, resulting in particle capture within the sampler. Quantitative analysis through PIV experiments allowed for a more robust understanding of the fluid dynamics within the collector to be developed. PIV results indicate that flow rate reduction within the sampler is conducive to the fallout of fine silts to clays from suspension. Although the modified design lacks the dead-zones noted in the original TIMS design due to the lack of insertion of the inflow tube into the main body, quantitative analysis of the fluid dynamics indicate that the modified design should collect fine grained silt and clay regardless of the presence of dead-zones within the sampler. Given similar trapping efficiency, the modified TIMS design is favorable for prevention of sample loss when emptying the unit in the field.

Sampler collection efficiency was assessed in both laboratory and field experiments, and in both assessments indicated the modified TIMS design is capable of collecting representative sediment samples. In laboratory experiments, the sampler had up to a 96% retention rate relative to total retained and outflow material, with 93% retention when ambient velocity was doubled. The fine-grained material exiting the sampler at the highest velocity during the experiment had a d_{50} of 7 µm or less and although that material was significantly different than the inflow material, there was no significant difference between inflowing sediment and the retained sample at either of the velocities tested.

Field experiments utilized single-time point samples and the modified TIMS design over a three day period in a marsh and agricultural environment within the estuary. Although differences in sediment distributions were noted between sampling locations, the retained

53

sediment within the modified TIMS design compares well with equivalent single-time point samples collected over the same period. Unlike the small mass collected in the single-time point samples, the bi-directional TIMS sampler retained up to two orders of magnitude more sediment (multiple grams) an amount required for many geochemical (i.e. stable and radioisotope, lipid, etc.) analysis. The bi-directional TIMS design also collects an integrated sediment sample over the collection period, allowing for collection over multiple time-scales. This study verifies the usefulness the modified bi-directional TIMS design for collection of suspended sediment in the tidal environment, allowing for an inexpensive time-integrated suspended sediment sampler for use within the estuarine environment.

CHAPTER 3: REFINING PB-210 AGE MODELS FOR USE IN ENERGETIC DEPOSITIONAL ENVIRONMENTS BY INCLUDING TEMPESTITES

3.1 Introduction

Developing an accurate record of sediment-accumulation rates is paramount in understanding depositional processes in aquatic environments. The naturally-occurring radioisotope, ^{210}Pb, is delivered from the atmosphere and sorbed onto sediment surfaces (excess or unsupported ^{210}Pb) and decays at a constant rate. The ^{210}Pb radioisotope is considered one of the most accurate methods for establishing recent sediment (0-150 years) geochronologies, especially in environments with constant sedimentation rates (Appleby 2001). To determine sedimentation rates during the past 150 years, the excess or unsupported ^{210}Pb that is sorbed onto the surface of particles is measured over multiple depth intervals, and various models can be applied to determine stratigraphic ages associated with the unsupported ^{210}Pb profile. However, before determining the appropriate age model, it is important to consider the sediment-transport and depositional setting of the site being examined, because each model has a unique set of assumptions that are based on environmental conditions.

The unsupported ^{210}Pb method was developed for use with lake and deep-sea sediments, where environments generally have a constant supply of ^{210}Pb and uniform sediment accumulation rates, with a relatively constant sediment supply (Appleby, 2001). This allows for the unsupported ^{210}Pb, once deposited, to decay exponentially as a function of the half-life of ^{210}Pb (22.3 yrs) and geochronologies to be calculated from the ^{210}Pb profile. Two simple models for ^{210}Pb geochronologies have been developed for use within these environments; the constant

initial concentration (CIC) model and the constant rate of supply (CRS) model (Pennington et al., 1976; Appleby and Oldsfield, 1978; Robbins, 1978; Appleby et al., 1979; Appleby 2001). These models differ in their basic assumptions regarding the constancy of sediment and ^{210}Pb flux to bed sediments. Both models assume that ^{210}Pb is quickly removed from solution onto particulate matter and that, once particulates are deposited, unsupported ^{210}Pb decays constantly through time. A simple application of both models also requires that there is no post-depositional mixing or removal within the sediment profile. The CIC model assumes a constant initial concentration of unsupported ^{210}Pb at the sediment surface, and that ^{210}Pb is quickly removed from solution onto particulate matter, ensuring exponential decay of ^{210}Pb in accordance with the radioactive decay law (Appleby and Oldfield, 1978; Appleby, 2001). The assumptions built into the CIC model requires sedimentation rates to be constant through time (Appleby, 2001). The CRS model assumes the rate of unsupported ^{210}Pb supply to bed sediments is constant (Appleby and Oldfield, 1978), allowing for sedimentation rates to vary inversely proportional to the unsupported ^{210}Pb activity. When applying the CRS model, the measured inventory of unsupported ^{210}Pb activity must be complete. To apply each model appropriately, researchers need to take into account the known sediment dynamics of a site and evaluate whether the specific assumptions of each model are being violated. The ideal sites for ^{210}Pb dating are relatively quiescent depositional environments, like small deep lakes and the deep ocean (Aston et al, 1973; Pennington, 1973; Pennington et al., 1976; Appleby and Oldfield, 1978; Appleby et al., 1979; Appleby and Oldfield, 1992).

It is becoming commonplace to apply ^{210}Pb age models within the dynamic coastal zone, which presents challenges for developing an accurate geochronology (e.g., Allison et al., 1995; Kirchner and Ehlers, 1998; Kirchner, 2011). Unlike many lake and deep-ocean settings, coastal

environments are energetic, with varying rates of sediment supply, deposition, and remobilization at the surface-sediment bed. These processes within the coastal system result in incomplete inventories for ^{210}Pb and violate assumptions of both ^{210}Pb age models.

Preservation of coastal sediments within estuaries has been observed over event to annual time-scales (Olsen et al., 1978; Corbett et al., 2007); however over scales greater than 1 year, portions of the sediment profile are often remobilized, making sedimentation rates difficult to resolve (Olsen et al. 1993; Elliott et al., 2015). Although episodic cycles of deposition and remobilization within estuarine environments can make the use of ^{210}Pb problematic, if not impossible, because the sediment record is incomplete, there are areas within the estuary and coastal environment where the long-term ^{210}Pb record is preserved. Deeper portions of estuarine environments (e.g., harbors, sink-holes, mining pits, settling basins) are capable of capturing sediment below the regional sedimentation base-level (Van Rijn, 2005), and are less prone to removal or mixing via currents and waves. Within these accumulation-dominated portions of the estuarine environment, the long-term, high-resolution sedimentary record can be preserved (Elliott et al, 2015).

Within accumulation-dominated portions of the estuarine environment that do not have complete inventories, the simple CIC and CRS models cannot be used to obtain high-resolution profiles. In these situations, composite models can be utilized to obtain reliable ages and sediment-accumulation rates. The reference-date method for the CRS model is one such composite model that utilizes independent dates, defined by chronostratigraphic marker horizons, to construct inventories and correct erroneous dates. In the case of incomplete inventories (eroded strata or partial sampling), the reference date CRS model can use known time horizons to develop complete inventories and dates above the incomplete portion of the record. Previous

work has highlighted using concentration peaks of artificial radionuclides, like ^{137}Cs, ^{90}Sr, or ^{230,240,241}Pu from atmospheric nuclear weapons testing, as time horizons in conjunction with ^{210}Pb when utilizing the reference date method (Appleby, 2001). However, lithologic markers within a ^{210}Pb profile with a defined reference date may also be used to validate the unsupported ^{210}Pb record. Tempestites, which are storm deposits, could be used as precise lithologic age horizons for use in the reference date method, as long as the timing of emplacement is well constrained.

^{210}Pb dating methods have been effectively utilized to establish records of sediment accumulation within continuously-accreting saltmarsh environments (French et al., 1994; Kirchner and Ehlers, 1998; Gunnell et al., 2010; Kirchner, 2011); however, work showing the effectiveness of applying modeled ^{210}Pb data to estuarine sedimentary records is not as well established. This paper aims to highlight the assumptions and demonstrate the proper application of the CIC, reference date CRS and multi-marker CRS models within the dynamic estuarine environment. The models were applied to a high-resolution ^{210}Pb dataset, obtained from a core collected within Cape Lookout Bight, NC, (CLB) a relatively undisturbed, rapidly accreting (~10 cm yr^{-1}) estuarine sediment basin. Comparing results from the reference date CRS model with sedimentation rates for CLB calculated using the CIC model (Elliott et al., 2015), and to a more rigorous multi-marker reference date CRS model for the basin using well-constrained tempestites as marker beds, reveals the relative strengths and weaknesses of each model for the characterization of sedimentation within this and other estuarine basins.

3.2 Background and Methods

The CLB sedimentary basin, represents an ideal setting for testing the implementation of both the CIC and CRS model within a dynamic estuarine environment. The embayment formed over the last century and multiple studies have shown it to be an efficient sediment trap with no significant post-depositional sediment redistribution or mixing (Martens, 1976; Chanton et al., 1983; Bartlett, 1981; Martens and Klump, 1984; Wells, 1988; Canuel et al., 1990; Elliott et al., 2015).

Previous work by Chanton et al. (1983) established a sedimentation rate in CLB of nearly 10 cm yr^{-1}, underscoring the great potential for generating a high-resolution record of sedimentation there. In 2010, a 4.65 m core was extracted from the deepest portion of the CLB basin, and subsamples were analyzed for grain-size, water content and radio-isotopic analyses. Lithologic units were similar to those presented in Chanton et al. (1983) and Wells (1988), with a basal highly modified marine shelf unit (465-385 cm), an overlaying marine-estuarine unit punctuated by hurricane washover beds (tempestites; 385-300 cm) and an upper estuarine unit (300-0 cm) with undisturbed sedimentary layers (Elliott et al., 2015). Alpha spectrometry was conducted at 1-cm intervals throughout the entirety of the core to obtain a high-resolution unsupported ^{210}Pb profile for the CLB basin and the CIC, CRS and multi-marker CRS models were applied to the dataset.

3.2.1 CIC Model

The simplest model that can be applied to the unsupported ^{210}Pb profile is the CIC model. The CIC model assumes a constant initial concentration of unsupported ^{210}Pb at the sediment surface, regardless of accumulation rates (Appleby, 2001). Therefore, the supply of ^{210}Pb to bed sediments must vary directly in proportion to the sediment supply, higher rates of sediment

59

supply require higher fluxes of ^{210}Pb to the bed sediment. One important assumption of the CIC model is that sedimentation rates are constant. Under this assumption, the date t of sediment layer at depth z can be calculated using the equation in Figure 3.1a, where $C(0)$ is the unsupported ^{210}Pb activity at the surface of the core, $C(z)$ is the unsupported ^{210}Pb activity at depth z and λ is the decay constant for ^{210}Pb (0.03118 yr^{-1}) (Appleby, 2001; Sanchez-Cabeza and Ruiz-Fernández, 2012). Since the initial concentration of ^{210}Pb is assumed to remain constant through time, a linear regression is fit to the data to determine the sediment-accumulation rate.

Figure 3.1- (a) Conceptual model and equation for calculating the timing of deposition for depth z for Constant Initial Concentration (CIC) model; (b) Applied CIC model utilizing binned 5-cm averaged excess ^{210}Pb concentrations in CLB core from Elliott et al. (2015); (c) excess ^{210}Pb profile with excess ^{210}Pb concentrations and CIC model sedimentation rate from regressions models from Elliott et al. (2015).

Multiple linear regressions can be identified and applied to the ^{210}Pb profile if applying a piece-wise regression model that acknowledges multiple sediment regimes. Although the CIC model is useful for determining long-term sediment-accumulation rates, for high-resolution

datasets, the CIC model is not sensitive enough for determining high-frequency changes in sedimentation rate through time.

3.2.2 Application of CIC Model at CLB

Chanton et al. (1983) performed ^{210}Pb analysis on sediment extracted from the central part of CLB, using the CIC model to determine ages and sedimentation rates down profile. Within the sediment profile, multiple sand concentrations were noted, with the upper-most sand concentration in the core deposited during Hurricane Ginger, which struck the study site on September 30, 1971. Chanton et al. (1983) probed down to this sand horizon with a measuring stick over a two year period to determine changes in sediment thickness through time, allowing for a secondary means of establishing sedimentation rates in the basin (Chanton et al., 1983). Wells (1988) also sampled this sand horizon and interpreted overwash of the barrier island during Hurricane Ginger as the process of deposition.

Elliott et al. (2015) constructed a high-resolution ^{210}Pb profile for CLB that showed high variability between measurements taken at 1-cm increments down core. For comparison to the lower resolution ^{210}Pb age profile established using the CIC model in the work by Chanton et al.(1983), the unsupported ^{210}Pb profile was binned into 5-cm intervals and the CIC model was used to establish ages down core (Figure 3.1b, c). As presented in Elliott et al. (2015) a multi-regression CIC model showed the best fit for those data, with a sand layer at 307.5 cm correlating to an age of ~1971, consistent with the previously-identified washover deposit emplaced during Hurricane Ginger. Although the CIC model was able to verify the placement of the 1971 Hurricane Ginger sand layer and identified average ages within the lithologic units, the model indicated an abrupt change in sedimentation rate from ~3 to ~10 (cm yr^{-1}) occurred at ~262.5 cm depth, with no corresponding change in the lithology. Additionally, when plotting the

raw (1-cm increment) excess ^{210}Pb profile, variation in the activity of excess ^{210}Pb was noted, indicating the CIC model may not be the most appropriate model for the dataset (Figure 3.1c). As noted in Elliott et al. (2015), a more robust age model, like the CRS model, which can account for changes in the activity of excess ^{210}Pb and in the sediment accumulation rate through time, should be applied to the profile.

3.2.3 CRS Model

The CRS model assumes that the ^{210}Pb activity of sediments being deposited on the surface of the bed and the rate of sedimentation vary inversely proportional to one another, making the CRS model useful for datasets that exhibit high-frequency changes in the sedimentation rate through time (Appleby and Oldfield, 1978). Using the CRS model, conceptually shown in Figure 3.2a and applied to data from Appleby (2002) in Figure 3.2b and 3.2c, date (*t*) for chronostratigraphic unit within the ^{210}Pb profile is calculated using the total unsupported ^{210}Pb inventory of the entire core, *A(0)* and the unsupported ^{210}Pb inventory below the layer being dated (*Ai*), where λ is the ^{210}Pb decay constant (Appleby & Oldfield, 1978; Appleby, 1997). Inventories for *A(0)* and *Ai* are determined through numerical integration of the ^{210}Pb profile. As the equation in Figure 3.2a expresses, dates for a specific layer are largely determined by the relationship between the total inventory of unsupported ^{210}Pb activity *A(0)* in the core, relative to the inventory (*Ai*) of the unsupported ^{210}Pb activity below the layer that is being dated. Therefore, accurate dates within the ^{210}Pb profile are dependent on reliable estimations of both A_0 and A_i.
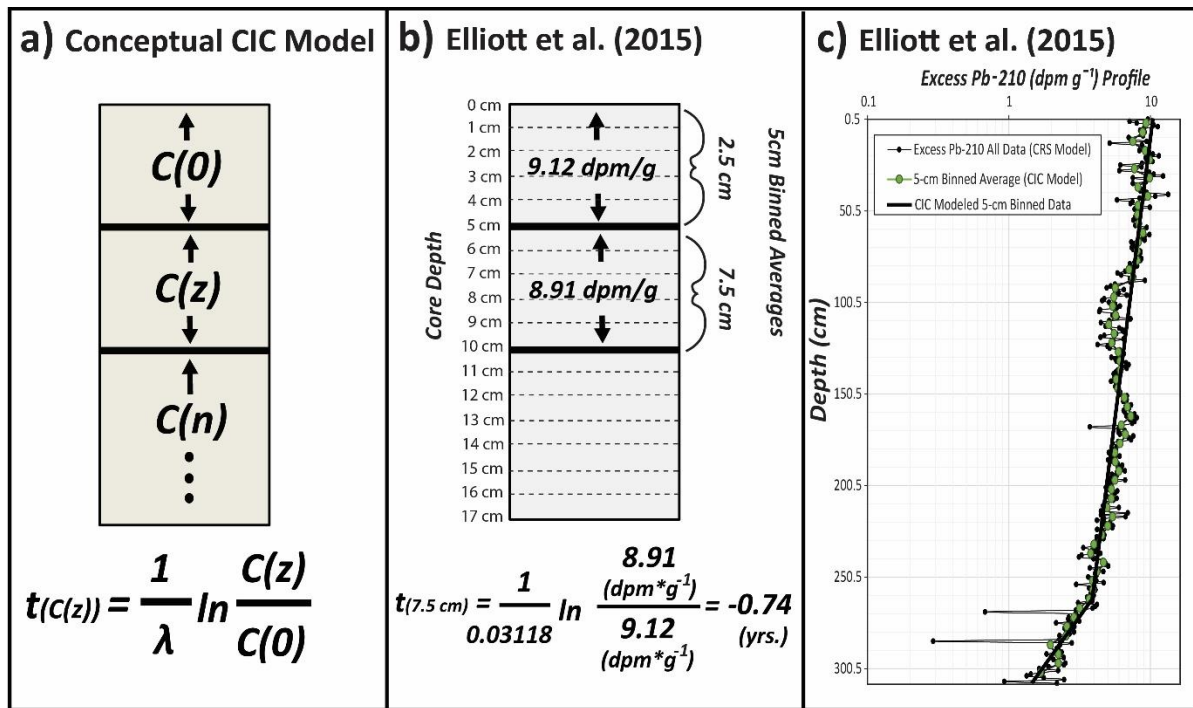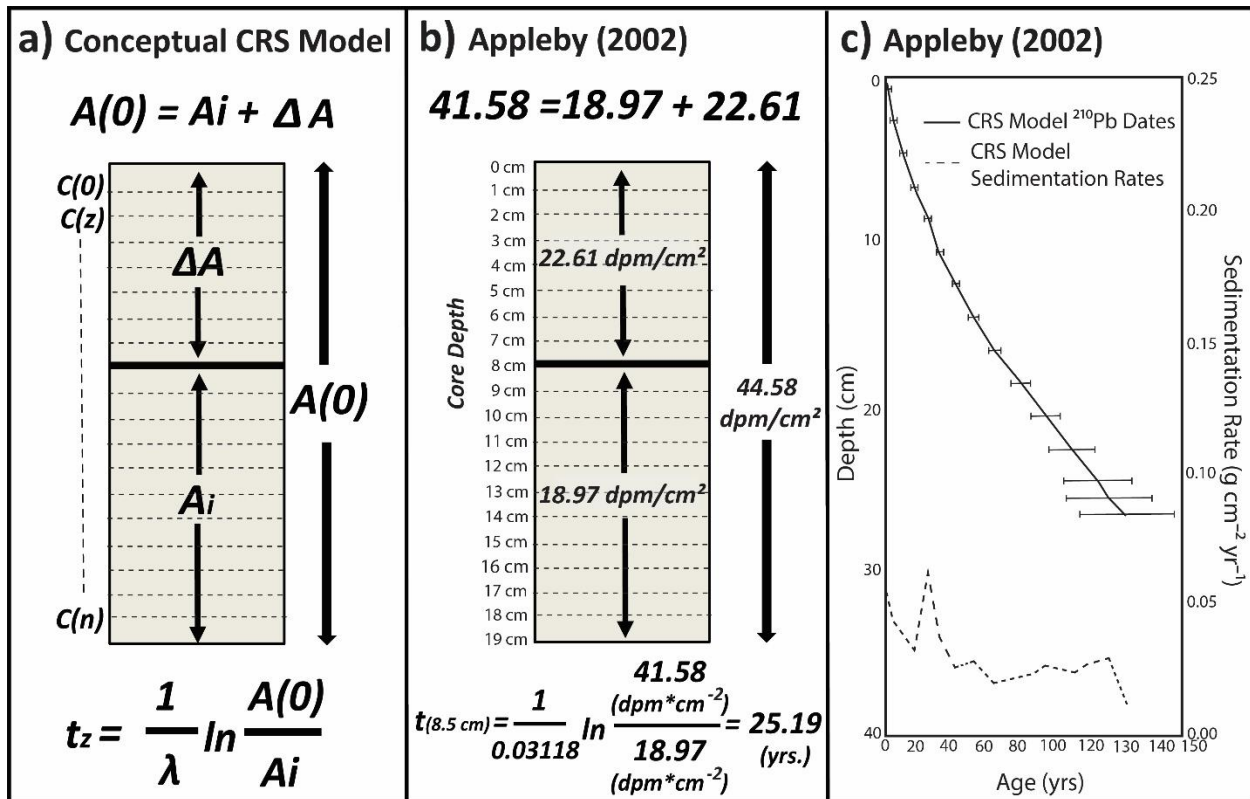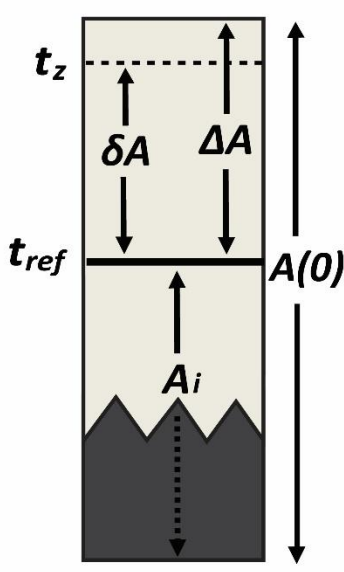
Figure 3.2- (a) Conceptual model and equation for calculating the timing of deposition for depth z for Constant Rate of Supply (CRS) model; (b) Applied CRS model utilizing activities and inventories presented in Appleby (2002); (c) CRS model application with date and sedimentation rate presented in Appleby (2002)

3.2.4 Reference Date CRS Method – Hurricane Layer Application in CLB
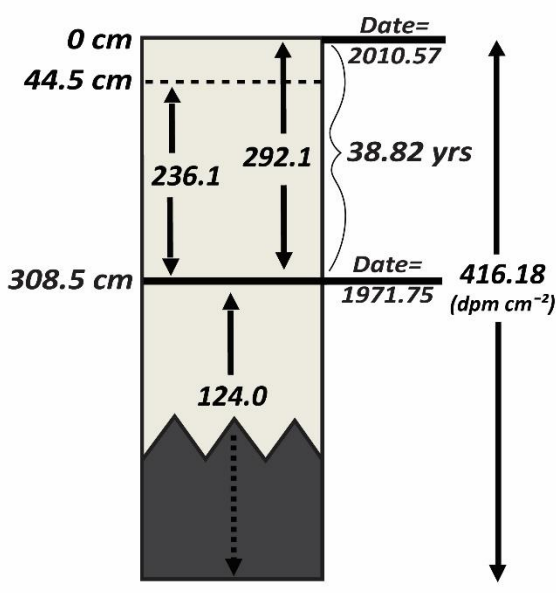
Common sources of error in measuring ^{210}Pb inventories are incomplete sediment records, where background values in ^{210}Pb were never sampled or portions of the record are missing. Both of these errors result in underestimation of the inventory or violation of the assumptions of the model itself. Where the record is incomplete due to gaps in the sedimentary record or background values of ^{210}Pb were never sampled, estimations of the *Ai* using a known reference layer can allow for accurate accumulation rates to be determined above the reference horizon (Appleby, 1997). The reference date CRS method, shown conceptually in Figure 3.3a, allows a known reference date to be applied to the ^{210}Pb profile to calculate

a) Conceptual Reference Date CRS Model

$$Ai = \frac{\Delta A}{e^{\lambda\, t_{ref}} - 1}$$

t_z

δA ΔA

t_{ref} $A(0)$

A_i

$$t_z = \frac{1}{\lambda} \ln\left(\frac{A(0)}{Ai + \delta A}\right)$$

b) Applied Reference Date CRS Model (CLB ²¹⁰Pb Profile)

$$124.05_{\text{(dpm cm}^{-2})} = \frac{292.1_{\text{(dpm cm}^{-2})}}{e^{(0.03118*38.82)} - 1}$$

0 cm   Date= 2010.57

44.5 cm

236.1   292.1   38.82 yrs

308.5 cm   Date= 1971.75   416.18 (dpm cm⁻²)

124.0

$$4.64_{\text{(yrs)}} = \frac{1}{0.03118} \ln\left(\frac{416.18_{\text{(dpm cm}^{-2})}}{124.0 + 236.1}\right)$$
$$\text{(dpm cm}^{-2}) \text{(dpm cm}^{-2})$$

Figure 3.3- (a) Conceptual model and equation for calculating the timing of deposition for depth z using single reference date CRS model; (b) Applied single-reference date CRS model utilizing activities and calculated inventories from tempestite deposit, Hurricane Ginger layer, dated at 1971.75 yrs. from excess ²¹⁰Pb profile and inventories from CLB core.

the inventory, *Ai,* below the known chronostratigraphic layer, where *ΔA* is the inventory above the reference layer and t_{ref} is the reference age applied to the middle of the associated lithologic horizon (Figure 3.3a).

Elliott et al. (2015) showed that the lithology below the Hurricane Ginger sand layer was variable due to episodic erosion and pulses of marine-sediment deposited in the basin, invalidating the simple CRS model due to an incomplete unsupported ²¹⁰Pb inventory. Using the composite reference date CRS model, a reference date (*t_{ref}*) of 1971.75 was applied to the middle of the Hurricane Ginger layer, 308.5 cm depth, to establish an inventory *Ai* for the lower highly-

modified portion of the core (Figure 3.3b). The newly-established *Ai*, the inventory *δA* above the reference layer to the layer being dated (*t_z*), and the total inventory for the ^{210}Pb profile *A(0)* are applied to the CRS age-model equation to obtain associated ages of depth interval *t_z*, calculated as shown in Figure 3.3a, and applied in Figure 3.3b.

3.2.5 Multi-Marker Reference Date CRS Model

Once the Hurricane Ginger reference age horizon was established, and the inventory within the core was calculated, the timing of smaller peaks in sand concentration appeared to be associated with other known hurricane impacts. Work presented in Elliott et al. (2015) showed that increases in elevation, width, and length of the CLB barrier spit made the basin more resistant to overwash through time, moving the predominant sediment source from marine to estuarine, resulting in less sand above the Hurricane Ginger layer. Those smaller peaks in sand concentration above the Hurricane Ginger layer are likely associated with high-energy events like hurricanes.

To increase the resolution of the ^{210}Pb profile, we applied the same principles presented in the composite reference date CRS method, by fitting the unsupported ^{210}Pb profile to the known tempestite dates throughout the core, shown conceptually in figure 3.4a, and applied in figures 3.4b. The piecewise CRS model presented in Appleby (1997) applies a similar method through use of known age horizons from artificial radionuclides like ^{137}Cs, ^{90}Sr or $^{239,240,\ 241}$Pu, emitted into the environment through nuclear-bomb testing. Ideally, ^{137}Cs, which is often used in combination with ^{210}Pb, could be used to further verify the profile, but unfortunately within this core, a clear spike in ^{137}Cs was not observed. Within saline environments, ^{137}Cs can

a) Conceptual Multi-Marker CRS Model

$$A_i = \frac{\Delta A}{e^{\lambda(t_{ref}{}^2 - t_{ref}{}^1)} - 1}$$

t_{ref2}

t_z —— ΔA

δA

t_{ref1}

$A(0)$

A_i
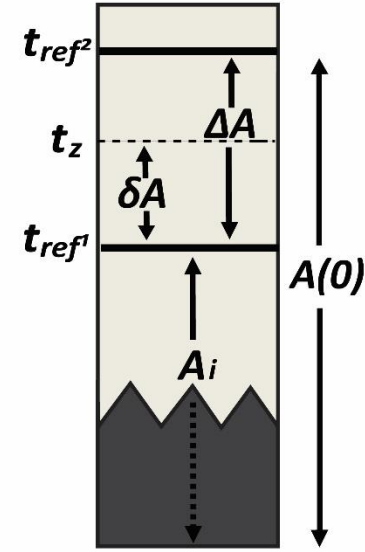
$$t_z = \frac{1}{\lambda} \ln\left(\frac{A(0)}{A_i + \delta A}\right)$$

b) Applied Multi-Marker CRS Model (CLB ^{210}Pb Profile)

$$124.8 \text{ (dpm cm}^{-2}) = \frac{235.04 \text{ (dpm cm}^{-2})}{e^{(0.03118*33.96)} - 1}$$

44.5 cm — Date= 2005.71

150.5 cm — 235.04 — 33.96 yrs

101.15

308.5 cm — Date= 1971.75 — 359.86 (dpm cm^{-2})

124.8

$$14.92 \text{ (yrs)} = \frac{1}{0.03118} \ln\left(\frac{359.86 \text{ (dpm cm}^{-2})}{124.8 + 101.15} \right)$$
$$\text{(dpm cm}^{-2})\text{(dpm cm}^{-2})$$
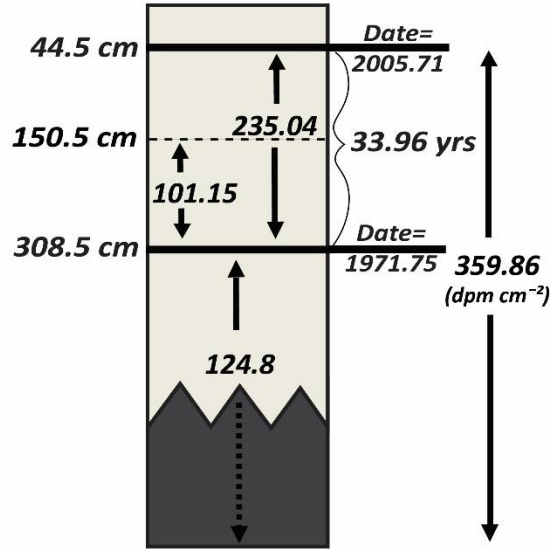
Figure 3.4- (a) Conceptual model and equation for calculating the timing of deposition for depth z using multi-marker reference date CRS model; (b) Applied multi-marker reference date CRS model utilizing activities and calculated inventories from tempestite deposit, Hurricane Ginger layer, dated at 1971.75, and Hurricane Ophelia, dated at 2005.71, from excess ^{210}Pb profile and inventories from CLB core.

become post-depositionally mobile. A new inventory A_i was determined for each tempestite reference date, and δA, the unsupported ^{210}Pb inventory, was determined between the reference date and the lithologic unit being dated (Figure 3.4a and 3.4b). Utilizing the known tempestite reference dates down-profile, increased the accuracy of the modeled excess ^{210}Pb profile, allowing for a more robust sediment-accumulation rate to be determined down-core

3.3 Results

3.3.1 CIC and CRS Reference Date Model Comparison

Using Hurricane Ginger as a reference date at 308.5-cm depth, the inventory to the base of the core was established and ages were determined above the reference date to establish an overall age profile and sediment-accumulation rate as shown in Figure 3.5. To examine differences in the resolution and accuracy of the CIC and CRS models, sediment-accumulation rates versus time derived from the simple CIC model, presented in Elliott et al. (2015), were compared to the sediment-accumulation rates versus time established through the composite reference date CRS model using the Hurricane Ginger layer (Figure 3.5).
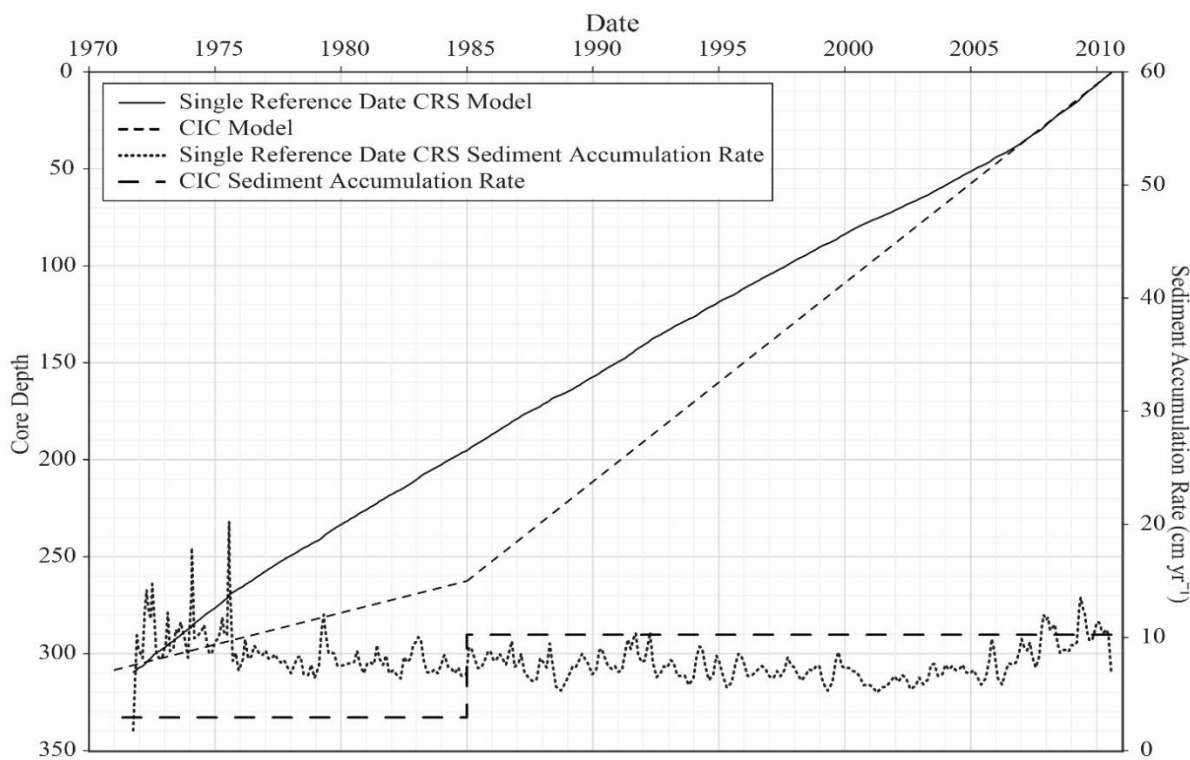
Figure 3.5 – Comparison plot of CIC and reference date CRS model 210Pb dates and sediment accumulation rates (cm yr^{-1}) for the CLB core.

The CIC and CRS age models and resulting sedimentation rates are markedly different. The CRS model shows high-frequency (sub-annual) variations in the sediment-accumulation rate with a maximum of 17.6 cm yr^{-1} and a minimum of 4.16 cm yr^{-1} and a standard deviation of 0.93 cm yr^{-1} in the 5-year running average of sediment accumulation rates. In contrast, the CIC model shows constant sediment accumulation at 2 cm yr^{-1} from 1971 to 1985, an abrupt increase in sediment accumulation at 1985, and constant sediment accumulation at 11 cm yr^{-1} from 1985 to 2011. When averaged over the entire record, the SAR for the CIC and CRS models are relatively similar, being 6.58 cm yr^{-1} and 7.93 cm yr^{-1}, respectively.

3.3.2 Establishment of Multiple-Marker Reference Date CRS Model

Once the reference date CRS model was applied to the dataset, ages were determined for every cm of sediment above the Hurricane Ginger sand layer. Small distinct peaks in the percent sand appear to be closely associated in time with other major hurricanes that impacted the study area (Figure 3.6). The most distinct peak at 44.5 cm is close in time with Hurricane Ophelia,
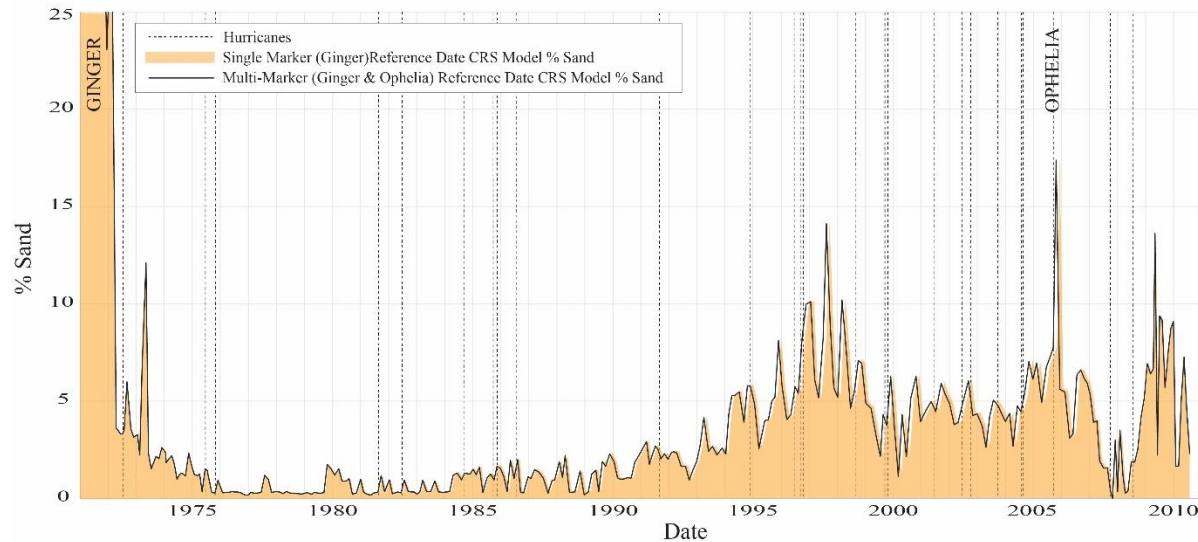
Figure 3.6 – Age model application for single marker (Ginger) and multi-marker (Ginger and Ophelia) reference date CRS model relative to % Sand within the core. Hurricane and tropical storms within 100 km of CLB marked through time, with Ophelia and Ginger indicated.

which has been categorized as an extremely slow moving storm that moved around the North Carolina coast between September 9th and 15th, 2005. A broad increase in percent sand is present between 124.5 and 83.5 cm depth, with multiple small distinct peaks in sand concentration through this interval. Based on the single-reference date CRS model, this core interval occurred between 1995 to 2000, with the distinct peaks in sand concentration corresponding to 1996, 1998 and 1999, which coincide with historically-intense hurricane seasons along the North Carolina coast.

Using the same techniques outlined above, Hurricanes Ophelia (September 16, 2005) and Ginger (September 30, 1971) reference dates for peaks at 44.5 and 308.5 cm depth, respectively, were recognized and applied in a multi-marker reference date CRS model. As referenced in Appleby (2001), using multiple reference layers allowed increased accuracy in the sediment accumulation rate profile. In regard to hurricane layers, which can deposit large pulses of sand and sediment within a single event, using reference layers becomes even more important because pulses of sand will not necessarily be recorded in the excess ^{210}Pb profile, due to slow sorption of ^{210}Pb to sand, and rapid deposition associated with events.

Using Hurricanes Ophelia and Ginger as reference layers within the CRS model, dates were determined for each 1.0-cm layer between the reference horizons to further tighten the age profile and establish more accurate sediment-accumulation rates (Figure 3.7). The age profile and sediment- accumulation rate established using the multi-marker reference date CRS model with Hurricane Ginger and Ophelia are compared with the results for the single reference date CRS model in Figure 3.7.
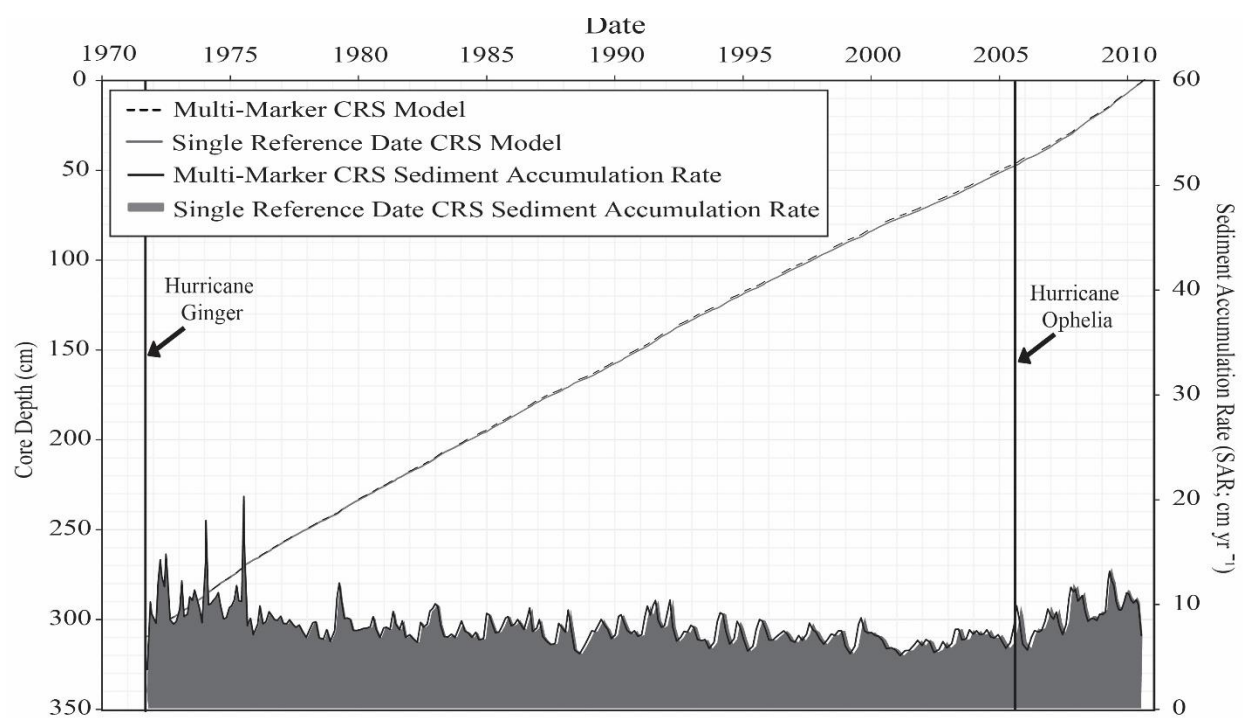
Figure 3.7 – Comparison plot of the single (Hurricane Ginger) and multi-marker (Ginger and Ophelia) reference date CRS model ^{210}Pb dates and sediment accumulation rates (cm yr^{-1}) for the CLB core. Timing of Hurricane Ginger and Hurricane Ophelia are indicated.

3.4 Discussion

3.4.1 CIC and simple CRS Reference Date Model

The apparent abrupt shift to a new increased rate of sedimentation at 1985 is an artifact of the CIC model itself, which assigns regressions to the dataset. At the lowest resolution, the two models show an average SAR within error of each other in both models (CIC and CRS). When the CIC model is applied to a high-resolution profile with significant changes in the rate of sedimentation through time, like the unsupported ^{210}Pb profile for CLB (Figure 3.5), it can only provide general long-term trends, but does not resolve the sediment dynamics of the system, and can lead to misinterpretations. The high sedimentation rates within CLB and the increased resolution provided by the CRS age model allows for short-term, high-frequency variations in the sedimentation rate to be used as a proxy for estuarine sediment flux, a powerful tool when

70

trying to determine physical mechanisms for changes in estuarine sedimentation through time.

As indicated by the geologic history developed for the CLB basin from Elliott et al. (2015), the CIC model is useful for determining long-term trends in the sediment profile and geologic context for the system. Unlike the reference date CRS model, which, for incomplete inventories can only determine ages and sedimentation rates above a known reference layer, the CIC model can be used to establish ages within portions of the profile that could be difficult or impossible to resolve using the CRS model alone. The CIC model assumes that concentration of excess ^{210}Pb is constant, and therefore at its highest concentration at the top of the profile, relying on radioactive decay for changes in concentration down profile. Using the CIC model, dates are determined based on concentration of excess ^{210}Pb down core, not overall inventory, and therefore, when data is binned appropriately, it can be used to determine long-term trends in a sediment profile. The CIC model also requires fewer samples to be analyzed, and within systems that are quiescent, with relatively low rates of sedimentation, not much information is gained by using a sensitive model like the CRS. In such situations, applying the CIC model using a few samples would be more efficient both from a time and financial perspective. When analyzing unsupported ^{210}Pb for dating, applying the CIC model is a simple first step for determining overall ages and rates of sedimentation within the profile, with the subsequent application of a more complex model, like the CRS model, if needed.

3.4.2 Comparison of Simple and Multi-Marker CRS Reference Date Models

A comparison of the simple, single Hurricane Ginger CRS reference date model to the multi-marker CRS reference date model, shown in Figure 3.7, shows very little variation in the age model or SAR profile, but highlights the increased precision provided by the multi-marker method. Using known hurricane strikes and associated peaks in sand concentration allow for the

71

age model to be pinned to 3 depth - time coordinates resulting in increased precision of modeled ages and establishment of more accurate sedimentation rates within the sediment profile.

Unlike using global impulse tracers preserved in the core (i.e. ^{137}Cs, ^{90}Sr, $^{230, 240, 241}$Pu, stable ^{210}Pb, carbon spherules), as known reference dates, assigning reference dates to tempestites is an iterative process of applying a reference date and checking the results against the overall sediment profile, storm history of the system and/or physical forcing mechanisms within the system. Ideally, multiple markers, especially regional markers (i.e. tempestite deposits, volcanic ash deposits, flooding surfaces, etc.) would be used to verify the profile. However, if tempestites are present within the profile, application of reference dates associated with tempestites does not only provide increased precision within the resolution of the age model; these hurricane deposits represent an impulse of sediment during an event, causing a large shift in the sedimentation rate at a temporal resolution that is difficult to constrain using the unsupported ^{210}Pb profile alone. Therefore, depending on frequency of change within the sediment accumulation rate profile, not including tempestite horizons could shift the age model and sedimentation rate by multiple months or even years. Since the high average sedimentation in the CLB core allows for interpolation of the age model to monthly resolution, a shift of a month or more could makes a large impact on the placement of ages and associated sedimentation rates within the profile.

3.5 Conclusions

The CIC and CRS models are useful tools for understanding sedimentation within the coastal system, but careful consideration of the assumptions built into each model is essential, and are often violated within the dynamic coastal zone. Additionally, when complete inventories of excess ^{210}Pb are not possible, the CRS model cannot be applied. Utilizing known reference

horizons within the profile, the reference date CRS model may be a useful tool for approximating the excess ^{210}Pb inventory to determine ages and sedimentation rates above the reference layer. Detailed recommendations about sample extraction, preparation and model application follow.

3.5.1 Site Location and Sample Preparation

Within dynamic coastal environments, the choice of a sampling location is key for successful application of any model. For all models, continuous profiles with minimal mixing or profiles that are continuous above a known reference date provide the best results. Although, as we have shown, it is possible to use the CRS model with an incomplete profile, having a complete inventory of excess ^{210}Pb is best when applying the CRS model.

Once a core is extracted, preparing the sample for analysis starts with the resolution of core dissection. The finest practical sampling interval is best, as it is always possible to bin data, or choose a lower resolution after core dissection has occurred. Bulk density analysis should then be performed along with grain-size analysis. Without bulk density, application of a more sensitive model, like the CRS model, will not be possible. Finally, when trying to decide which model is most appropriate for the dataset, plotting the excess ^{210}Pb versus depth will provide much needed insight into model selection; for example, intervals of increasing ^{210}Pb down-core indicates assumptions are violated within the CIC model, indicating another model, like the CRS model, may be more appropriate for the dataset.

3.5.2 Model Application

The CIC model should be used first when analyzing a core from a new location to get a general idea of sedimentation rates within the profile. Because the CIC model does not allow for increased unsupported ^{210}Pb concentration down-core, this may require binning the data to remove those apparent inversions. Once a general idea of sedimentation rates has been

established, assessment of the need for a more sensitive complex model, like the CRS model, is recommended. If sedimentation rates are low and appear constant, not much is likely gained by applying the CRS model. However, if the profile of excess ^{210}Pb appears to vary through time, or sedimentation rates appear to be high, it may be appropriate to consider application of the CRS model to extract more information from the dataset. The CRS model will provide higher resolution, and is appropriate for application in situations where sedimentation rates appear to vary through time. Due to the need for a complete inventory of excess ^{210}Pb, there are significant costs associated with analysis. Therefore, it is important to consider the trade-off between cost of analysis and information gained by application of the CRS model at the sampling location. If funding is limited and it is unknown whether the sedimentation rates vary, the CIC model may be more appropriate for getting an overall understanding of sedimentation within the system.

If the CRS model is applied, and tempestites are present within the dataset, it is recommended to apply either the simple or multi-marker method to increase precision. Application of reference dates to tempestite deposits is an iterative process, meaning that once the model is applied it is important to check that the ages and sedimentation rates determined correspond to the lithology present within the core. Where possible, application of more than one tracer (i.e. global impulse tracers plus tempestites) is useful for increasing the age model accuracy and resolution, as well as verification of reference dates applied to tempestite deposits.

This study highlights the importance of applying both the CIC and CRS models to high-resolution datasets to get a complete picture of sedimentation and geologic context on multiple timescales within the system.

CHAPTER 4: UTILIZING MULTI-DECADAL ESTUARINE SEDIMENT RECORDS TO DEFINE SOURCE AND THE ROLE OF STORMS ON SEDIMENT DELIVERY TO THE COASTAL OCEAN

4.1 Introduction

As the nexus between riverine and oceanic environments, estuaries play a critical role in the transport of sediment from the terrestrial to the oceanic environment. The estuarine basin has the capability of recording not only sediment flux from outside of the estuary, but sediment erosion, transport, and deposition from within the estuarine environment itself. To this end, there are numerous potential sources of sediment, both allochthonous (riverine, off-shore marine environments, anthropogenic sediment loading due to land-use variation along the estuary) and autochthonous (marsh erosion, estuarine sediment remobilization, autogenic creation of biological material) (Dalrymple et al., 1992; Figure 4.1) that pass through the estuarine system
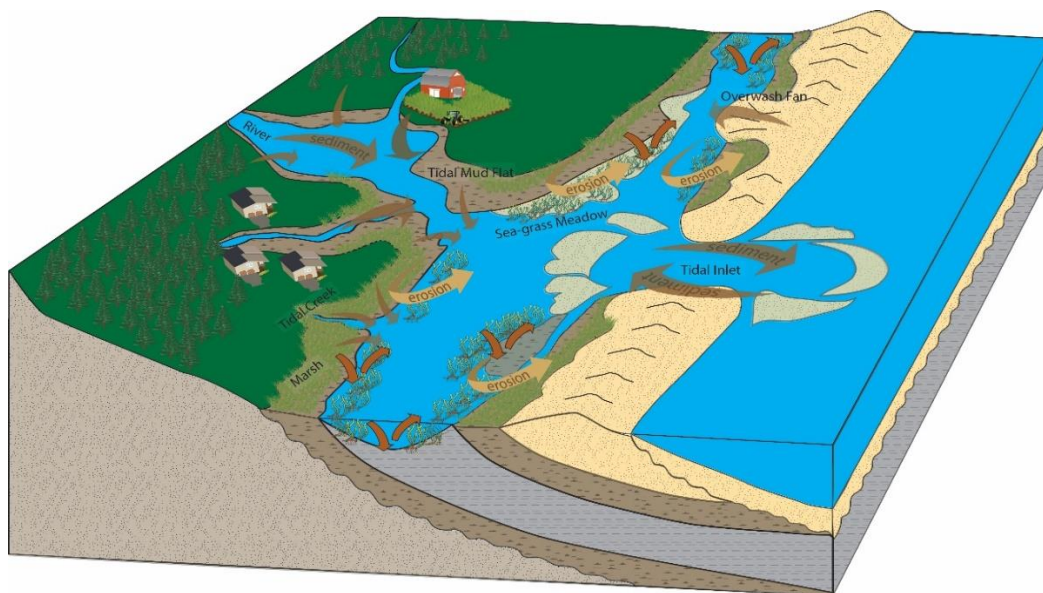
Figure 4.1 - Conceptual diagram of the sources and depositional environments within the coastal estuary (Symbols courtesy of the Integration and Application Network, University of Maryland Center for Environmental Science (ian.umces.edu/symbols/).

and have the potential to be recorded in basin deposits. Rivers flow into the estuary, carrying freshwater and terrestrial sediment into the system (Dyer, 1995; Figure 4.1). Tides and episodic storm events can wash beach and marine sediments into the estuary through wash-over fans and inlets (Figure 4.1). Additionally, population growth within and along the coastal zone has allowed for increased land modification along the estuarine shoreline, and allows for increased sediment run-off directly into tidal creeks and the estuary (Figure 4.1).

Determining the dominant source of sediment within the estuarine environment is a critical first step for understanding the erosion and transport of sediment within and through the estuarine environment over time. In addition to allochthonous sediment sources, erosion and remobilization within the estuary itself can increase the sediment load and change the shape of the estuary, causing increased fetch and a feedback loop that will exacerbate shoreline retreat (Schwimmer, 2001; Cowart et al., 2011). Estuarine shorelines are made up of fringing marshes, mangroves, mud-flats, sand-flats and sea-grass beds that border the back-barrier and mainland environments, which act as transition zones between terrestrial and estuarine systems (Figure 4.1). Through time, remobilization and erosion of these environments has largely been related to sea-level rise and wave action (Reed, 1995; Fagherazzi et al., 2006; Mattheus et al, 2010; Mariotti and Fagherazzi, 2010; Leonardi et al., 2016).

Along fringing marshes, multiple studies have shown wave energy can efficiently erode the marsh scarp edge (Fagherazzi et al., 2006; Leonardi et al., 2016). Additionally, unless sediment supply and *in situ* organic production is sufficient, sea-level rise will negatively impact marsh sustainability (Reed, 1995; Mattheus et al., 2010). Under normal conditions, sea-grass meadows reduce ambient energy and enhance sediment deposition, creating temporary repositories for sediment within the estuary. Under high-energy conditions and/or during

seasonal dieback, sediments can be remobilized from sea-grass meadows becoming a source of sediment to the estuarine basin (Robblee et al., 1991; Madsen et al., 2001). Tidal influence will impact the deposition and remobilization of sediment as well, especially on the marsh surface and along the marsh edge, as transport of material through tidal creeks impact sediment loading and flux within the estuary. Anthropogenic change due to land-use modification along the estuarine shoreline can rapidly increase the flux of sediment along the estuarine system (Mattheus et al., 2010).

The transport and source of sediment to the estuary and into the shallow-marine environment is not constant through time, which makes understanding the flux of sediment within and through the estuarine system complicated. Daily to monthly tidal fluctuations can remobilize sediment within the estuary, and seasonal variations (e.g., spring freshet, winter/summer storms, dry and wet seasons) can increase estuarine flow regimes, turbidity and overall sediment flux to and from the estuary, causing continual erosion, transport and deposition within the estuarine basin (Allen et al., 1980; Geyer et al., 2001; Fain et al., 2001; Grabemann and Krause, 2001). Over decadal to millennial timeframes, variations in anthropogenic influences (e.g., dams, land-use and cover modifications, shoreline armoring), sea level, and climate can also affect changes in sediment flux to the estuary (Patton and Horne, 1992; Small and Cohen, 2004; Poff et al., 2006; Mattheus et al., 2009; Walling 2012). Episodic events such as storms result in greater flux from rivers due to runoff, increased estuarine shoreline erosion from waves, remobilization of previously-deposited sediment on the estuary floor, and increased sediment influx from marine contributions (French and Spencer, 1993; Day et al., 1995; French, 2002; Yang et al., 2003; Ralston and Stacey, 2007; Ralston and Geyer, 2009). To this end, the type of storm is important as well. The direction and approach of a storm can impact associated

sediment sources, as well as, water-level and current-driven sediment regimes within the system. Hurricanes impact the estuary by increasing wave action, water level and flooding of adjacent environments with rain. However, the impact is often variable, and dependent on the approach, proximity and energy of the storm. Nor'easters tend to have less peak energy than tropical storms, however, the consistent wind direction over multiple days has the potential to move sediment through an estuarine system more efficiently, and impact erosion and resuspension of material on its transit to the offshore environment. Additionally, given the frequency of multiple nor'easter events during the course of one year relative to less frequent large hurricanes, it is important to consider the impact these storms have on sediment erosion, transport and deposition through the estuary.

In this work, we identify the current potential sources of material to Cape Lookout Bight (CLB) by comparing suspended sediment collected within the modern estuarine environment from two of the dominant sediment sources within Core Sound, NC, an anthropogenic (agricultural zone) and natural (fringing marsh) sediment source. We then compare the geochemical signature from these sources to current and historically-determined sediment sources in the CLB basin to evaluate if any changes in the dominant sediment source occurred through time in the system. We then compare historical hydrological and meteorological data to our established multi-decadal, high-resolution sediment accumulation rate record, available for the system from 1984-2010, to improve understanding of the mechanisms of sediment erosion and transport within the estuarine system through time. By investigating the long-term high-resolution record of sedimentation in CLB relative to known mechanisms of coastal change (sea-level rise, storms, etc.), our study identified the principle drivers of sediment transport to the marine environment.

4.2 Background and Methods

4.2.1 Sediment Source - Background

Understanding the principle sediment source within the estuarine system is critical to studies of sediment flux. In Cape Lookout Bight, NC, previous research has indicated that the fine-grained, organic material within the basin is largely derived from marsh detritus and peat, likely from erosion of the fringing marsh environments along the shoreline of Core Sound (Chanton et al., 1983; Canuel et al., 1990). However, as noted in Chapter 1 of this dissertation, a large 160 km^2 agricultural operation, Open Grounds Farm (OGF), lies directly adjacent to the fringing marshes that supply sediment to CLB, and transitioned to a large row-crop enterprise from the late 1970's to the early 1980's. It is possible that, in subsequent years, runoff from the farm ran directly into adjacent tidal creeks and added a new estuarine sediment source to CLB. It is therefore important to characterize the source of recent sedimentation to the basin and compare isotopic signatures of this sediment to previous studies that characterized the sediment source as fringing marsh.

4.2.2 Sediment Source – Methods

To further establish the principle sediment source to CLB, bi-directional TIMS samplers (described in Chapter 2) were deployed in tidal creeks adjacent to a fringing marsh and the agricultural site in Core Sound, North Carolina. The fringing marsh location (see study map in Figure 2.4 in Chapter 2 of this dissertation), represents the predominant natural environment within the coastal estuary, with high rates of fine grained suspended sediment erosion through both scarp retreat and resuspension of material along the marsh surface. The sampler deployed in the tidal creek next to the agricultural site drains overland flow from Open Grounds Farm, allowing for assessment of suspended sediment load from an anthropogenically-modified

79

environment within the tidal zone (see study map in Figure 2.4 in Chapter 2 of this dissertation).

Samplers were deployed at each location over the course of one year, from January 2013 through

January 2014, and samples were collected on a bi-monthly basis to assess grain-size, mass and

geochemical properties of the transported suspended sediment load to identify characteristics of

each proposed sediment source within the system. In conjunction, 50cm – 1 m cores were

collected from CLB for direct comparison of deposited sediment characteristics within the basin.

All samples were brought back to the laboratory for extraction, and were then freeze dried,

weighed and sub-sampled for particle size analysis. A portion of each sample was packed into

petri-dishes and analyzed for radio-isotopic signatures, including Be^7, using gamma spectrometry

methods (after Larsen and Cutshall, 1981; Olsen et al., 1986). Since Be^7 is delivered to coastal

environments from atmospheric deposition, and has a very short half-life (53.22 days), it is

assumed that runoff from the farm has a higher Be^7 concentrations than that of older, eroded

fringing marsh, which should have relatively low Be^7 concentrations. The remaining sample was

analyzed for carbon and nitrogen ($\delta^{13}C$, $\delta^{15}N$, C-N) using stable isotope analysis. Stable isotope

analysis was conducted at the Alabama Stable Isotope Laboratory (ASIL) at the University of

Alabama, using a Costech 4010 Elemental Analyzer, which was interfaced to a Thermo Delta V

Plus isotope ratio mass spectrometer with a Thermo Conflo IV. After analyzing the differences

between radio-isotopic and stable isotope signatures of sediment from the agricultural and marsh

site locations, $\delta^{15}N$ and Be^7 samples showed the most difference between sites, and are used in

comparison to the samples extracted from core sound.

4.2.3 Age Model and Sediment Accumulation Rate – Pb^{210} Age Model

The age model determined to fit the data based on tempestite deposits (established and

presented in Chapter 3) is presented as the sediment accumulation rate (SAR) for comparison to

historical datasets. The SAR record was interpolated for the entire data series to a monthly basis

for comparability to historical wind and water-level data for Cape Lookout Bight, NC. The long-

term trend in the SAR record was removed using a smoothing spline. The mean and standard

deviation was then determined for the residual SAR to identify 'sediment accumulation events'

(SAE), defined as peaks in the SAR above the mean, and 'significant sediment accumulation

events' (SSAE) that are defined as peaks in the SAR that fall above one standard deviation above

the mean. SAE and SSAE intervals are determined as half of the width (duration) between

troughs and full peak (Figure 4.7). The mass accumulation rate (MAR; g cm^{-2} yr^{-1}), determined

as the product of bulk density and SAR, is also presented.

4.2.4 Historical Datasets – Monthly Average Water-level and Wind-speed

A record of historical hurricanes that passed within 100 km of Cape Lookout Bight, NC

was determined through use of the NOAA Historical Hurricane Tracks mapping tool and are

presented with associated storm category, presented in Table 4.1.

Table 4.1 – Hurricane/tropical storm occurrence, category and date within 100 km of CLB
between 1970-2010

Storm		Date (1970-1990)	Storm		Date (1990-2000)	Storm		Date (2000-2010)
Doria	TS	8/25/1971	Bob	H2	8/19/1991	Allison	TD	6/14/2001
Ginger	H1	9/30/1971	Emily	H3	8/31/1993	Arthur	TD	6/14/2002
Agnes	TS	6/22/1972	Gordon	H2	11/18/1994	Kyle	TD	10/12/2002
Amy	TD	6/28/1975	Arthur	TS	6/19/1996	Isabel	H2	9/18/2003
Hallie	TS	10/27/1975	Bertha	H2	7/12/1996	Alex	H2	8/3/2004
Dennis	TS	8/20/1981	Fran	H3	9/6/1996	Bonnie	TD	8/13/2004
Diana	TS	9/14/1984	Josephine	H2	10/8/1996	Ophelia	H1	9/15/2005
Kate	TS	11/23/1985	Bonnie	H2	8/27/1998	Barry	ET	6/3/2007
Gloria	H2	9/27/1985	Dennis	TS	9/4/1999	Gabrielle	TS	9/9/2007
Charlie	H2	8/17/1986	Floyd	H2	9/16/1999	Cristobal	TS	7/20/2008
			Irene	H1	10/18/1999			

Water-level data was obtained by utilizing data collected from the NOAA station in

Beaufort, NC (8656483) the raw historical mean sea-level (m) hourly record from 1977-2010 were averaged to a monthly basis.

Wind-speed data was compiled and provided for Cape Lookout, NC (CLKN7) station at a 10 (m) height at an hourly basis by the State Climate Office (SCO) of North Carolina from 1984-2010. A vector average of hourly wind-speed (mps) data were averaged to a monthly basis from 1984-2010 for comparison to the long-term SAR profile.

A Welch power spectral density analysis was conducted on the detrended SAR profile, monthly wind-speed and water-level record to determine the distribution of variance as a function of frequency. A low-pass Butterworth filter was implemented on the wind-speed and water-level record for comparability to where the energy in the SAR profile appears greatest.

Low-pass water-level and wind-speed data were normalized and compared through regression analysis to the SAR profile over multi-year time periods to see if a relationship between wind-speed and water-level could be determined that would correlate with the established SAR profile.

4.2.5 Historical Datasets: Monthly Nor'Easter and Hurricane/Tropical Storm Occurrence

Hourly averaged daily wind-speed and direction data were also collected and analyzed from station CLKN7 to obtain a record of nor'easter events. Daily wind data was filtered to include consecutive days (2 days or more) with wind directions between 0-90 and daily wind speeds greater than 7 mps, to obtain a record of nor'easter events impacting the Core Sound and Cape Lookout Bight, NC from 1984-2010.

SAE and SSAE, determined from the peaks in the detrended SAR profile exceeding the mean and one standard deviations above the mean, respectively, are compared to monthly nor'easter events and the hurricane record for CLB to determine the impact different types of

storms may have on the SAR profile and therefore transport of sediment through the CLB basin.

4.2.6 Hurricane Irene Short Core Sediment Accumulation Rate

To identify the impact large storms have on sedimentation within the basin relative to normal activity, a 50 cm core was also taken before and one week after Hurricane Irene, which made landfall as a category 1 hurricane over CLB August 27, 2011. As a radioisotope with a short (53.22 days) half-life, Be^7 can be used to determine age and sedimentation rates over monthly timescales. Cores were extruded at 1-cm intervals, freeze dried, weighed and packed into petri-dishes and analyzed for Be^7 using gamma spectrometry method (after Larsen and Cutshall, 1981; Olsen et al., 1986). Be^7 inventories were established within the pre- and post-storm cores to determine the sedimentation that occurred during the storm, and compared work presented in Canuel et al. (1990) that established sedimentation determined from Be^7 inventories in CLB from 1986-1988 over a period with very little hurricane activity.

4.3 Results

4.3.1 Sediment Source

Sediment signatures for Be^7 and $\delta^{15}N$, as collected using bi-directional TIMS samplers, were different between the agricultural site relative to the fringing marsh location (Figure 4.2a). Upon comparison with the short cores, sediment deposited within the basin appears to be more strongly associated with the signatures of the fringing marsh location than that of the agricultural source (Figure 4.2b). Table 4.2 gives a list of expected $\delta^{15}N$ from salt-marshes, salt-marsh sediment and CLB. Further analysis of the $\delta^{15}N$ values for the long-core in CLB and the previously established dataset for the basin show $\delta^{15}N$ values consistent with values established in previous studies (Ream, 1997; Table 4.2). Given that previous work (Haddad and Martens, 1987; Canuel and Martens, 1993; Ream, 1997), also indicated the predominant source to the
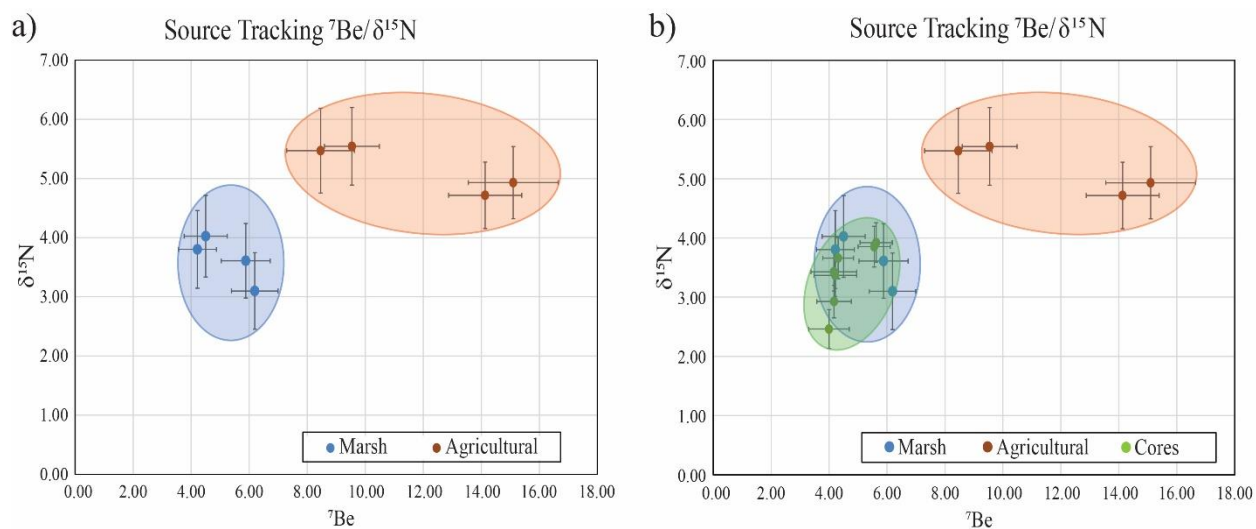
Figure 4.2 – Sediment source tracking using values of Be[7] relative to $\delta^{15}N$ to define sediment characteristics in a) the agricultural and marsh site locations from bi-directional TIMS sampler and b) comparison of the defined sediment characteristics at each source relative to sediment collected from short cores in CLB to characterize the source of sediment to the basin through time

Table 4.2 – Measured $\delta^{15}N$ values presented in previous work from marsh deposition and total suspended organic matter (SOM) (Couch, 1989; Currin, 1995), and sediment cores in CLB (Ream, 1997)

Sample Type	$\delta^{15}N$ (‰ AIR)	Source
Spartina alternaflora		
Live	3.9	Currin (1995)
Live	4.3	Couch (1989)
Standing Dead	2.9	
Detritus	2.8	
Total SOM	4.3	Couch (1989)
CLB Cores		
Core 1 (Avg)	4.0	Ream (1997)
Core 2 (Avg)	4.0	
Core 3 (Avg)	4.3	

basin is from natural sources (i.e. fringing marshes, sea-grass beds, algal/microbial alteration), it

is likely that the sediment source has remained consistent through time.

4.3.2 Sediment Accumulation Rate (SAR) Profile

Figure 4.3a and b presents the raw and interpolated SAR profile calculated in Chapter 3

of this dissertation.   As described in Chapter 3, high variability is present within the SAR

profile, indicating changes through time in the sediment accumulation rate. In addition to

fluctuations in the SAR profile on the monthly to annual time-scale, there is a long-term, multi-

year trend in the dataset, which was characterized by applying a smoothing spline to the data

(Figure 4.3b). Finally, the mass accumulation rate (MAR; $g \ cm^{-2} \ yr^{-1}$) is presented in figure

4.3d. The long-term trend in the MAR profile appears similar to the long-term trend identified in

the SAR profile, there are differences in the magnitude of the peaks in the MAR profile relative

to the SAR profile. Since MAR integrates mass, dry bulk density and sedimentation, the

observed differences in the SAR and MAR profiles are likely the result of changes in sediment

distribution and porosity within the core lithology.

Figure 4.3 – a) Raw sediment accumulation rate (SAR; cm mth^{-1}) profile relative to time; b) Monthly interpolated SAR profile with long-term trend identified using smoothing spline shown in green; c) Detrended (identified long-term trend removed) interpolated SAR profile; d) Mass accumulation rate (MAR; g cm^{-2} yr^{-1}) determined through SAR and bulk density.

To get a better idea of the amount of sediment deposition within the core through time and the impact of different types of sediment on the mass within the MAR profile, the MAR (g cm^{-2} yr^{-1}), is presented relative to the grain-size density diagram and storm occurrence in Figure 4.4. When we compare the grain-size density profile and the MAR relative to time, a similar trend is present. Concentrations of sand decrease after Hurricane Ginger, and then appear to
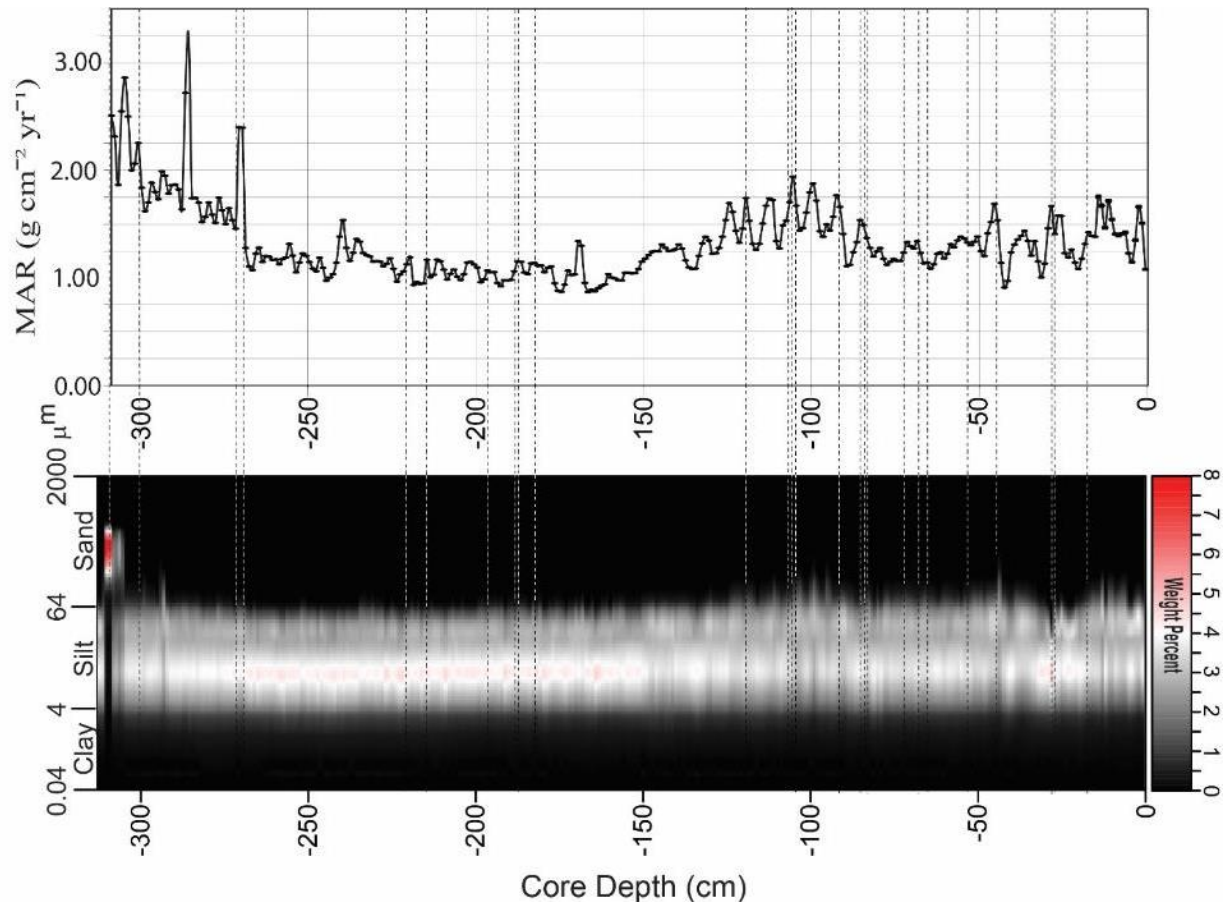
Figure 4.4 – Mass accumulation rate (MAR; g cm^{-2} yr^{-1}) profile relative to the grain-size distribution diagram throughout the depth of the core, with hurricane/tropical storm occurrence within the core noted by lines. This graphic depicts how the grain-size distribution within the core impacts the long-term trend present in both the MAR and SAR profiles through time, likely as a result of changing trapping efficiency within the basin through time.

increase in the late 1980's to early 1990's, with peaks in concentration that correlate to large storms, especially Hurricane Ophelia in 2005. The long-term trend in the profile for both the

SAR and MAR correlates well with the apparent shift in the lithology to slightly coarser

sediment through time, moving from predominantly silt to coarser silt and very fine sand in the

upper part of the profile. It is likely that this shift toward the upper part of the profile is related

to increased trapping efficiency within the basin.

4.3.3 Monthly averaged Water-level, Wind-speed and SAR Profile

In comparing the detrended SAR record to the monthly averaged wind-speed and water-

level records, no consistent relationship appears to be present. A Welch power spectral density

analysis, which partitions variance in the frequency domain, was generated using the monthly

water-level, wind-speed and interpolated detrended SAR profile data through time (Figure 4.5a).
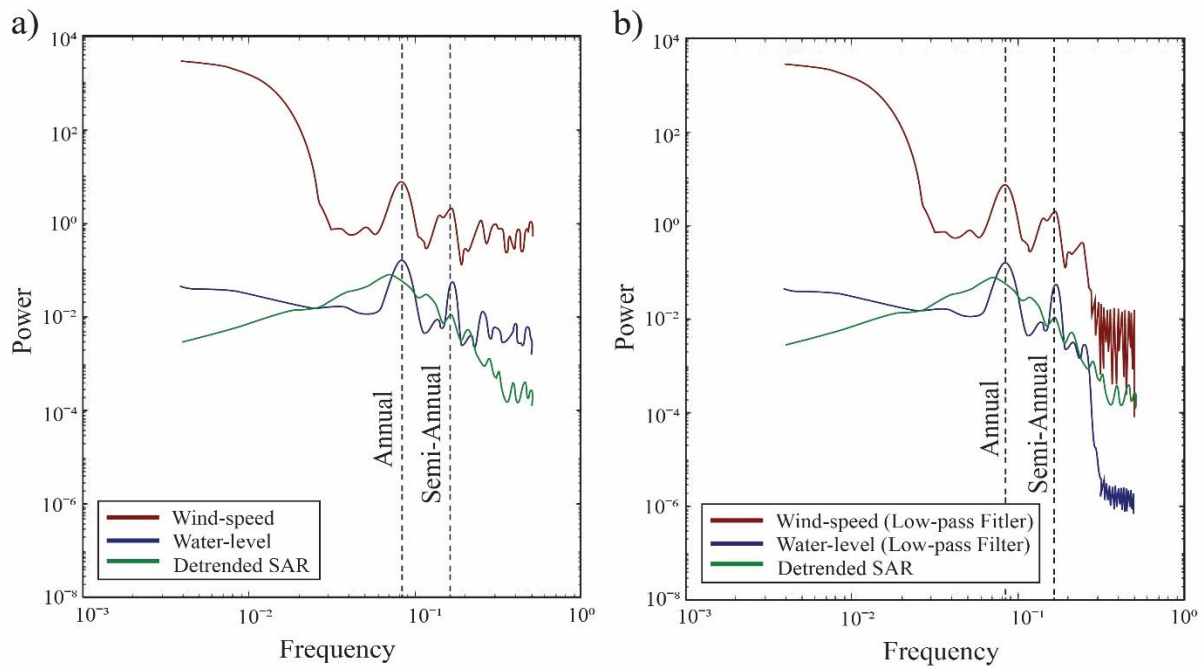
Figure 4.5 – Welch power spectral density analysis for a) monthly averaged wind-speed, water-level and monthly interpolated detrended SAR data; b) Welch power spectra of the Butterworth low-pass filter wind-speed and water-level record, used to remove the signal at 3 months or less, compared to the detrended SAR monthly interpolated dataset.

From the power spectra, the detrended SAR may have some 6-month to multi-year

timescale signal, but does not appear to show strong a strong frequency of repeatability in the

monthly dataset, whereas both wind-speed and water-level appear to show strong monthly,

seasonal and annual signals within the data. For comparability to the apparent energy in the

detrended SAR record, a Butterworth low-pass filter was applied to both the wind-speed and

water-level record to remove frequencies higher than a 3 month cycle in the data (Figure 4.5b).

The low-pass water-level and wind-speed data were then normalized, compared (Figure 4.6) and

analyzed in both an additive and interactive model using a multiple linear regression analysis

relative to the de-trended interpolated SAR profile. Both the additive and interactive models for
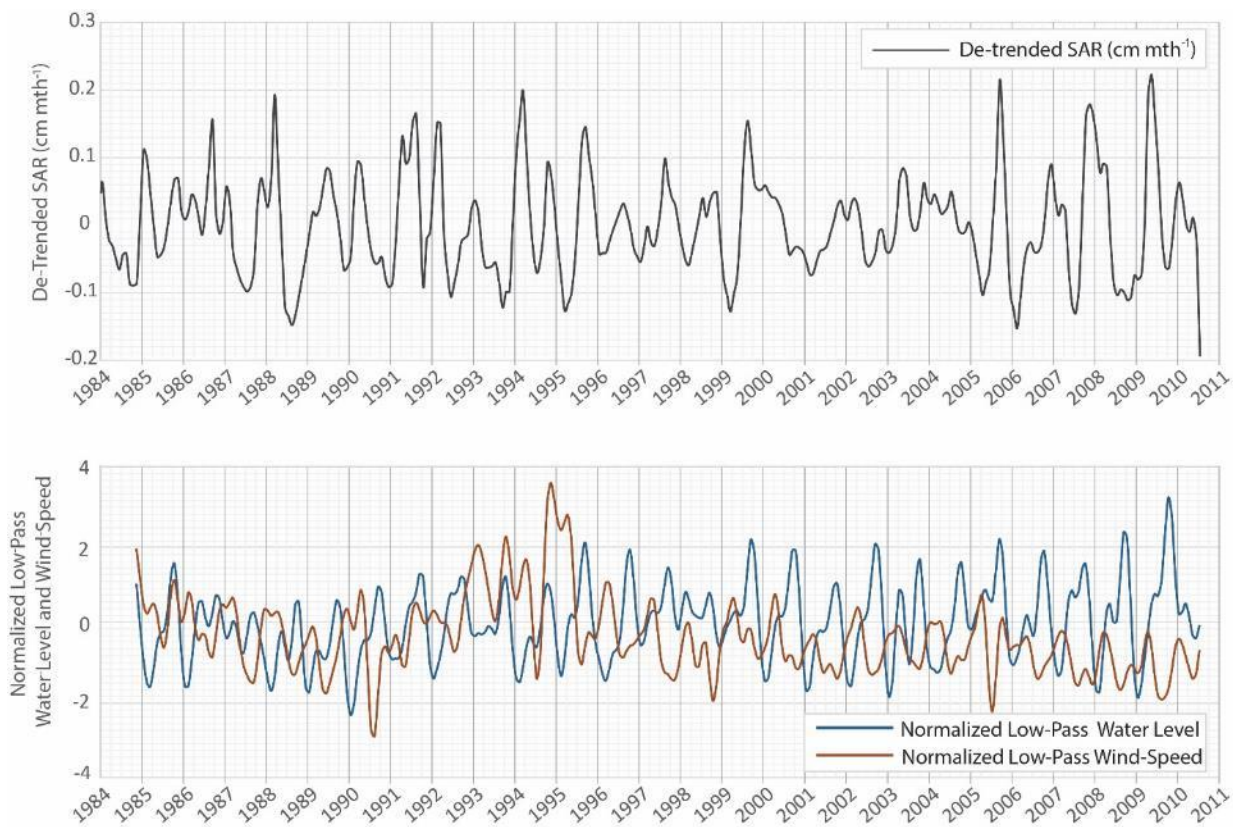
Figure 4.6 – (Top to bottom) Detrended monthly interpolated SAR profile through the
resolution of the historical wind-speed and water-level record near Cape Lookout Bight
(CLB), NC (1984-2010), relative to the normalized low-pass filtered wind-speed and
water-level record for CLB, showing that wind-speed and water-level move in and out
of phases with the detrended SAR record through time.

the filtered and normalized water-level and wind-speed data had low R^2 values of <0.1,

indicating that a quantitative relationship between wind and water-level explains less than 10%

of the SAR profile. Monthly averaged water-level and wind-speed data move in and out of phase

with the interpolated SAR profile, making a consistent simple relationship between monthly

water-level and wind-speed with the detrended SAR profile unlikely (Figure 4.6).

4.3.4 Sediment Accumulation Rate Events in SAR Profile

To identify and understand peaks in the SAR profile and the recurrence interval of these

events, peaks in the detrended SAR profile were identified as either 'sediment accumulation

events' (SAE) or 'significant sediment accumulation events' SSAE if they peaked above the

mean or one standard deviation above the mean (respectively; Figure 4.7). Within the detrended
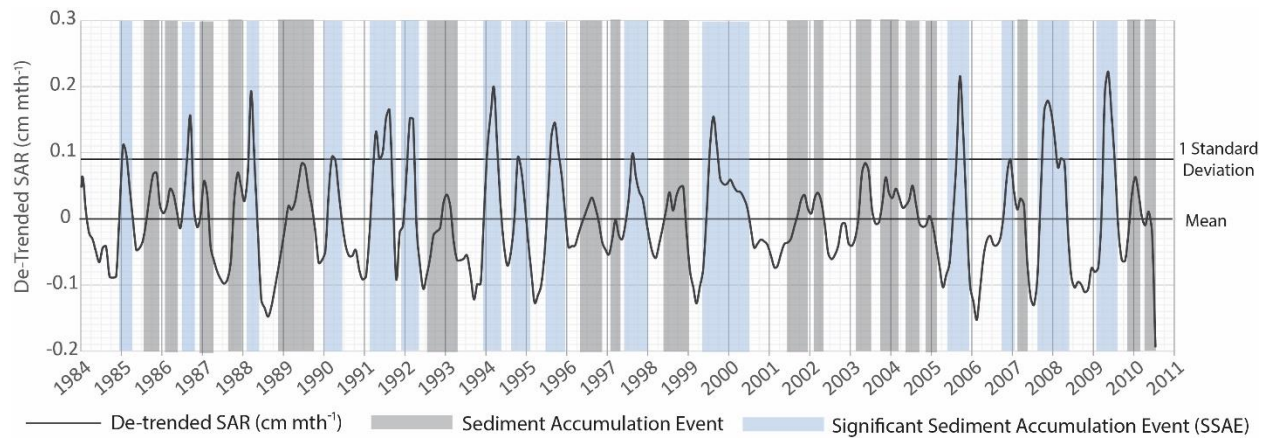
Figure 4.7 – Detrended SAR profile, with sediment accumulation events (SAE) defined as
any peak above the mean, and significant sediment accumulation events (SSAE) defined as a
peak one standard deviation above the mean; Peak determination for SAE and SSAE are
characterized by the full peak and half the width of the peak for each event.

SAR profile from 1984-2010, 33 SAE are identified, 15 of which are considered SSAE. There is

a recurrence interval of ~1 yr (+/- 0.25) between SSAE, marking significant peaks in the

accumulation rate, and between all SAE peaks, a recurrence interval of ~0.5 yrs (+/- 0.1). This is

consistent with the recurrence interval expected based on the Welch spectra for the detrended

SAR profile, and may explain why the peaks in the frequency domain were not as clear in the

Welch spectra due to the fact that the recurrence interval is not consistent between events

through time. This suggests that peaks in the SAR profile are not the result of predictable

monthly or seasonal trends within the data, but are instead the result of episodic events, like

storms.

4.3.5 Hurricane Irene Short Core

In 2011, Hurricane Irene made landfall over Cape Lookout Bight on August 27th as a

strong category 1 hurricane. Be^7 inventories for cores taken pre- and post- hurricane Irene were

calculated and utilized to determine sedimentation within the basin over the course of one week,

and presented in Figure 4.8. Based on the calculated new inventory of Be^7 that occurred after the
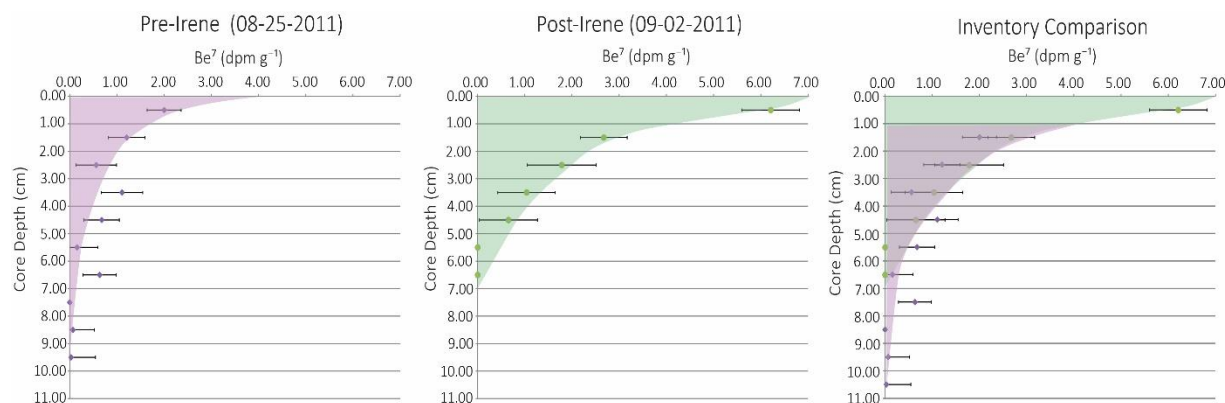
Figure 4.8 – (From left to right) Inventories of Be^7 obtained from pre- and post-
Hurricane Irene short cores in CLB, and comparison of Be^7 inventories indicating 1-cm
of sedimentation in the week after the storm

storm, ~1 cm of sediment was deposited during and in the week following Hurricane Irene.

When considering the SAR profile, this deposition represents what would be considered a SSAE.

This indicates the potential for relatively instantaneous sedimentation and flux of sediment

through the basin to the ocean during a large storm event impacting the system.

4.3.6 Storm Record and SAR Profile

To understand the role of storms on the SAR profile, a record of nor'easter events by

month was compiled from wind-speed and direction data for Cape Lookout (characterized as 2 or

more consecutive days, 0-90° wind directions and wind speeds greater than 7 mps) and

hurricane/tropical storm activity from 1984-2010. The storm records are compared to the

detrended SAR profile with marked SAE and SSAE peaks in Figure 4.9a. Correlations between

shaded areas where SAE and SSAE peaks are present and nor'easter or hurricane occurrence are

made through qualitative visual inspection, where increased storm activity occurs relative to the

surrounding, non-SAE or SSAE time periods. Of the 33 SAE and 15 SSAE peaks, 32 SAE and

14 SSAE are directly associated with months of either intense nor'easter activity or

hurricane/tropical storm influence to the system. Section 4.9b shows the lows in the SAR profile

(troughs in the SAR profile that fall below the mean). Of the 29 lows in the SAR profile

identified, 22 (76%) are associated with months of decreased nor'easter activity.

As a comparison, a profile of consecutive (2+) days of wind-speeds greater than 7 mps,

regardless of direction, is compared to the SAR profile relative to SAE, SSAE (4.9c) and lows in

the SAR profile (4.9d) through the same qualitative analysis of increased or decreased wind

activity relative to surrounding months described above is implemented. The relationship

between peaks in the SAR profile (SAE and SSAE) and lows in the SAR profile relative to wind-

speed appears to move in and out of phase, with many months with multiple days of increased

wind-speeds occurring during periods of low sedimentation rate within the SAR profile (4.9d).

Of the 33 SAE and SSAE identified, 24 show an association with peaks in consecutive days with

wind-speeds greater than 7mps (72% correlation), and 15 out of the 29 troughs (52%) are

associated with decreased high-wind activity. There are also places where SAE or SSAE events

are located that are not only not associated with the record of consecutive days with 7mps wind-

speeds or greater, but appear to have an inverse relationship to the wind-speed profile. This

qualitative comparison suggests that both storm energy and direction, (i.e., prolonged periods of

increased wind-speed from a north-easterly direction) are more closely correlated with peaks in
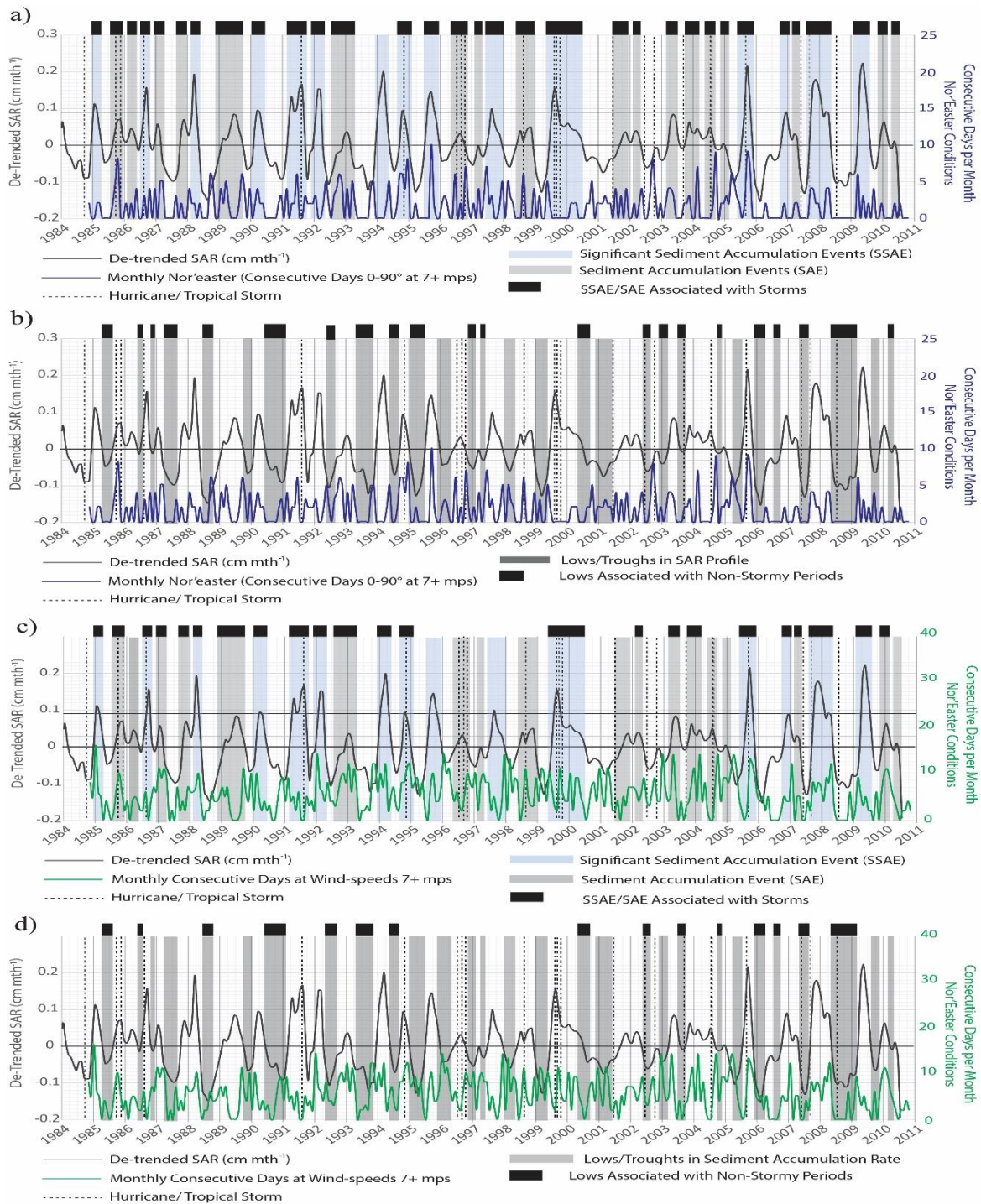
Figure 4.9 – Historical hurricane occurrence and monthly Nor'easter activity (2+ consecutive days of wind-speeds greater than 7mps and 0-90° wind-directions) and qualitative association (shown along the top of the graph) relative to a) SAE and SSAE peaks and b) lows in the SAR profile that fall below the mean (non-stormy periods); c) Comparison of SAE and SSAE peaks relative to all days in the month with consecutive days (2+) of wind-speeds greater than 7mps (regardless of direction) and d) lows in the SAR below the mean relative to all wind-direction 7mps profile.

93

the SAR profile than simply prolonged periods of increased wind-speed alone. However, the relationship between wind-speed, direction and peaks in the SAR profile is not completely consistent. At times the peaks in the SAR profile correspond directly to storm influence, yet there are some SSAE peaks a quarter to half a year after the peak in nor'easter activity. There are also places in the profile where nor'easter activity or hurricane/tropical storm activity is present, but a corresponding or expected SSAE is not present.

4.4 Discussion

4.4.1 Sediment Source

Analysis of recently deposited suspended sediment within the CLB basin and comparisons to a newly established agricultural source of OGF and the established fringing marsh source indicate a strong correlation to the established fringing marsh or sea-grass sediment source to the basin. Comparison to previously established isotopic signatures in the basin for $\delta^{15}N$ verify the correlation to the fringing marsh source, with little indication of a new agricultural source to the basin. Although it is likely that suspended sediment from the land-use modification along the estuarine shoreline, including from the agricultural source, is entering the estuary, the predominant source of sediment to the basin appears to be from erosion of the fringing marsh scarp or remobilization from sea-grass beds through time. Although other sediment sources are present within the estuarine system and could impact the SAR through time, it is likely that these sediment sources have at least temporary residence in sediment repositories within the system, like sea-grass beds or the surface of the marsh, and therefore change their isotopic signature before deposition in CLB. Given that the predominant source of sediment to the basin has remained consistent through time, it can be assumed that changes in the rate of sedimentation through time are not primarily associated with changes in sediment

94

sources, but instead are the result of disconnected processes of erosion, resuspension and transport of material from the existing source within the system, marshes and sea-grass beds.

4.4.2 Sediment Accumulation Rate Record

The SAR record is not constant through time, as was suggested from the CIC model results from Chanton et al. (1983) and work presented in Chapter 1 of this dissertation. Instead, when sedimentation is examined with higher temporal resolution, the SAR record shows high variability through time, with peaks in the record that indicate multiple periods of increased sedimentation at the CLB site, as our core from CLB sampled the sediment flux from the overall estuary through the basin to the ocean. As discussed previously, sediment source tracking within the system does not indicate a new source of sediment from land-use modification within the system, as was suggested as a possible source of increased sediment flux in Chapter 1, but instead indicates that the predominant source of sediment within the basin carries the signature of marsh or sea-grass beds. This is similar to the results of previous studies that indicate the dominant source and signature of sediment is from natural sources within the estuary (i.e. fringing salt-marshes, sea-grass beds, or algal/microbial alteration; Canuel and Martens, 1993). This means that the sediment flux within the basin is likely a result of remobilization, erosion and transport of material from within the estuary through the basin to the coastal ocean.

These variations in the SAR record are also not consistent through time. They do not follow a strictly monthly or seasonal variation. Erosion of material along the estuarine shoreline is largely a result of wave-action and tidal influence, with wave-action driven by wind-speed and direction, especially during storms working to remobilize sediment along the shoreline (Fagherazzi et al., 2006; Leonardi et al., 2016). Additionally, variations in water-level through tidal variation, seasonal and annual variations in water-level variation or long-term sea-level rise

impact sediment erosion and the suspended sediment load on a constant basis (Mariotti and Fagherazzi, 2010). At a simplistic level, monthly wind-speed and water-level should capture this interaction and, as shown in Figure 4.5, have consistent seasonal and annual trends. However, when we compare records of wind-speed and water-level to the SAR record, no consistent relationship, either separately or interacting, appears to be present within the record. It is also likely that monthly wind-speed and water-level cannot fully capture on their own the influence of wave regime within the estuary, especially when we consider high-energy, short term storm influence that may not be captured in the monthly averaged wind-speed and water-level record. To capture this quantitatively, wave models may give a better indication of changes within the basin through time, but semi-quantitative analysis of storm occurrence relative to the SAR profile, discussed later, does indicate a relationship to the SAR profile.

What is apparent is that at least part of the reason for a lack of direct correlation could be because the wind-speed and water-level records reflect instantaneous conditions, whereas the SAR record integrates variations in the sediment supply, transport and retention of material, as sediment flux may have lag periods or be deposited temporarily on transit to the basin. As such a direct correlation between water-level and wind-speed and the SAR profile is unlikely, as erosion, transport, deposition and accumulation processes, which are all integrated in the SAR profile, may not always be contemporaneous within the system.

It is important to acknowledge that another possibility for the lack of correlation between the SAR profile and that the instantaneous measurement of physical processes (i.e., wind-speed and water-level) are uncertainties within the age model itself. An error within the age mode of between 1-3 months is possible, and will impact the timing and magnitude associated with the SAR profile. It is likely that age model uncertainty contributes, at least in part, to the disconnect

between the SAR profile and instantaneous measures of physical data in the historical record.

4.4.3 Storm Influence – Impact of Storm Direction on Sediment Transport

Although a quantitative relationship through time-series analysis could not be established between the SAR record and the historical dataset, a qualitative assessment of storm occurrence relative to the SAR profile indicates the potential that sediment flux to the basin through time may be associated with high-energy events. These events could remobilize and flush sediment from temporary repositories (i.e., fringing marshes, sea-grass beds, mud-flats, etc.) into the basin and onward to the coastal ocean. In the SAR profile, it appears that high-energy events like storms transport sediment through the basin, and are responsible for the majority of SAE and SSAE present in the SAR profile. However, it also appears that the directionality of the storm has a large impact on whether an SAE or SSAE will be recorded in the profile. Hurricanes, have a clear impact on the wave dynamics, water-level, precipitation and erosion within the estuary, and many studies have shown the clear role hurricanes have on sediment erosion and transport within and through the estuary (Collins et al., 1999; Turner et al., 2006; Tweel and Turner, 2012; Tweel and Turner, 2014; Smith et al., 2015; Bost, 2016). However, hurricanes are short term, relatively infrequent events, and not all hurricanes are associated with either SAE or SSAE within the SAR profile. Hurricanes with the specific approach and energy needed to move sediment within the estuary do not occur every year, and cannot explain the recurrence interval of SAE or SSAE events within the SAR profile.

Nor'easter events, which impact the mid-Atlantic states each year, are counter-clockwise rotating cyclonic events that are characterized by strong winds that blow from the north-east to the southwest. Nor'easters, like hurricanes, are generally associated with heavy precipitation, and often cause increased flooding and erosion in and near the coastal zone. Although the wind and

wave energy associated with such storms may not be as great as a large hurricane, they are often characterized by multiple days of direct north-easterly wind directions. Nor'easters can occur anytime during the year, but are strongest during winter months (November to March) and occur much more frequently than large hurricane impacts. In our record of nor'easter events (defined as consecutive days of 7 mps wind speeds at 0-90 degrees wind direction) there is an average of 8 significant nor'easter events per year.

Figure 4.10b shows the SAE and SSAE that are associated with different types of storm events. Of the 14 SSAEs identified as being related to storm influence, 9 are associated only with nor'easter activity, and not hurricanes, and an additional 12 SAEs are associated with only nor'easter activity. Of the hurricanes that impact the system, only one peak is associated strongly with only hurricanes and does not correlate directly with nor'easter activity. This extended peak is correlated with Hurricanes Dennis, Floyd and Irene in 1999, historically intense hurricanes which previous work has shown were responsible for causing significant sedimentation and flushing in the New River estuary (Bost, 2016). Of the 33 SSAE and SAE peaks, 31 are associated with either nor'easter or nor'easter and hurricane occurrence, and 21 of those peaks are associated with only nor'easter activity (Figure 4.10b). These results indicate a relationship between storm type and direction relative to increases in the sediment accumulation rate. Results from the sedimentation associated with Hurricane Irene in 2011 further substantiates the idea that hurricanes with specific directions can nearly instantaneously impact sedimentation and sediment flux to the coastal ocean.

When SSAE and SAE with associated storm are plotted against the core profile, of the 197 cm represented during the historical storm record for CLB, 155 are directly related to storm
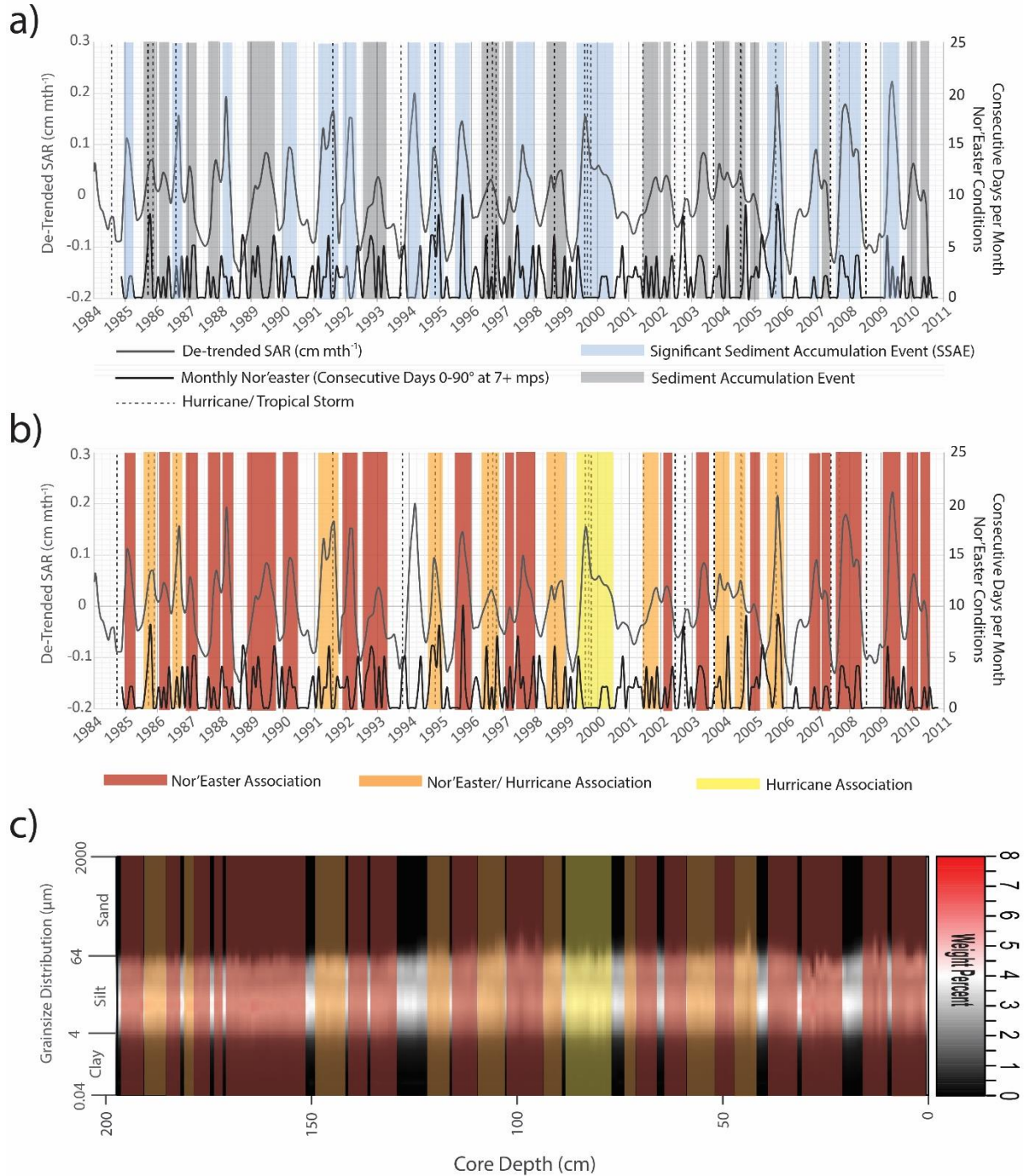
Figure 4.10 a) Record of SAE, SSAE, monthly nor'easter and hurricane activity b) SAE and SSAE peaks with storm association as nor'easter, nor'easter and hurricanes or hurricanes alone and c) Sediment grain-size distribution profile and core depth relative to associated storm influence based on timing within the SAR profile, used to define percentage of the core qualitatively assessed to be associated with deposition during different types of storm events within the system.

99

influence, meaning that 79% of the sediment profile in CLB is directly related to storm influence (nor'easters and hurricanes). Of the 155 cm related to storm deposition, 99 cm are the result of nor'easters alone, and 46 cm the result of nor'easter and hurricane activity, equivalent to 50% of the sediment profile as the result of nor'easter activity, and 23% nor'easter and hurricane activity. In the sediment profile, 10 cm are related to storm deposition from Hurricane Floyd, Dennis and Irene in 1999, representing ~5% of the sediment profile. It is clear from this analysis that the vast majority of sedimentation within the profile represented during deposition within the historical profile is related to storm influence, and more directly, deposition during storms with north easterly wind direction for multiple days.

In Core Sound, winds that dominate from the northeast at high-speeds over multiple days likely flush water and sediment down the estuary, transporting sediment from the estuary through CLB to the coastal ocean (Wells, 1988; Canuel and Martens, 1993). Canuel et al. (1990) indicated similar findings for the transport of material and sedimentation into CLB, showing enhanced delivery of particulate matter to the bight as a result of meteorological drivers during predominantly north-northeasterly wind conditions. In work presented in Wells (1988), currents were also shown to be enhanced through CLB during nor'easter activity, and thought to enhance the delivery of sediment through the basin and into the coastal ocean (Canuel et al., 1990). This indicates that storm direction, in addition to increased wind and wave energy associated with the storms appears to dictate the presence of a SSAE event, and therefore the flux of sediment through Core Sound from repositories, through CLB, and out into the coastal ocean.

4.4.4 Estuarine Buffers and Sediment Flux

As discussed previously, although there appears to be an association between sediment accumulation within CLB and storm occurrence, this relationship is not always consistent

through time, and there are some times where the SSAE peaks a quarter to half a year after the storm event. As discussed earlier, error within the age model could be responsible for some of this disconnect. Another possible explanation is that there could be buffers within the estuary that could impact when sediment is able to move through the system. Buffers within the estuary could impact when and how much sediment can be delivered during storm events into the estuary, buffering the connectivity between estuarine sediment source and eventual sink in the basin and coastal ocean. Potential buffers could be physical features (sand bars, barriers, tidal flats, mud- or sand flats, etc.) or biological (sea-grass beds, marshes) that prevent sediment from moving directly from one position to another.

There are clear physical buffers that appear to dictate the lithologic profile within the CLB core. After 1971 Hurricane Ginger, the % sand within the lithologic profile is greatly reduced, likely as a result of increased width and elevation of the sand spit surrounding CLB, which prevents overwash of marine sediment into the basin, making the dominant source estuarine (as discussed in Chapter 1). However, between 1988-1998, there is a small increase in the MAR profile, with a transition to slightly coarser silt to very fine sand. Peaks appear closely related to storm influence within the system, although it is possible that changes in the geomorphology within the basin (like a sand bar along the inlet eroded between 1988-1998), could impact the trapping efficiency and buffer the sediment flux to the basin. It is likely that the long-term trend observed within the SAR and MAR profiles are related to changes in the trapping efficiency within the basin due to geomorphic changes within the basin.

Biological buffers within the system could also impact the flux and distribution of sediment within the estuary prior to transport through the bight into the coastal ocean. Sea-grass beds have been shown to greatly impact the transport and deposition of sediment within the

estuarine system (Madsen et al., 2001). Sea-grass beds have the potential to attenuate wave energy during large scale events, preventing erosion along the marsh scarp, and allowing for the deposition of fine-grained sediment as a temporary repository within the basin. Nearly 2000 ha of seagrass beds are present within Core Sound (Kelly et al., 2001), making it likely that these systems could act as buffers to sediment transport during storms. Like sea-grass beds, the marsh surface could be a potential repository of sediment. During high-tides, suspended sediment is moved onto the surface of the marsh, and deposits on the marsh surface as a result of the grasses that reduce energy along the marsh surface. The remobilization of sediment from the marsh surface is difficult due to cohesion of fine-grained sediment on the surface of the marsh and the increased energy needed to remobilize this sediment.

Like physical barriers, the removal of these biological buffers will impact the ability to remobilize temporarily deposited material to the basin during large storm events. For example, sea-grass bed die offs, which can result from storm influence, anthropogenic disturbance or changes in water quality, have been associated with increased suspended sediment flux. Sea-grass beds can reduce wave energy and allow fine-grained sediment to fall out of suspension and be deposited within the sea-grass bed. When these biological features are removed, energy that would normally be dissipated within the sea-grass bed (i.e. wave action, tidal action, etc.) directly impacts the deposited sediment, allowing for this sediment is available for remobilization and movement within the system (Robblee et al., 1991; Madsen et al., 2001). These buffers are likely to make the transport of material within the coastal estuary more complex; possibly explaining the variation in correlation between high-energy storm events and observed increases in sedimentation rates.

4.5 Conclusions

Understanding the timing and source of sediment through the estuarine environment, especially during estuarine flushing events, is critical to our understanding of sediment delivery to the coastal ocean. The source of sediment to CLB appears to be largely associated with natural sources within the estuary (i.e., marshes, sea-grass beds, and appears to be relatively consistent through time, indicating that changes in the sedimentation rate through time are driven by physical mechanisms that remobilize sediment within the estuary rather than a new source.

In the literature, hurricanes/tropical storms have been shown exhibit strong controls on sediment delivery both within and from the estuarine environment (Collins et al., 1999; Turner et al., 2006; Tweel and Turner, 2012; Tweel and Turner, 2014; Smith et al., 2015; Bost, 2016). Although large storm events, like hurricanes, clearly impact the promotion of sediment erosion, transport, deposition within and through the estuarine environment, the frequency of these events are at multi-year to decadal timescales rather than annual events. The recurrence interval of sediment accumulation events (SAE) and significant sediment accumulation events (SSAE) within the CLB core is between ~0.5-1 yr., indicating much more frequent sedimentation than can be explained by hurricane events alone. Since the occurrence interval of nor'easter activity within CLB and relationship to sedimentation events within the CLB core would suggest that more frequent, less intense storms may play a role in sediment erosion and transport through the estuarine system, and that directionality may play an important role in the sediment transport through the system. The relationship between sediment erosion and transport within the estuary is more complicated than just storms driving sedimentation, and buffers (i.e., biological and physical) likely play an important role in when and where sediment delivery occurs. However, sedimentation within the CLB core suggests the potential more frequent flushing events of the

estuary occur, and that more frequent, less intense storms, like nor'easters, may play an important role in the delivery within the estuary to the coastal ocean. This finding correlates well with theoretical and quantified models of estuarine erosion within the estuary and along coastal fringing marshes (Leonardi et al., 2016) and with previous work in the CLB basin that suggests nor'easters may play an important role in the delivery of sediment from the estuary to basin (Canuel et al., 1990). The sediment record presented in this work corroborates these findings at a high-frequency, intra-annual basis over multi-decadal timescales. This work indicates that estuarine sediment flushing events occur at potentially annual timescales, indicating that sediment flux occurs not only during high-energy, multi-year to decadal events like hurricanes, but at annual timescales. Future work should focus on further quantification and timing of estuarine sedimentation events and the role that frequent storms, like nor'easters play on the estuarine sediment flux.

APPENDIX

Analyzed data for core CLB-10-6 are presented in the following table, including sampling interval, sample weight (mg), excess [210]Pb (dpm g[-1]), excess ^{210}Pb accounting for sand content ('No Sand'), grain-size percent by category (sand, silt, clay), organic and porosity information for the entirety of the core.

Depth (cm)	Sample Mass (mg)	Excess Pb-210 (dpm g⁻¹)	Excess Pb-210 (No Sand)	±	Yield (%)	Sand (%)	Silt (%)	Clay (%)	Organic (%)	Porosity (φ)
0.5	1560	9.35	9.59	0.02	44.61	2.31	88.17	9.52	11.57	0.81
1.5	1570	6.76	7.12	0.01	53.24	4.63	87.39	7.98	9.45	0.77
2.5	1530	7.37	8.01	0.02	46.65	7.26	85.42	7.32	6.38	0.75
3.5	1580	9.97	10.54	0.02	58.18	5.05	86.1	8.85	9.44	0.79
4.5	1570	11.07	11.27	0.02	59.54	1.67	88.82	9.51	10.81	0.81
5.5	1530	8.85	9.01	0.01	67.73	1.64	88.06	10.3	6.14	0.80
6.5	1520	7.63	8.47	0.02	51.01	9.1	82.21	8.69	8.59	0.78
7.5	1540	8.25	9.11	0.02	44.70	8.75	82	9.25	9.32	0.77
8.5	1580	7.91	8.61	0.02	44.03	7.45	83.47	9.08	9.24	0.77
9.5	1530	8.34	8.88	0.02	50.85	5.71	85.04	9.25	9.34	0.79
10.5	1540	6.32	7.03	0.01	51.94	9.16	81.91	8.93	8.48	0.77
11.5	1580	6.50	7.24	0.02	55.10	9.38	81.26	9.36	7.08	0.77
12.5	1560	9.19	9.42	0.02	43.36	2.23	86.08	11.69	10.68	0.81
13.5	1520	4.35	5.15	0.01	48.14	13.62	77.09	9.29	5.65	0.70
14.5	1560	8.07	8.70	0.02	54.27	6.66	82.71	10.63	8.04	0.78
15.5	1540	8.21	8.82	0.02	51.19	6.4	83.96	9.64	9.57	0.77
16.5	1560	7.89	8.53	0.02	49.03	6.93	83.62	9.45	8.60	0.77
17.5	1520	7.91	8.38	0.02	42.80	5.15	85.41	9.44	8.49	0.78
18.5	1530	9.40	9.84	0.02	55.30	4.22	85.07	10.71	9.29	0.80
19.5	1550	10.15	10.43	0.02	54.46	2.51	86.18	11.31	8.82	0.80
20.5	1560	11.27	11.49	0.02	56.29	1.86	85.59	12.55	10.94	0.81
21.5	1580	9.08	9.27	0.02	59.56	1.87	87.4	10.73	9.86	0.79
22.5	1540	9.39	9.43	0.02	55.15	0.38	88.01	11.61	9.89	0.80
23.5	1550	10.34	10.37	0.02	50.36	0.27	88.89	10.84	12.30	0.83
24.5	1590	8.63	8.74	0.02	56.64	1.15	88.56	10.29	11.11	0.81
25.5	1580	5.89	6.13	0.01	58.04	3.51	86.58	9.91	7.54	0.76
26.5	1550	8.64	8.67	0.02	57.37	0.35	87.74	11.91	8.94	0.80
27.5	1530	7.62	7.88	0.02	42.45	2.99	86.05	10.96	6.85	0.78
28.5	1550	6.04	6.04	0.01	54.04	0	86.22	13.78	10.64	0.77
29.5	1570	9.78	9.82	0.02	49.11	0.37	87.47	12.16	10.96	0.82

30.5	1550	10.38	10.55	0.02	50.90	1.56	86.09	12.35	12.03	0.82
31.5	1580	12.12	12.32	0.02	41.28	1.57	86.7	11.73	12.71	0.84
32.5	1560	7.37	7.53	0.02	47.38	1.93	85.92	12.15	10.06	0.78
33.5	1520	9.09	9.49	0.02	49.78	3.99	84.91	11.1	11.11	0.79
34.5	1580	8.94	9.33	0.02	43.53	3.91	85.27	10.82	9.81	0.80
35.5	1530	7.08	7.52	0.02	51.45	5.34	84.67	9.99	9.71	0.77
36.5	1540	7.66	8.18	0.02	47.15	5.92	84.49	9.59	9.63	0.78
37.5	1580	7.46	8.00	0.02	50.45	6.16	85.35	8.49	9.00	0.77
38.5	1580	7.91	8.52	0.02	48.45	6.61	83.88	9.51	8.67	0.76
39.5	1560	7.93	8.52	0.02	52.64	6.35	83.42	10.23	10.02	0.77
40.5	1510	9.10	9.44	0.02	53.48	3.31	84.93	11.76	10.75	0.77
41.5	1540	12.93	13.36	0.02	49.49	3.1	84.2	12.7	11.89	0.80
42.5	1550	10.21	10.84	0.02	59.09	5.46	83.17	11.37	10.21	0.79
43.5	1550	7.88	8.39	0.02	50.71	5.62	83.76	10.62	9.19	0.76
44.5	1560	4.67	5.81	0.01	48.73	17.38	74.31	8.31	6.64	0.72
45.5	1510	6.84	7.48	0.01	56.38	7.76	82.73	9.51	6.67	0.76
46.5	1570	6.66	7.24	0.01	55.50	7.29	83.72	8.99	9.21	0.76
47.5	1510	7.86	8.48	0.02	49.16	6.76	83.09	10.15	10.13	0.76
48.5	1520	9.39	9.91	0.02	45.52	4.93	84.42	10.65	8.17	0.77
49.5	1520	7.14	7.73	0.02	48.45	6.95	83.08	9.97	9.08	0.75
50.5	1540	7.56	8.10	0.02	47.36	6.12	83.53	10.35	9.03	0.76
51.5	1550	7.59	8.22	0.02	54.22	7.03	82.51	10.46	8.83	0.76
52.5	1570	7.94	8.44	0.02	56.90	5.43	83.43	11.14	9.55	0.77
53.5	1550	7.47	7.85	0.02	55.10	4.46	84.7	10.84	9.33	0.77
54.5	1580	7.52	7.93	0.01	60.71	4.75	83.98	11.27	6.91	0.77
55.5	1560	7.36	7.59	0.01	56.64	2.69	86.5	10.81	8.19	0.78
56.5	1550	7.87	8.26	0.02	58.70	4.37	84.27	11.36	8.26	0.78
57.5	1540	7.93	8.28	0.02	57.53	3.95	84.94	11.11	7.86	0.77
58.5	1510	7.46	7.83	0.02	45.16	4.33	84.89	10.78	8.95	0.76
59.5	1570	8.93	9.42	0.02	49.14	4.77	84.29	10.94	10.06	0.78
60.5	1530	7.89	8.35	0.02	53.72	5.05	82.63	12.32	8.67	0.78
61.5	1590	8.12	8.51	0.02	46.14	4.21	84.03	11.76	8.46	0.77
62.5	1570	8.28	8.52	0.02	55.30	2.62	85.65	11.73	9.99	0.78
63.5	1540	9.46	9.85	0.02	49.13	3.7	84.94	11.36	9.45	0.78
64.5	1570	8.67	9.10	0.02	57.31	4.36	84.22	11.42	9.72	0.78
65.5	1580	8.44	8.85	0.02	58.39	4.26	84.58	11.16	9.53	0.78
66.5	1530	8.51	9.11	0.02	54.85	6.05	82.88	11.07	9.21	0.77
67.5	1550	6.94	7.34	0.01	50.25	4.92	84.04	11.04	8.69	0.75
68.5	1550	7.38	7.71	0.02	52.80	3.9	84.5	11.6	9.66	0.76
69.5	1560	7.73	8.07	0.02	54.81	3.79	84.1	12.11	9.54	0.76
70.5	1580	6.98	7.37	0.01	56.75	4.87	84.16	10.97	9.28	0.76
71.5	1510	7.09	7.54	0.01	60.84	5.37	83.14	11.49	8.59	0.76
72.5	1570	7.95	8.49	0.02	51.31	5.92	83.63	10.45	9.01	0.77

73.5	1590	8.09	8.50	0.02	51.68	4.46	83.97	11.57	8.83	0.77
74.5	1550	7.93	8.38	0.02	44.59	4.98	83.49	11.53	10.16	0.77
75.5	1560	7.77	8.17	0.02	45.43	4.51	83.48	12.01	10.59	0.77
76.5	1510	8.29	8.66	0.02	56.27	3.94	84.71	11.35	10.00	0.78
77.5	1550	7.94	8.52	0.02	55.91	6.27	83.2	10.53	9.15	0.78
78.5	1540	7.31	7.75	0.02	55.71	5.17	83.49	11.34	9.11	0.77
79.5	1580	7.00	7.17	0.02	51.03	2.14	83.52	14.34	10.16	0.78
80.5	1540	7.69	8.07	0.02	39.97	4.3	83.52	12.18	9.90	0.78
81.5	1590	7.59	7.69	0.01	54.27	1.14	84.17	14.69	11.02	0.79
82.5	1570	6.73	7.02	0.01	66.92	3.68	82.92	13.4	9.03	0.78
83.5	1530	6.17	6.63	0.01	50.07	6.26	82.53	11.21	8.74	0.76
84.5	1550	5.61	5.85	0.01	56.91	3.75	84.69	11.56	9.69	0.77
85.5	1570	5.92	6.22	0.01	60.66	4.31	83.58	12.11	9.54	0.78
86.5	1550	7.48	7.67	0.01	63.01	2.16	84.85	12.99	9.87	0.80
87.5	1560	6.93	7.18	0.01	63.09	3.19	84.62	12.19	10.08	0.78
88.5	1570	8.70	9.16	0.02	37.64	4.63	83.75	11.62	10.50	0.78
89.5	1590	6.84	7.23	0.01	42.98	4.9	83.42	11.68	9.47	0.79
90.5	1560	5.19	5.63	0.01	51.42	6.95	83.3	9.75	7.63	0.76
91.5	1550	4.83	5.25	0.01	51.07	7.09	82.46	10.45	7.89	0.74
92.5	1580	4.60	4.91	0.01	54.95	5.5	83.52	10.98	8.30	0.74
93.5	1510	6.16	6.50	0.01	49.52	4.64	83.46	11.9	9.67	0.77
94.5	1550	5.38	5.87	0.01	44.79	7.4	80.87	11.73	9.07	0.76
95.5	1540	5.29	5.97	0.01	49.36	10.2	78.4	11.4	8.31	0.75
96.5	1530	6.40	6.79	0.01	54.48	5.2	83.83	10.97	8.73	0.78
97.5	1540	5.11	5.46	0.01	57.07	5.69	83.38	10.93	9.41	0.76
98.5	1560	4.22	4.72	0.01	61.83	9.04	80.48	10.48	8.86	0.75
99.5	1570	3.82	4.57	0.01	49.43	14.12	76.85	9.03	7.59	0.72
100.5	1540	4.62	5.10	0.01	58.16	8.27	81.34	10.39	8.50	0.74
101.5	1580	5.32	5.65	0.01	60.61	5.17	83.56	11.27	9.16	0.75
102.5	1540	5.68	6.10	0.01	59.54	6.09	82.36	11.55	9.16	0.75
103.5	1530	5.13	5.79	0.01	59.01	10.12	79.26	10.62	7.83	0.73
104.5	1570	3.89	4.41	0.01	71.36	9.98	79.18	10.84	3.57	0.73
105.5	1580	3.92	4.34	0.01	56.97	8.28	80.44	11.28	7.42	0.74
106.5	1590	5.24	5.58	0.01	56.29	5.4	83.1	11.5	7.87	0.76
107.5	1580	5.05	5.40	0.01	54.52	5.74	82.85	11.41	7.69	0.75
108.5	1560	5.57	5.85	0.01	55.16	4.29	84.37	11.34	9.14	0.77
109.5	1540	6.92	7.24	0.02	46.43	4.06	83.54	12.4	10.83	0.80
110.5	1520	4.78	5.11	0.01	57.12	5.76	82.12	12.12	7.83	0.76
111.5	1580	4.05	4.47	0.01	52.74	8.12	80.65	11.23	7.34	0.73
112.5	1560	4.69	4.98	0.01	50.23	5.2	83.57	11.23	8.53	0.77
113.5	1540	4.55	4.83	0.01	50.74	5.01	83.62	11.37	7.58	0.76
114.5	1590	5.75	6.03	0.01	48.86	4.06	83.29	12.65	8.96	0.78
115.5	1510	6.05	6.33	0.01	44.71	3.99	82.99	13.02	9.13	0.78

116.5	1580	6.30	6.48	0.01	51.15	2.55	84.86	12.59	8.78	0.77
117.5	1530	5.43	5.74	0.01	50.83	4.86	82.31	12.83	8.05	0.77
118.5	1590	4.41	4.72	0.01	48.90	5.75	81.8	12.45	7.98	0.75
119.5	1550	4.13	4.43	0.01	52.88	5.8	81.72	12.48	6.65	0.70
120.5	1550	6.18	6.46	0.02	52.37	3.91	83.38	12.71	9.40	0.77
121.5	1570	5.13	5.47	0.01	55.21	5.48	82.36	12.16	8.81	0.75
122.5	1550	5.15	5.48	0.01	54.81	5.29	83.18	11.53	8.67	0.77
123.5	1550	3.97	4.24	0.01	48.33	5.29	83.39	11.32	7.89	0.76
124.5	1570	4.74	4.98	0.01	57.46	4.34	84.12	11.54	8.13	0.78
125.5	1520	5.02	5.15	0.01	49.66	2.27	85.25	12.48	9.31	0.77
126.5	1550	5.89	6.07	0.02	52.81	2.59	85.32	12.09	8.72	0.77
127.5	1520	5.85	6.00	0.02	45.54	2.23	85.43	12.34	9.66	0.78
128.5	1550	6.30	6.49	0.02	48.66	2.67	85.49	11.84	8.84	0.78
129.5	1570	5.83	5.99	0.01	55.13	2.42	85.83	11.75	8.70	0.78
130.5	1520	5.05	5.30	0.01	56.65	4.16	84.51	11.33	8.96	0.78
131.5	1530	5.49	5.66	0.01	48.61	2.69	85.88	11.43	8.97	0.78
132.5	1580	5.64	5.76	0.01	53.56	1.92	85.16	12.92	9.53	0.78
133.5	1560	6.62	6.73	0.01	51.15	1.48	85.49	13.03	9.52	0.79
134.5	1520	6.95	7.02	0.02	52.00	0.94	83.56	15.5	9.83	0.79
135.5	1580	6.58	6.71	0.01	47.47	1.65	85.05	13.3	9.78	0.79
136.5	1540	6.69	6.81	0.01	46.76	1.64	86.19	12.17	9.85	0.79
137.5	1560	5.73	5.88	0.01	50.41	2.33	85.8	11.87	8.55	0.79
138.5	1560	5.54	5.69	0.01	54.13	2.4	85.55	12.05	9.51	0.79
139.5	1530	5.36	5.51	0.01	46.75	2.37	85.6	12.03	9.47	0.80
140.5	1580	5.89	6.03	0.02	51.65	2.01	86.04	11.95	10.02	0.80
141.5	1570	5.44	5.58	0.01	52.69	2.3	84.09	13.61	9.46	0.80
142.5	1550	5.88	6.02	0.01	51.04	2.03	84.8	13.17	9.92	0.80
143.5	1580	5.13	5.28	0.01	52.00	2.52	83.14	14.34	9.82	0.77
144.5	1560	5.54	5.71	0.02	45.16	2.69	84.84	12.47	9.16	0.78
145.5	1595	5.67	5.82	0.02	43.68	2.25	84.8	12.95	10.08	0.79
146.5	1525	5.53	5.64	0.01	43.90	1.75	84.55	13.7	9.89	0.79
147.5	1595	5.65	5.84	0.02	40.56	2.93	83.87	13.2	9.42	0.78
148.5	1535	5.71	5.88	0.02	31.41	2.58	83.89	13.53	9.54	0.78
149.5	1570	5.97	6.12	0.02	43.49	2.2	85.25	12.55	9.53	0.77
150.5	1550	6.00	6.12	0.02	42.33	1.86	83.92	14.22	11.14	0.76
151.5	1540	6.74	6.82	0.02	39.21	1.05	87.1	11.85	10.85	0.77
152.5	1560	6.47	6.55	0.02	52.04	1.06	86.97	11.97	11.29	0.77
153.5	1590	6.73	6.81	0.02	47.05	1	86.64	12.36	10.58	0.77
154.5	1575	6.36	6.43	0.02	50.68	0.99	86.76	12.25	9.93	0.77
155.5	1560	6.68	6.76	0.02	41.95	1.06	87.17	11.77	11.28	0.78
156.5	1520	7.17	7.32	0.02	40.87	1.88	86.26	11.86	9.69	0.77
157.5	1560	6.50	6.67	0.01	49.10	2.29	86.03	11.68	10.70	0.77
158.5	1575	6.92	7.05	0.02	47.08	1.66	86.82	11.52	10.47	0.77

159.5	1520	6.32	6.46	0.01	44.80	1.89	86.69	11.42	11.49	0.76
160.5	1530	6.58	6.61	0.01	50.99	0.36	87.47	12.17	10.81	0.77
161.5	1565	7.61	7.73	0.02	47.88	1.45	87.43	11.12	10.65	0.77
162.5	1570	6.66	6.76	0.02	44.55	1.26	87.36	11.38	11.04	0.77
163.5	1570	8.00	8.03	0.02	37.37	0.33	88.18	11.49	10.95	0.78
164.5	1580	7.16	7.17	0.02	39.40	0.19	86.56	13.25	8.67	0.75
165.5	1570	7.63	7.75	0.02	35.90	1.41	85.77	12.82	10.62	0.75
166.5	1510	7.41	7.43	0.02	44.28	0.33	86.78	12.89	10.55	0.76
167.5	1530	6.28	6.30	0.02	37.17	0.32	86.94	12.74	10.10	0.76
168.5	1560	3.64	3.73	0.01	65.58	2.21	86.04	11.75	11.51	0.75
169.5	1580	5.87	5.94	0.02	48.73	1.07	86.59	12.34	12.25	0.81
170.5	1530	6.44	6.58	0.02	32.74	1.89	86.67	11.44	10.23	0.79
171.5	1550	5.91	5.97	0.02	33.07	0.96	86.81	12.23	10.70	0.77
172.5	1585	6.01	6.07	0.01	52.87	0.94	86.96	12.1	7.79	0.78
173.5	1530	7.55	7.57	0.02	44.86	0.27	86.31	13.42	10.71	0.79
174.5	1580	6.96	7.04	0.02	51.79	1.05	86.48	12.47	10.99	0.78
175.5	1530	7.21	7.32	0.02	44.25	1.35	86.66	11.99	8.90	0.78
176.5	1550	5.83	5.93	0.02	36.82	1.48	86.62	11.9	10.57	0.77
177.5	1560	5.33	5.40	0.01	46.96	1.02	87.49	11.49	10.59	0.83
178.5	1570	5.97	6.05	0.02	44.62	1.11	86.58	12.31	8.03	0.78
179.5	1580	5.74	5.76	0.01	55.64	0.29	85.18	14.53	12.38	0.79
180.5	1580	5.35	5.37	0.01	58.96	0.31	85.76	13.93	11.19	0.79
181.5	1550	5.61	5.74	0.01	45.85	2	85.24	12.76	8.93	0.78
182.5	1560	5.02	5.08	0.01	49.49	1.03	87.99	10.98	10.96	0.79
183.5	1580	5.59	5.72	0.02	42.46	1.96	86.63	11.41	11.77	0.78
184.5	1530	6.04	6.07	0.01	53.20	0.36	86.47	13.17	12.15	0.78
185.5	1550	5.46	5.53	0.01	40.16	1.12	86.45	12.43	11.45	0.79
186.5	1560	4.93	5.02	0.01	56.01	1.55	86.3	12.15	11.84	0.78
187.5	1560	5.36	5.46	0.01	42.15	1.65	86.51	11.84	10.83	0.79
188.5	1580	5.81	5.87	0.01	48.27	0.95	86.69	12.36	12.83	0.80
189.5	1550	6.24	6.32	0.01	56.19	1.26	86.97	11.77	12.80	0.80
190.5	1590	5.84	5.91	0.01	55.82	1.05	87.14	11.81	12.41	0.80
191.5	1560	6.21	6.23	0.01	59.83	0.3	86.28	13.42	12.12	0.81
192.5	1565	6.48	6.60	0.01	55.25	1.6	86.24	12.16	11.68	0.80
193.5	1510	5.71	5.79	0.01	39.82	1.22	86.31	12.47	7.67	0.80
194.5	1575	5.28	5.37	0.01	45.82	1.5	85.77	12.73	10.81	0.80
195.5	1545	5.68	5.76	0.01	45.79	1.25	86.9	11.85	11.30	0.80
196.5	1560	5.06	5.13	0.01	51.33	1.3	86.77	11.93	11.61	0.79
197.5	1530	6.56	6.63	0.02	40.53	0.96	85.89	13.15	12.07	0.80
198.5	1515	5.32	5.40	0.01	41.55	1.31	85.75	12.94	11.34	0.79
199.5	1540	5.03	5.10	0.01	36.13	1.2	86.51	12.29	11.46	0.80
200.5	1530	5.07	5.09	0.01	48.60	0.35	86.8	12.85	9.81	0.79
201.5	1550	4.83	4.85	0.01	44.85	0.33	86.48	13.19	11.28	0.80

202.5	1545	5.08	5.10	0.02	46.57	0.32	86.91	12.77	9.78	0.80
203.5	1570	5.82	5.85	0.01	46.62	0.34	86.97	12.69	11.57	0.79
204.5	1560	5.58	5.64	0.02	46.42	0.9	86.11	12.99	11.15	0.79
205.5	1550	5.42	5.44	0.02	38.27	0.35	87.06	12.59	11.56	0.80
206.5	1590	4.91	4.93	0.01	48.58	0.35	87.5	12.15	11.79	0.70
207.5	1520	5.72	5.78	0.01	43.58	0.93	85.67	13.4	11.88	0.88
208.5	1570	5.45	5.47	0.01	55.36	0.35	87.02	12.63	11.35	0.81
209.5	1510	4.78	4.79	0.01	48.88	0.22	85.68	14.1	11.45	0.81
210.5	1560	4.74	4.76	0.01	53.61	0.33	85.98	13.69	10.66	0.80
211.5	1580	4.61	4.63	0.01	52.84	0.34	86.28	13.38	10.52	0.79
212.5	1570	5.97	5.99	0.02	44.44	0.36	86.34	13.3	10.87	0.80
213.5	1580	4.77	4.82	0.01	48.77	0.94	85.83	13.23	11.00	0.80
214.5	1550	4.46	4.47	0.01	51.67	0.29	85.64	14.07	12.03	0.80
215.5	1570	6.90	6.93	0.02	47.28	0.34	85.57	14.09	9.14	0.80
216.5	1550	4.46	4.47	0.01	51.67	0.24	85.49	14.27	11.48	0.80
217.5	1540	6.62	6.69	0.02	50.06	0.96	85.64	13.4	11.33	0.80
218.5	1540	4.69	4.71	0.01	54.87	0.35	86.13	13.52	10.86	0.79
219.5	1550	4.13	4.19	0.01	52.88	1.18	85.43	13.39	10.64	0.79
220.5	1550	5.18	5.20	0.01	31.98	0.32	85.04	14.64	11.43	0.80
221.5	1570	4.71	4.73	0.01	38.13	0.28	85.65	14.07	11.20	0.81
222.5	1510	5.43	5.45	0.01	49.28	0.18	84.29	15.53	11.65	0.81
223.5	1540	5.38	5.39	0.01	44.58	0.21	83.6	16.19	11.88	0.80
224.5	1550	4.18	4.20	0.01	47.90	0.32	85.06	14.62	11.51	0.80
225.5	1560	4.53	4.58	0.01	46.10	0.99	84.26	14.75	11.13	0.79
226.5	1580	4.53	4.54	0.01	48.14	0.28	84.91	14.81	11.89	0.80
227.5	1540	4.71	4.73	0.01	38.18	0.22	84.89	14.89	11.37	0.80
228.5	1520	4.12	4.17	0.01	50.90	1.02	83.94	15.04	11.79	0.80
229.5	1540	4.62	4.67	0.01	37.74	0.89	84.08	15.03	10.98	0.80
230.5	1580	4.12	4.16	0.02	31.82	0.89	84.35	14.76	11.11	0.79
231.5	1545	4.21	4.29	0.01	40.93	1.53	84.53	13.94	11.23	0.79
232.5	1560	3.98	4.03	0.01	47.34	1.2	84.48	14.32	4.72	0.79
233.5	1590	4.05	4.12	0.01	50.41	1.49	83.85	14.66	9.42	0.78
234.5	1545	3.29	3.36	0.01	39.83	1.75	83.8	14.45	8.37	0.75
235.5	1575	3.94	3.96	0.01	44.77	0.3	84.19	15.51	10.18	0.80
236.5	1550	4.07	4.09	0.01	37.66	0.27	84.58	15.15	10.78	0.82
237.5	1500	4.43	4.44	0.01	48.33	0.28	85.01	14.71	11.91	0.80
238.5	1550	3.25	3.27	0.01	27.81	0.32	85.14	14.54	12.87	0.80
239.5	1565	3.12	3.13	0.01	62.32	0.22	83.52	16.26	12.53	0.80
240.5	1540	3.95	3.96	0.01	45.80	0.25	83.54	16.21	12.64	0.80
241.5	1565	4.60	4.62	0.01	51.36	0.3	84.37	15.33	12.44	0.80
242.5	1560	4.77	4.78	0.01	59.01	0.23	83.33	16.44	12.64	0.80
243.5	1510	4.85	4.86	0.01	52.17	0.25	83.4	16.35	12.49	0.80
244.5	1530	5.03	5.04	0.01	46.80	0.26	82.26	17.48	11.53	0.79

245.5	1510	3.73	3.74	0.01	52.29	0.28	83.4	16.32	10.29	0.80
246.5	1540	4.29	4.31	0.01	52.37	0.36	84.72	14.92	12.30	0.82
247.5	1545	4.64	4.66	0.01	51.75	0.25	84.09	15.66	12.86	0.81
248.5	1515	4.05	4.07	0.01	46.94	0.33	84.25	15.42	12.30	0.78
249.5	1600	4.15	4.17	0.01	40.15	0.36	84.15	15.49	11.89	0.79
250.5	1585	3.62	3.64	0.01	30.41	0.31	83.46	16.23	12.42	0.82
251.5	1570	3.96	4.01	0.01	40.22	0.99	83.41	15.6	11.71	0.81
252.5	1590	4.10	4.16	0.01	44.32	1.19	84.53	14.28	10.57	0.80
253.5	1520	4.66	4.68	0.01	44.51	0.31	84.4	15.29	11.39	0.81
254.5	1560	2.98	2.99	0.01	52.20	0.28	83.55	16.17	12.28	0.81
255.5	1570	4.01	4.02	0.01	50.87	0.27	84.2	15.53	12.04	0.80
256.5	1560	3.68	3.69	0.01	40.41	0.31	83.71	15.98	11.53	0.81
257.5	1540	4.09	4.10	0.01	50.95	0.17	82.48	17.35	13.13	0.81
258.5	1530	3.98	3.99	0.01	45.00	0.19	83.72	16.09	12.99	0.80
259.5	1530	3.76	3.77	0.01	46.80	0.28	84.38	15.34	11.07	0.80
260.5	1570	3.97	3.98	0.01	37.95	0.33	84.86	14.81	12.67	0.80
261.5	1520	3.55	3.57	0.01	43.60	0.33	85.51	14.16	11.43	0.81
262.5	1535	3.90	3.92	0.01	47.32	0.35	80.87	18.78	11.78	0.80
263.5	1580	3.87	3.89	0.01	36.38	0.32	84.97	14.71	12.94	0.80
264.5	1570	3.07	3.08	0.01	53.63	0.31	85.62	14.07	12.67	0.80
265.5	1590	4.18	4.19	0.01	51.76	0.29	85.85	13.86	13.36	0.79
266.5	1510	4.03	4.07	0.01	49.75	0.94	85.24	13.82	11.70	0.79
267.5	1535	3.89	3.90	0.01	47.51	0.26	85.74	14	9.93	0.79
268.5	1640	2.97	2.98	0.01	53.66	0.33	85.75	13.92	11.62	0.78
269.5	1530	0.66	0.68	0.01	44.06	1.24	85.15	13.61	9.49	0.78
270.5	1520	2.92	2.97	0.01	37.29	1.42	85.81	12.77	10.61	0.78
271.5	1590	2.96	3.02	0.01	55.92	1.53	84.92	13.55	18.36	0.78
272.5	1580	2.63	2.64	0.01	48.63	0.34	86.03	13.63	11.36	0.77
273.5	1550	2.59	2.63	0.01	39.61	1.25	84.93	13.82	11.15	0.77
274.5	1540	3.10	3.14	0.01	35.17	1.17	85.12	13.71	10.74	0.76
275.5	1560	2.12	2.16	0.01	42.42	1.23	84.64	14.13	11.32	0.76
276.5	1550	2.71	2.77	0.01	54.08	1.67	84.48	13.85	6.47	0.76
277.5	1540	2.82	2.90	0.01	42.37	2.34	84.22	13.44	8.40	0.76
278.5	1570	2.43	2.47	0.01	43.71	1.15	84.54	14.31	8.19	0.73
279.5	1520	2.49	2.53	0.01	44.92	1.3	84.44	14.26	10.68	0.76
280.5	1570	2.84	2.88	0.01	53.49	1.26	84.51	14.23	10.52	0.76
281.5	1580	2.66	2.69	0.01	36.38	0.98	84.1	14.92	9.96	0.75
282.5	1540	2.23	2.28	0.01	59.71	1.75	83.81	14.44	10.41	0.75
283.5	1520	2.47	2.54	0.01	51.88	2.2	83.08	14.72	10.27	0.74
284.5	1580	2.22	2.28	0.01	61.75	2.04	84.38	13.58	10.28	0.74
285.5	1590	0.27	0.29	0.01	52.84	1.84	82.59	15.57	10.90	0.74
286.5	1560	2.70	2.78	0.01	42.69	2.35	84.9	12.75	11.18	0.73
287.5	1570	2.22	2.30	0.01	58.82	2.62	84.74	12.64	10.26	0.73

288.5	1580	2.19	2.25	0.01	57.82	2.05	83.63	14.32	8.32	0.73
289.5	1510	2.12	2.18	0.01	59.60	2.16	83.51	14.33	9.68	0.74
290.5	1540	2.20	2.25	0.01	54.88	1.84	84.19	13.97	9.75	0.76
291.5	1550	2.31	2.36	0.01	54.48	1.53	84.35	14.12	10.01	0.76
292.5	1570	1.79	1.85	0.01	51.53	2.32	85.02	12.66	8.53	0.73
293.5	1560	1.90	2.26	0.01	41.71	12.1	76.2	11.7	8.80	0.72
294.5	1580	2.22	2.44	0.01	39.07	6.86	80.59	12.55	7.98	0.74
295.5	1590	2.01	2.07	0.01	59.15	2.24	84.48	13.28	8.53	0.74
296.5	1550	2.13	2.23	0.01	60.67	3.28	84.32	12.4	8.26	0.73
297.5	1550	2.41	2.51	0.01	32.77	3.15	83.91	12.94	7.74	0.73
298.5	1590	2.34	2.45	0.01	41.80	3.58	83.22	13.2	8.79	0.73
299.5	1550	1.75	1.91	0.01	50.48	5.99	80.77	13.24	8.92	0.70
300.5	1580	1.55	1.63	0.01	57.27	3.52	83.68	12.8	7.61	0.69
301.5	1540	2.13	2.23	0.01	43.87	3.31	83.68	13.01	8.82	0.70
302.5	1600	1.66	1.74	0.01	50.25	3.31	83.52	13.17	5.98	0.68
303.5	1520	1.35	1.43	0.01	49.99	3.54	83.33	13.13	7.92	0.68
304.5	1580	1.26	1.33	0.01	48.54	3.58	83.47	12.95	6.87	0.66
305.5	1580	1.31	1.76	0.01	38.57	18.07	71.15	10.78	5.90	0.63
306.5	1530	1.48	2.46	0.01	51.55	30.69	60.41	8.9	6.39	0.66
307.5	1540	0.54	0.93	0.01	47.78	23.07	66.9	10.03	7.33	0.59
308.5	1540	1.41	2.19	0.01	49.40	26.5	63.26	10.24	4.55	0.66
309.5	1540	0.49	12.90	0.01	32.68	91.01	7.32	1.67	0.61	0.60
310.5	1630	-0.34	6.37	0.01	48.45	94.45	4.41	1.14	0.95	0.45
311.5	1550	1.16	1.29	0.01	43.30	6.28	81.13	12.59	4.03	0.66
312.5	1510	0.53	0.55	0.01	50.28	1.32	86.01	12.67	6.02	0.57
313.5	1570	0.40	0.43	0.01	51.10	2.47	85.07	12.46	5.47	0.57
314.5	1570	0.26	0.50	0.01	43.54	19.5	70.48	10.02	3.12	0.46
315.5	1570	-0.08	0.21	0.01	54.54	30.64	60.44	8.92	1.25	0.51
316.5	1585	0.94	1.01	0.01	42.29	4.28	83.67	12.05	6.67	0.65
317.5	1530	0.50	0.67	0.01	57.24	12.25	76.34	11.41	3.62	0.60
318.5	1570	0.96	1.03	0.01	55.14	4.01	83.31	12.68	4.25	0.63
319.5	1580	0.05	0.41	0.01	60.00	31.47	59.6	8.93	2.07	0.50
320.5	1575	0.34	1.35	0.01	49.55	48.41	44.97	6.62	3.10	0.53
321.5	1550	0.67	0.73	0.01	41.27	4.1	84.09	11.81	5.00	0.58
322.5	1570	0.91	1.19	0.01	60.43	14.74	74.64	10.62	5.49	0.64
323.5	1560	0.99	1.20	0.01	32.41	10.94	77.33	11.73	4.83	0.66
324.5	1550	0.59	0.81	0.01	64.13	13.88	75.19	10.93	5.47	0.65
325.5	1520	-0.23	-0.20	0.01	54.56	4.22	83.91	11.87	5.05	0.63
326.5	1520	0.39	0.54	0.01	54.50	11.73	77.21	11.06	6.17	0.58
327.5	1570	0.57	0.97	0.01	67.23	23.31	66.17	10.52	4.59	0.64
328.5	1540	2.01	2.38	0.01	33.79	11.72	75.8	12.48	5.00	0.68
329.5	1560	2.56	2.91	0.01	37.84	9.83	77.68	12.49	7.12	0.69
330.5	1580	2.38	2.72	0.01	39.35	9.87	78.21	11.92	7.53	0.70

331.5	1580	2.61	2.94	0.01	32.40	9.14	78.24	12.62	8.37	0.70
332.5	1580	1.22	1.49	0.01	56.52	12.48	75.06	12.46	6.46	0.68
333.5	1560	1.36	1.69	0.01	56.06	13.3	74.95	11.75	6.20	0.68
334.5	1560	1.09	1.36	0.01	60.48	12.68	75.03	12.29	6.78	0.66
335.5	1580	1.36	1.46	0.01	56.48	4.46	82.78	12.76	7.53	0.69
336.5	1580	1.46	1.82	0.01	53.86	14.11	74.86	11.03	6.59	0.67
337.5	1540	1.21	1.43	0.01	53.14	10.36	78.29	11.35	5.49	0.68
338.5	1540	1.32	1.52	0.01	57.64	9.29	79.23	11.48	5.99	0.69
339.5	1580	1.01	1.11	0.01	46.26	5.38	81.66	12.96	6.15	0.68
340.5	1520	1.29	1.38	0.01	56.74	4.13	83.65	12.22	7.63	0.71
341.5	1520	1.47	1.49	0.01	48.28	1.11	87.04	11.85	7.39	0.71
342.5	1550	1.47	1.49	0.01	55.00	1.14	86.59	12.27	6.77	0.72
343.5	1580	1.21	1.24	0.01	55.71	1.92	85.55	12.53	5.68	0.72
344.5	1500	0.86	0.96	0.01	55.99	6	81.25	12.75	4.91	0.66
345.5	1510	1.51	2.41	0.01	46.06	28.65	62.65	8.7	5.30	0.70
346.5	1530	1.82	1.99	0.01	38.88	6.12	82.17	11.71	5.99	0.71
347.5	1560	0.92	1.00	0.01	50.67	4.26	83.83	11.91	7.14	0.67
348.5	1550	0.75	1.14	0.01	47.94	20.85	69.36	9.79	5.35	0.63
349.5	1570	0.61	1.75	0.01	50.59	45.94	47.44	6.62	4.26	0.62
350.5	1550	0.54	0.84	0.01	42.15	19.27	71.2	9.53	5.43	0.60
351.5	1550	0.54	1.09	0.01	57.38	30.48	60.69	8.83	4.99	0.62
352.5	1540	0.69	0.87	0.01	50.74	11.33	76.96	11.71	4.26	0.62
353.5	1510	-0.01	0.71	0.01	51.05	49.73	44	6.27	2.80	0.50
354.5	1500	0.14	0.67	0.01	54.79	37.81	54.07	8.12	2.65	0.54
355.5	1530	0.46	1.15	0.01	55.46	36.57	54.92	8.51	4.66	0.58
356.5	1570	0.47	1.22	0.01	51.66	38.2	54.23	7.57	3.13	0.57
357.5	1520	0.51	1.38	0.01	62.00	41.24	51.45	7.31	4.11	0.60
358.5	1550	0.58	1.12	0.01	49.48	28.93	62.01	9.06	4.76	0.62
359.5	1590	-0.73	0.53	0.01	55.58	26.05	64.6	9.35	4.15	0.53
360.5	1540	0.13	2.61	0.01	51.16	74.34	21.92	3.74	2.26	0.52
361.5	1580	0.21	2.83	0.01	45.61	73.57	22.92	3.51	1.33	0.52
362.5	1570	0.04	1.27	0.01	51.15	61.76	33.31	4.93	1.93	0.46
363.5	1580	-0.29	1.76	0.01	25.96	82.47	14.87	2.66	1.31	0.38
364.5	1510	-0.25	2.96	0.01	41.63	87.04	11	1.96	0.85	0.46
365.5	1550	-0.13	0.13	0.01	26.11	29.37	61.64	8.99	2.66	0.49
366.5	1570	-0.10	1.71	0.01	35.10	74.08	22.31	3.61	1.52	0.47
367.5	1530	-0.01	1.72	0.01	43.23	70.47	25.47	4.06	3.16	0.53
368.5	1510	0.37	1.88	0.01	43.70	57.87	36.13	6	3.21	0.58
369.5	1520	0.94	1.61	0.01	41.33	28.65	61.89	9.46	6.25	0.66
370.5	1520	0.55	0.87	0.01	30.45	19.84	69.71	10.45	6.58	0.61
371.5	1515	0.20	0.54	0.01	39.24	26.77	64.61	8.62	4.65	0.57
372.5	1580	0.08	0.34	0.01	29.69	24.57	66.27	9.16	4.58	0.55
373.5	1530	0.21	0.65	0.01	28.79	31.87	59.6	8.53	2.77	0.54

374.5	1560	0.00	0.30	0.01	29.30	29.11	61.93	8.96	3.44	0.48
375.5	1530	0.27	0.75	0.01	62.37	32.81	58.82	8.37	3.21	0.54
376.5	1600	0.27	0.98	0.01	53.19	41.22	51.36	7.42	4.20	0.57
377.5	1520	0.50	0.74	0.01	53.96	16.28	72.65	11.07	5.85	0.59
378.5	1580	0.36	0.66	0.01	54.98	22.04	67.76	10.2	4.21	0.55
379.5	1560	-0.05	0.34	0.01	43.03	36.32	56.04	7.64	4.79	0.49
380.5	1550	-0.23	0.47	0.01	56.22	58.02	36.44	5.54	1.49	0.44
381.5	1585	0.03	0.74	0.01	52.88	48.32	45.01	6.67	2.81	0.52
382.5	1580	0.79	1.08	0.01	51.35	16.31	72.87	10.82	4.86	0.66
383.5	1540	0.72	0.86	0.01	50.52	8.76	79.93	11.31	5.22	0.65
384.5	1560	0.28	0.58	0.01	52.61	22.67	68.04	9.29	5.03	0.57
385.5	1580	0.12	0.57	0.01	53.49	34.56	57.53	7.91	2.66	0.57
386.5	1580	-0.25	0.14	0.01	32.39	44.97	47.9	7.13	3.07	0.41
387.5	1550	-0.32	0.53	0.01	37.43	67.68	28.3	4.02	1.44	0.40
388.5	1590	-0.30	0.38	0.01	30.65	61.18	33.31	5.51	1.38	0.39
389.5	1550	0.19	1.21	0.01	41.89	52.47	40.99	6.54	2.72	0.52
390.5	1520	-0.03	0.10	0.01	48.36	15.51	73.14	11.35	2.96	0.51
391.5	1570	0.22	1.33	0.01	33.87	53.91	40.12	5.97	1.73	0.54
392.5	1530	0.28	0.32	0.01	50.66	4.22	83.87	11.91	4.15	0.58
393.5	1520	-0.37	0.42	0.01	57.59	68.44	27.28	4.28	3.66	0.41
394.5	1580	-0.07	2.14	0.01	54.19	77.04	19.87	3.09	2.79	0.48
395.5	1560	-0.10	0.57	0.01	46.61	51.67	41.96	6.37	2.47	0.46
396.5	1580	-0.56	-0.45	0.01	52.64	38.7	53.39	7.91	2.04	0.37
397.5	1585	-0.52	0.07	0.01	41.02	73.38	23.04	3.58	1.57	0.35
398.5	1580	-0.55	2.50	0.01	50.18	94.38	4.58	1.04	0.50	0.37
399.5	1540	-0.58	3.60	0.01	46.62	96.55	2.62	0.83	0.23	0.37
400.5	1630	-0.46	0.13	0.01	69.16	68.29	26.97	4.74	1.23	0.41
401.5	1560	-0.27	0.39	0.01	58.40	59.17	35.52	5.31	1.38	0.46
402.5	1580	0.29	0.91	0.01	51.38	37.94	53.92	8.14	4.61	0.57
403.5	1580	0.03	0.33	0.01	42.34	28.28	62.13	9.59	3.21	0.51
404.5	1550	-0.18	0.10	0.01	59.47	33.52	57.72	8.76	3.44	0.49
405.5	1590	0.00	0.46	0.01	50.37	39.02	52.79	8.19	2.42	0.48
406.5	1550	0.10	0.79	0.01	39.59	45.3	47.02	7.68	2.97	0.50
407.5	1520	0.35	0.86	0.01	52.00	31.6	58.88	9.52	2.99	0.51
408.5	1570	0.13	0.69	0.01	39.74	39.9	51.74	8.36	3.00	0.53
409.5	1530	0.18	0.63	0.01	38.89	32.86	57.99	9.15	3.27	0.53
410.5	1550	0.04	0.42	0.01	51.23	33.29	57.52	9.19	2.28	0.51
411.5	1510	0.04	0.19	0.01	42.28	15.42	72.32	12.26	2.47	0.50
412.5	1590	-0.10	0.63	0.01	47.92	53.61	39.5	6.89	2.34	0.45
413.5	1530	0.10	0.61	0.01	54.58	38.08	52.61	9.31	3.34	0.46
414.5	1520	0.15	1.23	0.01	42.11	55.08	38.47	6.45	2.49	0.49
415.5	1540	-0.19	1.02	0.01	53.54	69.01	26.31	4.68	2.73	0.43
416.5	1550	-0.19	0.34	0.01	48.64	49.49	43.45	7.06	2.32	0.43

417.5	1510	-0.15	0.31	0.01	52.48	44.32	47.72	7.96	2.95	0.42
418.5	1520	-0.13	0.24	0.01	45.87	37.5	53.98	8.52	2.56	0.44
419.5	1560	-0.15	0.32	0.01	50.68	45.21	47.74	7.05	3.22	0.42
420.5	1520	-0.20	0.20	0.01	53.32	43.22	49.03	7.75	2.81	0.41
421.5	1520	-0.07	0.54	0.01	49.46	47.53	44.8	7.67	2.01	0.41
422.5	1580	-0.13	0.54	0.01	39.28	52.57	40.63	6.8	3.14	0.41
423.5	1520	-0.17	0.24	0.01	43.05	42.16	49.41	8.43	2.81	0.41
424.5	1550	-0.01	0.62	0.01	36.21	46.45	45.76	7.79	3.25	0.43
425.5	1580	-0.11	0.14	0.01	61.05	28.89	61.29	9.82	3.40	0.42
426.5	1560	-0.05	0.54	0.01	40.53	46.8	45.22	7.98	3.39	0.42
427.5	1550	0.05	0.32	0.01	47.99	26.39	63.37	10.24	3.61	0.43
428.5	1590	-0.07	0.22	0.01	53.57	30.76	59.36	9.88	3.38	0.42
429.5	1560	-0.11	0.51	0.01	50.51	49.73	43.24	7.03	2.45	0.43
430.5	1560	-0.13	0.32	0.01	50.49	42.89	49.31	7.8	3.17	0.44
431.5	1560	-0.13	0.21	0.01	50.49	36.36	55.06	8.58	2.78	0.44
432.5	1570	0.03	0.43	0.01	48.38	34.6	56.55	8.85	2.82	0.45
433.5	1530	0.01	0.64	0.01	49.49	45.9	46.63	7.47	2.50	0.43
434.5	1550	0.00	0.40	0.01	44.83	35.01	55.8	9.19	2.80	0.44
435.5	1550	0.11	0.72	0.01	35.81	42.26	49.54	8.2	3.38	0.45
436.5	1570	0.04	0.59	0.01	34.59	41.57	49.87	8.56	3.93	0.44
437.5	1570	0.03	1.27	0.01	49.46	62.12	32.36	5.52	2.45	0.45
438.5	1500	-0.04	0.30	0.01	26.31	32.93	57.68	9.39	1.71	0.45
439.5	1580	0.10	0.70	0.01	42.36	42.33	49.18	8.49	3.45	0.45
440.5	1580	0.12	0.99	0.01	34.92	50.35	41.95	7.7	3.56	0.45
441.5	1540	-0.05	0.45	0.01	34.48	42.95	48.47	8.58	3.43	0.41
442.5	1590	0.04	0.25	0.01	41.81	21.24	67.14	11.62	4.72	0.43
443.5	1560	-0.01	0.18	0.01	34.27	20.86	66.95	12.19	4.49	0.45
444.5	1550	0.08	0.32	0.01	42.46	23.2	65.22	11.58	3.65	0.47
445.5	1580	-0.04	0.23	0.01	50.62	27.94	61.56	10.5	6.72	0.47
446.5	1590	-0.02	0.29	0.01	48.93	30.53	59.28	10.19	3.31	0.48
447.5	1590	-0.02	0.33	0.01	50.66	33.38	57.04	9.58	4.84	0.46
448.5	1560	0.01	0.16	0.01	48.50	17.03	70.68	12.29	6.17	0.48
449.5	1500	0.33	0.46	0.01	49.72	11.3	76.04	12.66	4.03	0.48
450.5	1630	-0.01	0.17	0.01	61.28	19.7	68.76	11.54	7.19	0.49
451.5	1500	0.25	0.40	0.01	49.32	12.88	74.87	12.25	7.38	0.50
452.5	1510	0.30	0.98	0.01	39.77	39.67	52.04	8.29	8.58	0.53
453.5	1510	0.41	0.80	0.01	45.20	25.65	63.67	10.68	6.78	0.53
454.5	1520	0.23	0.73	0.01	48.79	34.79	56.17	9.04	6.54	0.53
455.5	1550	0.40	0.65	0.01	52.55	18.08	70.01	11.91	5.89	0.50
456.5	1590	0.30	0.55	0.01	54.77	19.68	69.46	10.86	5.35	0.51
457.5	1500	0.21	0.34	0.01	37.49	12.65	74.29	13.06	6.36	0.51
458.5	1570	0.44	0.72	0.01	47.70	19.38	68.8	11.82	6.37	0.52
459.5	1520	0.17	0.31	0.01	51.43	13.6	73.43	12.97	5.26	0.49

460.5	1580	0.35	0.42	0.01	54.80	5.73	79.66	14.61	5.11	0.51
461.5	1580	0.33	0.45	0.01	60.99	10.48	76.4	13.12	6.08	0.52
462.5	1560	0.38	0.70	0.01	46.00	22.04	66.47	11.49	6.11	0.51
463.5	1550	0.40	0.58	0.01	50.05	13.68	73.43	12.89	5.96	0.53
464.5	1590	0.33	0.39	0.01	54.12	5.74	81.06	13.2	5.37	0.54

REFERENCES

Allan, R.J., 1986. The role of particulate matter in the fate of contaminants in aquatic ecosystems. Inland Waters Directive Science Series, 142. National Water Research Institute, Burlington, Canada.

Allen, G.P., et al., 1980. Effects of tides on mixing and suspended sediment transport in macrotidal estuaries. Sediment. Geol. 26, 69-90.

Allison, M.A., Nittrouer, C.A. and Faria, L.E.C., 1995. Rates and mechanisms of shoreface progradation and retreat downdrift of the Amazon river mouth. Marine Geology, 125(3-4), 373-392.

Appleby, P.G., 2001. Chronostratigraphic techniques in recent sediments. In Last, W.M. and Smol, J.P., editors, Tracking environmental change using lake sediments volume 1: basin analysis, coring, and chronological techniques. Kluwer Academic, 171–203.

Appleby, P. G., 1997. The use of 210 Pb and 137 Cs as tracers in modelling transport processes in lake catchment systems. *Studies in Environmental Science* 68 (1997): 441-448.

Appleby, P.G. and Oldfield, F., 1992. Applications of lead-210 to sedimentation studies. In Uranium-series disequilibrium: applications to earth, marine, and environmental sciences. 2. ed.

Appleby, P.G. and Oldfield, F. 1978. The calculation of 210Pb dates assuming a constant rate of supply of unsupported 210Pb to the sediment. Catena 5, 1–8.
—— 1983: The assessment of 210Pb data from sites with varying sediment accumulation rates. Hydrobiologia 103, 29–35.

Appleby, P.G., Oldfield, F., Thompson, R., Huttunen, P. and Tolonen, K., 1979. 210Pb dating of annually laminated lake sediments from Finland. *Nature*, *280*(5717), pp.53-55.

Ankers, C., Walling, D.E., Smith, R.P., 2003. The influence of catchment characteristics on suspended sediment properties. Hydrobiologia 494, 159–167.

Aston, S.R., Bruty, D., Chester, R. & Padgham, R.C., 1973: Mercury in lake sediments, a possible indicator of technological growth. Nature London. 241, 450 - 451.

Audrey, S., Schäfer, J., Blanc, G., Bossy, C., Lavaux G., 2004. Anthropogenic components of heavy metal (Cd, Zn, Cu, Pb) budgets in the Lot-Garonne fluvial system (France). Applied Geochemistry 19, 769–786.

Avnimelech, Y., Troeger, B.W., Reed, L.W. 1982. Mutual flocculation of algae and clay, evidence and implications. Science 216, 63-65.

Bartlett, K.B., 1981. Macrofauna Distribution and Seasonal Influences on Interstitial Water Chemistry of Cape Lookout Bight. N.C. University of North Carolina, Chapel Hill, U.S.A. Master of Science thesis.

Bianchi, T.S., Mead, A.A. 2009. Large-river delta-front estuaries as natural "recorders" of global environmental change. Proceedings of the National Academy of Sciences 106, 8085-8092.

Bost, M.C., 2016. How storms affect carbon burial in the New River Estuary, North Carolina (Masters Thesis).

Canuel, E.A., Martens, C.S. and Benninger, L.K., 1990. Seasonal variations in 7Be activity in the sediments of Cape Lookout Bight, North Carolina. Geochimica et Cosmochimica Acta, 54(1), pp.237-245.

Canuel, E.A. and Martens, C.S., 1993. Seasonal variations in the sources and alteration of organic matter associated with recently-deposited sediments. Organic Geochemistry, *20*(5), pp.563-577.

Canuel, E.A., Freeman, K.H., Wakeham, S.G., 1997. Isotopic compositions of lipid biomarker compounds in estuarine plants and surface sediments. Limnol. Oceanogr. 42, 1570-1583.

Chanton, J.P., Martens, C.S., Kipphut, G.W., 1983. Lead-210 sediment geochronology in a changing coastal environment. Geochim. Cosmochim. Acta 47, 1791-1804.

Cheung, K.C., Poon, B.H.T., Lan, C.Y., Wong, M. H. 2003. Assessment of metal and nutrient concentrations in river water and sediment collected from the cities in the Pearl River Delta, South China. Chemosphere 52, 1431-1440.

Collins, E.S., Scott, D.B. and Gayes, P.T., 1999. Hurricane records on the South Carolina coast: can they be detected in the sediment record? Quaternary International, 56(1), pp.15-26.

Collins A.L., Walling D.E., Stroud R.W., Robson M., Peet L.M., 2010. Assessing damaged road verges as a suspended sediment source in the Hampshire Avon catchment, southern United Kingdom. Hydrological Processes, 24, 1106-1122.

Cooper, J.A.G., 2002. The role of extreme floods in estuary-coastal behaviour: contrasts between river-and tide-dominated microtidal estuaries. Sediment. Geol. 150, 123-137.

Corbett, D.R., et al., 2007. Decadal-scale sediment dynamics and environmental change in the Albemarle Estuarine System, North Carolina. Estuar. Coast. Shelf Sci. 71, 717-729.

Correll, D.L., Jordan, T.E., Weller, D.E., 1992. Nutrient flux in a landscape, effects of coastal land use and terrestrial community mosaic on nutrient transport to coastal waters. Estuaries 15, 431-442.

Couch, C. A. (1989). Carbon and nitrogen stable isotopes of meiobenthos and their food resources. Estuarine, Coastal and Shelf Science, 28(4): 433–441.

Cowart, L.D., Corbett, D.R., Walsh, J.P., 2011. Shoreline change along sheltered coastlines: insights from the Neuse River Estuary, NC, USA. Remote Sens. 3, 1516-1534.

Cuffney, T.F., Wallace, J.B., 1988. Particulate Organic Matter Export from Three Headwater Streams, Discrete versus Continuous Measurements. Canadian Journal of Fisheries and Aquatic Sciences, 45, 2010-2016.

Currin, C.A., Newell, S.Y. and Paerl, H.W., 1995. The role of standing dead Spartina alterniflora and benthic microalgae in salt marsh food webs: considerations based on multiple stable isotope analysis. Marine Ecology Progress Series, 121, 99-116.

Dalrymple, R.W., Zaitlin, B.A., Boyd, R., 1992. Estuarine facies models: conceptual basis and stratigraphic implications: perspective. J. Sediment. Res. 62.

Day, J.W., et al., 1995. Impacts of sea-level rise on deltas in the Gulf of Mexico and the Mediterranean: the importance of pulsing events to sustainability. Estuaries 18, 636-647.

DeMaster, D.J., et al., 1985. Rates of sediment reworking at the HEBBLE site based on measurements of Th-234, Cs-137 and Pb-210. Mar. Geol. 66, 133-148.

Donnelly, J.P., Woodruff, J.D., 2007. Intense hurricane activity over the past 5,000 years controlled by El Nino and the West African monsoon. Nature 447, 465-468.

Donnelly, J.P., Anderson, J.B., Hawkes, A.D., Otvos, E.G., Toomey, M.R., van Hengstum, P.J., Wallace, D.J., Woodruff, J.D., 2014. The geological legacy of Hurricane Irene: implications for the fidelity of the paleo-storm record. By Hippensteel, S.P, Eastin, M.D, Garcia, W.J (REPLY). GSA Today 24, 28.

Dyer, K.R., 1995. Sediment transport processes in estuaries. Geomorphol. Sedimentology Estuaries 53, 423-449.

Evans, D.J., Gibson, C.E., Rossell, R.S., 2006. Sediment loads and sources in heavily modified Irish catchments, a move towards informed management strategies. Geomorphology 79, 93–113.

Elliott, E.A., McKee, B.A. and Rodriguez, A.B., 2015. The utility of estuarine settling basins for constructing multi-decadal, high-resolution records of sedimentation. Estuarine, Coastal and Shelf Science, 164, pp.105-114.

Fagherazzi, S., Carniello, L., D'Alpaos, L. and Defina, A., 2006. Critical bifurcation of shallow microtidal landforms in tidal flats and salt marshes. Proceedings of the National Academy of Sciences, 103(22), 8337-8341.

Fagherazzi, S., et al. 2012. Numerical models of salt marsh evolution, Ecological, geomorphic, and climatic factors. Reviews of Geophysics 50, RG1002.

Fain, A.M., Jay, D.A., Wilson, D.J., Orton, P.M., Baptista, A.M., 2001. Seasonal and tidal monthly patterns of particulate matter dynamics in the Columbia River estuary. Estuaries 24, 770-786.

Fox, J.F., Papanicolaou, A.N., 2008. An un-mixing model to study watershed erosion processes. Advances in Water Resources 31, 96–108.

Fox, J.F., Papanicolaou, A.N., 2007. The use of carbon and nitrogen isotopes to study watershed erosion processes. Journal of the American Water Resources Association 43, 1047–1064.

Frank, R., 1981. Pesticides and PCBs in the Grand and Saugeen River basins. Journal of Great Lakes Research 7, 440-454.

French, P., 2002. Coastal and Estuarine Management. Routledge.

French, J.R., Spencer, T., 1993. Dynamics of sedimentation in a tide-dominated backbarrier salt marsh, Norfolk, UK. Mar. Geol. 110 (3), 315-331.

Fukuyama, T., Onda, Y., Gomi, T., Yamamoto, K., Kondo, N., Miyata, S., Kosugi, K., Mizugaki, S., Tsubonuma, N., 2010. Quantifying the impact of forest management practice on the runoff of the surface-derived suspended sediment using fallout radionuclides. Hydrological Processes 24, 596–607.

Geyer, W.R., Woodruff, J.D., Traykovski, P., 2001. Sediment transport and trapping in the Hudson River estuary. Estuaries 24, 670-679.

Grabemann, I., Krause, G., 2001. On different time scales of suspended matter dynamics in the Weser Estuary. Estuaries 24, 688-698.

Grieve, I.C., 1984. Concentrations and annual loading of dissolved organic matter in a small moorland stream. Freshwater Biology 14, 533 - 537.

Gunnell, J.R., Rodriguez, A.B. and McKee, B.A., 2013. How a marsh is built from the bottom up. Geology, 41(8), pp.859-862.

Haddad, R.I. and Martens, C.S., 1987. Biogeochemical cycling in an organic-rich coastal marine basin: 9. Sources and accumulation rates of vascular plant-derived organic material. Geochimica et Cosmochimica Acta, 51(11), 2991-3001.

Hess, K.W., Spargo, E.A., Wong, A., White, S.A., Gill, S.K., 2005. VDatum for Central Coastal North Carolina: Tidal Datums, Marine Grids, and Sea Surface Topography. Silver Spring. National Oceanic and Atmospheric Administration Technical Report 46, NOS-CS-21.

Hippensteel, S.P., Eastin, M.D., Garcia, W.J., 2013. The geological legacy of Hurricane Irene: implications for the fidelity of the paleo-storm record. GSA Today 23.

Hippensteel, S.P., 2008. Preservation potential of storm deposits in back-barrier marshes. J. Coast. Res. 24, 594-601.

Horowitz, A.J., Elrick, K.A., Smith, J.J., 2008. Monitoring urban impacts on suspended sediment, trace element, and nutrient fluxes within the City of Atlanta, Georgia, USA, program design, methodological considerations, and initial results. Hydrological Processes 22, 1473–1496.

Jha, R., Ojha, C.S.P., Bhatia, K.K.S., 2007. Non-point source pollution estimation using a modified approach. Hydrological Processes 21, 1098–1105.

Keesstra, S.D., van Dam, O., Verstraeten, G., van Huissteden, J., 2009. Changing sediment dynamics due to natural reforestation in the Dragonja catchment, SW Slovenia. Catena 78, 60-71.

Kelly, N.M., Fonseca, M. and Whitfield, P., 2001. Predictive mapping for management and conservation of seagrass beds in North Carolina. Aquatic Conservation: Marine and Freshwater Ecosystems, 11(6), 437-451.

Kirchner, G., 2011. 210 Pb as a tool for establishing sediment chronologies: examples of potentials and limitations of conventional dating models. Journal of Environmental Radioactivity, 102(5), 490-494.

Kirchner, G. and Ehlers, H., 1998. Sediment geochronology in changing coastal environments: potentials and limitations of the 137Cs and 210Pb methods. Journal of Coastal Research, 483-492.

Kirwan, M.L., et al. Limits on the adaptability of coastal marshes to rising sea level. Geophysical Research Letters 37, L23401.

Kronvang, B., Laubel, A., Larsen, S. E., Friberg, N., 2003. Pesticides and heavy metals in Danish streambed sediment. *The Interactions between Sediments and Water*. Springer Netherlands. 93-101.

Larsen, I.L. and Cutshall, N.H., 1981. Direct determination of ^{7}Be in sediments. Earth and Planetary Science Letters, 54, 379-384.

Laubel A, Kronvang B, Fjorback C, Larsen SE., 2003. Time-integrated sediment sampling from a small lowland stream. International Association of Theoretical and Applied Limnology, Proceedings 28, 1420–1424.

Leonard, L. A., Luther, M.E., 1995. Flow hydrodynamics in tidal marsh canopies. Limnology and Oceanography 40, 1474–1484.

Leonardi, N., Ganju, N.K. and Fagherazzi, S., 2016. A linear relationship between wave power and erosion determines salt-marsh resilience to violent storms and hurricanes. Proceedings of the National Academy of Sciences, 113(1), 64-68.

Liu, K., Fearn, M.L., 2000. Reconstruction of prehistoric landfall frequencies of catastrophic hurricanes in northwestern Florida from lake sediment records. Quat. Res. 54, 238-245.

Ludwig, W., Probst, J., 1998. River sediment discharge to the oceans; present-day controls and global budgets. American Journal of Science 298.4, 265-295.

Madsen, J.D., Chambers, P.A., James, W.F., Koch, E.W. and Westlake, D.F., 2001. The interaction between water movement, sediment dynamics and submersed macrophytes. Hydrobiologia, 444(1), 71-84.

Mann, M.E., et al., 2009. Atlantic hurricanes and climate over the past 1,500 years. Nature 460, 880-883.

Mariotti, G. and Fagherazzi, S., 2010. A numerical model for the coupled long-term evolution of salt marshes and tidal flats. Journal of Geophysical Research: Earth Surface, 115(F1).

Martens, C.S., Klump, J.V., 1984. Biogeochemical cycling in an organic-rich coastal marine basin: An organic carbon budget for sediments dominated by sulfate reduction and methanogenesis. Geochim. Cosmochim. Acta 48, 1987-2004.

Martens, C.S., 1976. Control of methane sediment-water bubble transport by macroinfaunal irrigation in Cape Lookout Bight, North Carolina. Science 192, 998-1000.

Martin, J.M., Meybeck M., 1979. Elemental mass balance of material carried by major world rivers. Marine Chemistry 7, 173–206.

Mattheus, C.R., Rodriguez, A.B., McKee, B.A. and Currin, C.A., 2010. Impact of land-use change and hard structures on the evolution of fringing marsh shorelines. Estuarine, Coastal and Shelf Science, 88(3), 365-376.

Mattheus, C.R., Rodriguez, A.B., McKee, B., 2009. Direct connectivity between upstream and downstream promotes rapid response of lower coastal-plain rivers to land-use change. Geophys. Res. Lett. 36, L20401. http://dx.doi.org/10.1029/ 2009GL039995.

McDonald D.M., Lamoureux, S.F., Warburton, J., 2010. Assessment of a time-integrated fluvial suspended sediment sampler in a high arctic setting. Geografiska Annaler Series A–Physical Geography 92A:225–235.

McDowell, R.W.,Wilcock, R.J., 2007. Sources of sediment and phosphorus in stream flow of a highly productive dairy farmed catchment. Journal of Environmental Quality 36, 540–548.

McKee, B.A., Cohen, A.S., Dettman, D.L., Palacios-Fest, M.L., Alin, S.R., Ntungumburanye, G.R., 2005. Paleolimnological investigations of anthropogenic environmental change in Lake Tanganyika: II. Geochronologies and mass sedimentation rates based on 14C and 210Pb data. J. Paleolimnol. 34, 19-29.

McKee, B.A., Nittrouer, C.A., DeMaster, D.J., 1983. Concepts of sediment deposition and accumulation applied to the continental shelf near the mouth of the Yangtze River. Geology 11, 631-633.

Meybeck, M., 1984.Les fleuves et le cycle geochemique des e le ments, The se de Doctorat d'Etat, Universite Pierre et Marie Curie, Paris.

Milligan, T. G., Hill, P.S., 1998. A laboratory assessment of the relative importance of turbulence, particle composition, and concentration in limiting maximal floc size and settling behaviour. Journal of Sea Research 39.3, 227-241.

NOAA Historical Hurricane Tracks (2017). (https://coast.noaa.gov/hurricanes/)

NOAA Tides and Currents (2013). (https://tidesandcurrents.noaa.gov/waterlevels)

Nichols, M., Boon, J.D., 1994. Sediment transport processes in lagoons. In: Kferfve, B. (Ed.), Coastal Lagoon Processes. Elsevier Science, Amsterdam, pp. 157-220.

Nichols, M., 1989. Sediment accumulation rates and relative sea-level rise in lagoons. Mar. Geol. 88, 201-219.

Nittrouer, C.A., et al., 1979. The use of Pb-210 geochronology as a sedimentological tool: application to the Washington continental shelf. Mar. Geol. 31, 297-316.

Olsen, C.R., Larsen, I.L., Mulholland, P.J., Von Damm, K.L., Grebmeier, J.M., Schaffner, L.C., Diaz, R.J., Nichols, M.M., 1993. The concept of an equilibrium surface applied to particle sources and contaminant distributions in estuarine sediments. Estuaries 16, 683-696.

Olsen, C.R., Larsen, I.L., Lowry, P.D., Cutshall, N.H., 1986. Geochemistry and deposition of [7]Be in river-estuarine and coastal waters. Journal of Geophysical Research, 91, 896-908.

Olsen, C.R., Simpson, H.J., Bopp, R.F., Williams, S.C., Peng, T.H., Deck, B.L., 1978. Geochemical analysis of the sediments and sedimentation in the Hudson estuary. J. Sediment. Petrol. 48, 401-418.

Ongley E.D., 1992. Environmental quality, changing times for sediment programs. International Association Hydrological Sciences.

Onishi, Y., Wells, B. E., Hartley, S. A., Cooley, S. K., 2002. Pipeline Cross-Site Transfer Assessment for Tank 241-SY-101.

Oroskar, A.R., Turian, R.M., 1980. The critical velocity in pipeline flow of slurries. AIChE Journal 26.4, 550-558.

Owens, P.N., Blake, W.H., Giles, T.R., Williams, N.D., 2012. Determining the effects of wildfire on sediment sources using 137Cs and unsupported 210Pb, the role of landscape disturbances and driving forces. Journal of Soils and Sediments 12, 982–994.

Patton, P.C., Horne, G.S., 1992. Response of the Connecticut river estuary to late Holocene sea level rise. Geomorphology 5, 391-417.

Pennington, W., Cambray, R.S., Eakins, J.D. and Harkness, D.D., 1976. Radionuclide dating of the recent sediments of Blelham Tarn. *Freshwater Biology*, *6*(4), pp.317-331.

Pennington W, Cambray RS, Fisher EMR. Observations on lake sediments using fallout ^{137}Cs as a tracer. Nature 1973; 242:324 – 6.

Perks, M.T., Warburton, J., Bracken, L., 2014. Critical assessment and validation of a time-integrating fluvial suspended sediment sampler. Hydrological Processes 28.17, 4795-4807.

Phillips, J.M., Russell, M.A., Walling, D.E., 2000. Time-integrated sampling of fluvial suspended sediment, a simple methodology for small catchments. Hydrological Processes 14, 2589–2602.

Poff, L.N., Bledsoe, B.P., Cuhaciyan, C.O., 2006. Hydrologic variation with land use across the contiguous United States: geomorphic and ecological consequences for stream ecosystems. Geomorphology 79, 264-285.

Poulenard, J., Perrette, Y., Fanget, B., Quentin, P., Trevisan, D., Dorioz, J.M., 2009. Infrared spectroscopy tracing of sediment sources in a small rural watershed (French Alps). Science of the Total Environment 407, 2808–2819.

Ralston, D.K., Geyer, W.R., 2009. Episodic and long-term sediment transport capacity in the Hudson River estuary. Estuaries Coasts 32, 1130-1151.

Ralston, D.K., Stacey, M.T., 2007. Tidal and meteorological forcing of sediment transport in tributary mudflat channels. Cont. Shelf Res. 27 (10), 1510-1527.

Ream, B.J., 1997. Bomb-radiocarbon tracing of reactive organic matter in coastal North Carolina sediments (Masters Thesis).

Reed, D.J., 1995. The response of coastal marshes to sea-level rise: Survival or submergence?. Earth Surface Processes and Landforms, 20(1), 39-48.

Riggs, S.R., 2001. Shoreline Erosion in North Carolina Estuaries: the Sound front Series, V. North Carolina Sea Grant, Raleigh, p. 68. UNC-SG-01-11.

Robbins, J.A., 1978. Geochemical and geophysical applications of radioactive lead. In: Triage, J.O. (Ed.), The Biogeochemistry of Lead in the Environment, 285-393.

Robbins, J.A., Edgington, D.N., 1975. Determination of recent sedimentation rates in Lake Michigan using Pb-210 ad CS-137. Geochim. Cosmochim. Acta 39, 288-304.

Robblee, M.B., Barber, T.R., Carlson Jr, P.R., Durako, M.J., Fourqurean, J.W., Muehlstein, L.K., Porter, D., Yarbro, L.A., Zieman, R.T. and Zieman, J.C., 1991. Mass mortality of the tropical seagrass Thalassia testudinum in Florida Bay(USA). Marine ecology progress series. Oldendorf, 71(3), 297-299.

Ruiz-Fernandez, A.C., et al., 2009. Changes of coastal sedimentation in the Gulf of Tehuantepec, South Pacific Mexico, over the last 100 years from short-lived radionuclide measurements. Estuar. Coast. Shelf Sci. 82, 525-536.

Russell, M. A., Walling, D.E., Hodgkinson, R.A., 2000. Appraisal of a simple sampling device for collecting time-integrated fluvial suspended sediment samples. *IAHS Publication (International Association of Hydrological Sciences)* 263, 119-127.

Sanchez-Cabeza, Ruiz-Fernandez, A.C., 2012. 210Pb sediment radiochronology: an integrated formulation and classification of dating models. Geochim. Cosmochim. Acta 82, 183-200.

Schwimmer, R.A., 2001. Rates and processes of marsh shoreline erosion in Rehoboth Bay, Delaware, USA. J. Coast. Res. 672-683.

Scileppi, E., Donnelly, J.P., 2007. Sedimentary Evidence of Hurricane Strikes in Western Long Island. Geochemistry, Geophysics, Geosystems, New York, p. 8.

Simms, A.R., Rodriguez, A.B., 2015. The influence of valley morphology on the rate of bayhead delta progradation. J. Sediment. Res. 85, 38-44.

Slagle, A.L., et al., 2006. Late-stage estuary infilling controlled by limited accommodation space in the Hudson River. Mar. Geol. 232, 181-202.

Small, C., Cohen, J.E., 2004. Continental physiography, climate, and the global distribution of human population. Curr. Anthropol. 45, 269-277.

Smith, J.E., Bentley, S.J., Snedden, G.A. and White, C., 2015. What role do hurricanes play in sediment delivery to subsiding river deltas? Scientific reports, 5.

Smith, T.B., Owens, P.N., 2014. Flume-and field-based evaluation of a time-integrated suspended sediment sampler for the analysis of sediment properties. Earth Surface Processes and Landforms 39.9, 1197-1207.

Smith, S. V., Renwick, W. H., Buddemeier, R. W., Crossland, C. J., 2001. Budgets of soil erosion and deposition for sediments and sedimentary organic carbon across the conterminous United States. Global Biogeochemical Cycles 15.3, 697-707.

State Climate Office of North Carolina (SCO-NC). (2016). Data and Products. (http:// http://climate.ncsu.edu/cronos)

Stevenson, J.C., Ward, L.G., Kearney, M.S., 1986. Vertical accretion in marshes with varying rates of sea level rise. In: Wolfe, D.A. (Ed.), Estuarine Variability. Academic Press, Orlando, pp. 241-260.

Syvitski, J.P.M, Vörösmarty, C.J., Kettner, A.J., Green, P., 2005. Impact of humans on the flux of terrestrial sediment to the global coastal ocean. Science 308, 376–380.

Turner, R. E., Baustian, J. J., Swenson, E. M., Spicer, J. S., 2006. Wetland sedimentation from Hurricanes Katrina and Rita. Science 314, 449–452.

Turner, A., Millward, G.E., 2002. Suspended particles, their role in estuarine biogeochemical cycles. Estuarine, Coastal and Shelf Science 55.6, 857-883.

Tweel, A.W. and Turner, R.E., 2014. Contribution of tropical cyclones to the sediment budget for coastal wetlands in Louisiana, USA. Landscape ecology, 29(6), pp.1083-1094.

Tweel, A.W. and Turner, R.E., 2012. Landscape-scale analysis of wetland sediment deposition from four tropical cyclone events. PloS one, 7(11), e50528.

Van Leussen, W., 1988. Aggregation of particles, settling velocity of mud flocs a review. Physical processes in estuaries. Springer Berlin Heidelberg 347-403

Van Rijn, L.C., 2005. Estuarine and coastal sedimentation problems. Int. J. Sediment Res. 20, 39-51.

Voli, M.T., Wegmann, K.W., Bohnenstiehl, D.R., Leithold, E.,Osburn, C.L., Polyakov, V., 2013. Fingerprinting the sources of suspended sediment delivery to a large municipal drinking water reservoir, Falls Lake, Neuse River, North Carolina, USA. Journal of Soils and Sediments 13, 1692–1707.

Walling, D.E., 2012. The role of dams in the global sediment budget. In: Erosion and Sediment Yields in the Changing Environment. IAHS Publication, p. 6, 356.

Walling, D.E., Collins, A.L., Stroud, R.W., 2008. Tracing suspended sediment and particulate phosphorus sources in catchments. Journal of Hydrology 350, 274–289.

Walling, D.E., 2005. Tracing suspended sediment sources in catchments and river systems. Science of the Total Environment, 344, 159-184.

Walling, D.E., Fang, D. 2003. Recent trends in the suspended sediment loads of the world's rivers. Global and Planetary Change 39, 111-126.

Walling, D.E., Webb, B., 1996. Erosion and Sediment Yield, Global and Regional Perspectives. Proceedings of an International Symposium Held at Exeter, UK, from 15 to 19 July 1996. No. 236. IAHS, 1996.

Walling D.E., 1989. Physical and chemical properties of sediment, the quality dimension. International Journal of Sediment Research 4(1), 27-39.

Walling, D. E., Webb, B.W., 1987. Suspended load in gravel-bed rivers, UK experience. Sediment Transfer in Gravel-Bed Rivers. John Wiley & Sons New York., 691-723.

Wasp, E.J., Kenny, J.P., Gandhi, R.L., 1977. Solid-Liquid Flow Slurry Pipeline Transportation. Trans Tech Publications, Rockport, MA

Wells, J.T., 1988. Accumulation of fine-grained sediments in a periodically energetic clastic environment, Cape Lookout Bight, North Carolina. J. Sediment. Res. 58.

Westerweel, J. 1997. Fundamentals of digital particle image velocimetry. Measurement Science and Technology 8, 1379-1392.

Wilson, C.G., Papanicolaou, A.N.T., Denn, K.D., 2012. Partitioning fine sediment loads in a headwater system with intensive agriculture. Journal of Soils and Sediments 12, 966–981.

Winterwerp, J.C., 1998. A simple model for turbulence induced flocculation of cohesive sediment. Journal of Hydraulic Research 36.3, 309-326.

Wren, D.G., Barkdoll, B.D., Kuhnle, R.A., Derrow R.W., 2000. Field techniques for suspended-sediment measurement. Journal of Hydraulic Engineering 126, 97–104.

Yang, S.L., Friedrichs, C.T., Shi, Z., Ding, P.X., Zhu, J., Zhao, Q.Y., 2003. Morphological response of tidal marshes, flats and channels of the outer Yangtze River mouth to a major storm. Estuaries 26 (6), 1416-1425.

Zaitlin, B.A., Dalrymple, R.W., Boyd, R., 1994. The stratigraphic organization of incised valley systems associated with relative sea-level change. In: Dalrymple, R.W., Boyd, R., Zaitlin, B.A. (Eds.), Incised-valley Systems: Origin and Sedimentary Sequences, SEPM (Society for Sedimentary Geology) Special Publication, vol. 51, pp. 45-60